

Fredrik Håland

Combining fully coupled analysis and linear potential theory time domain analysis to obtain cross sectional loads in the substructure of a floating offshore wind turbine

Master's thesis in Marine Technology

Supervisor: Prof. Zhen Gao

Co-supervisor: Jonas Gullaksen Straume, Håkon Drengsrud

June 2022

Fredrik Håland

Combining fully coupled analysis and linear potential theory time domain analysis to obtain cross sectional loads in the substructure of a floating offshore wind turbine

Master's thesis in Marine Technology

Supervisor: Prof. Zhen Gao

Co-supervisor: Jonas Gullaksen Straume, Håkon Drengsrud

June 2022

Norwegian University of Science and Technology

Faculty of Engineering

Department of Marine Technology



Norwegian University of
Science and Technology

PREFACE

This master's thesis is written by Stud. Techn. Fredrik Håland in cooperation with Dr. techn. Olav Olsen at the Norwegian University of Science and Technology (NTNU). The thesis serves as the final assignment for obtaining the Master of Science degree in Marine technology with specialisation in Marine structures. The work was carried out during the spring of 2022 and is a continuation of the Project thesis work submitted in the fall of 2021.

The objective of the thesis is to study a proposed method of combining fully coupled analysis and potential flow theory time domain analysis for obtaining cross sectional loads in the hull of floating offshore wind turbines.

Fredrik Håland

Fredrik Håland

Trondheim, 11th June 2022

ACKNOWLEDGEMENTS

My main supervisor from NTNU during the master's thesis work has been Prof. Zhen Gao. I would like to thank Prof. Zhen Gao for sharing his vast knowledge within floating offshore wind turbine technology, for always being available to help and providing relevant feedback. Thanks should also be extended to Prof. Erin Bachynski-Polić. Prof. Bachynski-Polić was my supervisor during the Project thesis work, and the master thesis work before her maternity leave, early 2022.

Jonas Gullaksen Straume has been my supervisor from Dr. techn. Olav Olsen. I would like to thank Jonas for being available for regular meetings, sharing his knowledge and helping me with problems that have occurred along the way. I would also like to thank Håkon Drengsrud who has been involved. I am grateful for the opportunity to cooperate with Dr. techn. Olav Olsen during my master thesis work. The task provided to me has been challenging, but in return developed me a lot as an engineer. I feel highly confident that the knowledge I have gained will benefit me a lot going forward in my engineering career.

A special thanks should also be given to Postdoc. Shuaishuai Wang at the department of Marine technology, NTNU. Shuaishuai has been doing many of the same investigations as me, and he has given me a lot of useful tips along the way. This has helped me avoid pitfalls, saved me a lot of time and guided me in the right direction.

There is a lot of people that has helped me also on a personal level. I want to thank my friends at office A2.011 at MTS for all the good memories we have made during the last five years as well as the good cooperation we have had with the school work. I also want to thank my friends from Karmøy, my brother and my sister.

Finally I want to thank my parents for always supporting me and believing in me.



MASTER THESIS IN MARINE TECHNOLOGY

SPRING 2022

for

Stud. Techn. Fredrik Håland

Combining fully coupled analysis and linear potential theory time domain analysis to obtain cross sectional loads in the substructure of a floating offshore wind turbine

Metoder for å kombinere koblet analyse og lineær potensialteori i tidsdomene for å evaluere indre laster i skroget på flytende havvindturbiner

Large volume structures of floating wind turbines (FWTs) do not have a well-defined methodology for transfer of loads to a structural model. In recent years a methodology of combining fully coupled analysis with a linear potential theory time domain analysis has been proposed, aiming at solving this issue. The thesis work will investigate this approach, if possible with comparison against an alternative approach using a beam model in SIMA. The proposed tasks to be carried out include:

1. As needed, extend the literature review into wave and wind loads, potential flow theory, FWT dynamics, and methods for obtaining internal loads in the hull of FWTs or other types of offshore platforms.
2. Make a panel model and structural model based on the Lifes50+ 10MW OOSTAR floater for the potential theory solver Wasim (based on previous modelling for Wadam).
3. Run the set-up between a fully coupled analysis run (Sima) to a time series potential theory solver (Wasim) for obtaining panel pressures for structural analysis. Motions and waves are transferred between the programs to ensure correct panel pressure for the structural model. Auxiliary forces from mooring line fairlead forces and tower base are also transferred.
4. Verify the method by comparing the loading at the tower interface between the fully coupled model and the structural model of substructure
5. Run a ULS analysis for idling turbine with the method of investigation and compare the cross sectional loads with those from a frequency domain analysis in Wadam.
6. If time permits, develop a beam element model in SIMA with distributed potential flow and compare obtained sectional loads with those from Wasim.
7. Conclusions and recommendations for further work.





The work scope may prove to be larger than initially anticipated. Subject to approval from the supervisors, topics may be deleted from the list above or reduced in extent.

In the thesis report, the candidate shall present his personal contribution to the resolution of problems within the scope of the project work

Theories and conclusions should be based on mathematical derivations and/or logic reasoning identifying the various steps in the deduction.

The candidate should utilise the existing possibilities for obtaining relevant literature.

Thesis format

The thesis should be organised in a rational manner to give a clear exposition of results, assessments, and conclusions. The text should be brief and to the point, with a clear language. Telegraphic language should be avoided.

The report shall contain the following elements: A text defining the scope, preface, list of contents, summary, main body of thesis, conclusions with recommendations for further work, list of symbols and acronyms, references and (optional) appendices. All figures, tables and equations shall be numerated.

The supervisors may require that the candidate, in an early stage of the work, presents a written plan for the completion of the work.

The original contribution of the candidate and material taken from other sources shall be clearly defined. Work from other sources shall be properly referenced using an acknowledged referencing system.

The report shall be submitted in electronic format (.pdf):

- Signed by the candidate
- The text defining the scope shall be included (this document)
- Drawings and/or computer models that are not suited to be part of the report in terms of appendices shall be provided on separate (.zip) files.

Ownership

NTNU has according to the present rules the ownership of the thesis. Any use of the report has to be approved by NTNU (or external partner when this applies). The department has the right to use the report as if the work was carried out by a NTNU employee, if nothing else has been agreed in advance.





Thesis supervisors:

Prof. Zhen Gao, NTNU, zhen.gao@ntnu.no

Jonas Gullaksen Straume, Dr. Tech. Olav Olsen, jgs@olavolsen.no

Håkon Drengsrud, Dr. Tech. Olav Olsen, hdr@olavolsen.no

Deadline: June 11, 2022

Trondheim, January 2022

Zhen Gao

Jonas Gullaksen Straume

Håkon Drengsrud

Zhen Gao

Jonas G. Straume

Håkon D

Candidate – date and signature:

11/06/2022

Fredrik Haland



Verification

Transaction 09222115557470988765

Document

Thesis_description_fredrik_håland-signedzgao

Main document

3 pages

Initiated on 2022-06-08 14:23:34 CEST (+0200) by Intility

eSign (le)

Finalised on 2022-06-08 14:29:05 CEST (+0200)

Initiator

Intility eSign (le)

esign@intility.no

Signing parties

Jonas Gullaksen Straume (JGS)

On behalf of Dr Techn Olav Olsen AS

jgs@olavolsen.no

95298697



Signed 2022-06-08 14:24:11 CEST (+0200)

Håkon Drengsrud (HD)

On behalf of Dr.techn.Olav Olsen AS

hdr@olavolsen.no

97511657



Signed 2022-06-08 14:29:05 CEST (+0200)

This verification was issued by Scrive. Information in italics has been safely verified by Scrive. For more information/evidence about this document see the concealed attachments. Use a PDF-reader such as Adobe Reader that can show concealed attachments to view the attachments. Please observe that if the document is printed, the integrity of such printed copy cannot be verified as per the below and that a basic print-out lacks the contents of the concealed attachments. The digital signature (electronic seal) ensures that the integrity of this document, including the concealed attachments, can be proven mathematically and independently of Scrive. For your convenience Scrive also provides a service that enables you to automatically verify the document's integrity at: <https://scrive.com/verify>



ABSTRACT

Large volume floating offshore wind turbine (FOWT) substructures do not have a well-defined methodology for transfer of loads to a structural model and new methods are needed in order to improve analyses.

This study investigates a new suggested method for load transfer of FOWTs that uses a combination of coupled analysis in Sima, and time domain potential flow analysis in Wasim. Hydrodynamic coefficients are first sent to Sima for the substructure representation. Coupled analysis is subsequently done before motions, waves and auxiliary forces are sent back to Wasim. Wasim computes hydro pressures and loads are afterwards transferred to a structural model. The work is carried out in cooperation with Dr. techn. Olav Olsen and models are based on the published Lifes50+ 10 MW design of their patented FOWT concept, the OO-Star.

Compatibility between the models in Sima and Wasim was ensured by comparing RAOs obtained from the two programs. FFT was used to calculate RAOs from Sima since the motion response is nonlinear. The obtained RAOs were very much alike expect some small differences around the resonance peaks, which is expected.

Correct data transfer between programs was ensured by comparing the input data from Sima with the output from Wasim analysis. It was also important to ensure that the hydrodynamic and hydrostatic pressure mapping to the structural model in Wasim worked as intended. The verification work showed that the method works as intended and the method is straightforward to implement.

The method of investigation was used for a ULS analysis with idling turbine. The M_y bending moment following body-fixed coordinate system was investigated in three cross sections along one of the pontoons and one in the central column close to the tower base. The largest pontoon bending moments were found in the pontoon cross section closest to the central column. The bending moment in the central column were relatively low which is expected for a turbine in idling condition where aerodynamic loads have been minimized.

The bending moments from the ULS analysis were also compared with a frequency domain analysis in Wadam, using the same sea state. Obtained bending moments were relatively close to the bending moments from the time domain analysis, which indicates that the cross sectional loads are mainly wave driven. The largest ratio between the bending moments from the time domain-, and frequency domain analysis was found to be 1.17 and occurred for the cross section closest to the central column.

The method of investigation is consistent with the rigid body approximation and future work should include looking further into the effect of hull flexibility.

Keywords: Floating offshore wind turbines, Renewable energy transition, Sesam package, Load-transfer, Potential flow theory

SAMMENDRAG

Storvolum skrog i flytende havvindturbiner har ikke en veldefinert metode for lastoverføring til strukturmodell og nye metoder trengs for å forbedre analyser.

Dette studiet undersøker en ny metode for lastoverføring på skroget i flytende vindturbiner som bruker en kombinasjon av koblet analyse i Sima og potensialteori i tidsdomene i Wasim. Hydrodynamiske koeffisienter blir først sendt til Sima for skroget. Koblet analyse blir så utført for bevegelser, bølger og krefter fra tårn og forankring sendes tilbake til Wasim. Wasim regner det hydrodynamiske og hydrostatiske trykket på skroget og laster kan etterpå overføres til en strukturmodell. Arbeidet er utført i samarbeid med Dr. techn. Olav Olsen og baserer seg på en 10 MW vindturbin med deres eget patenterte skrogdesign, OO-Star, presentert i Lifes50+ prosjektet.

Kompatibilitet mellom modeller i Sima og Wasim ble undersøkt ved å sammenligne RAOer fra programmene. FFT ble brukt til å beregne RAOer fra Sima siden responsen er ulineær. Beregnede RAOer var like, utenom små forskjeller rundt resonansfrekvensene, som var forventet på forhånd.

Korrekt dataoverføring mellom programmene ble undersøkt ved å sammenligne input dataen fra Sima med resultatene gitt fra Wasim analyse. Det var også viktig å sikre seg at hydrodynamiske og hydrostatiske trykk fra analysen ble skikkelig overført til strukturmodellen i Wasim. Verifikasjonsarbeidet viser at metoden fungerer som tiltenkt, og metoden er rett frem å implementere.

Den undersøkte metoden ble bruk til en ULS analyse med parkert turbin. M_y bøyemomenter i kroppsfast koordinatsystem ble undersøkt i tre tverrsnitt langs den ene pontongen, og ett i senterkraftet like ved tårnbasen. De største bøyemomentene i pontongene ble funnet i ble funnet i pontongtverrsnittet nærmest senterkolonnen. Bøyemomentene i senterkraftet var relativt små, noe som er forventet for en parkert turbin hvor aerodynamiske krefter har blitt minimert.

Bøyemomentene fra ULS analysen ble også sammenlignet med en frekvensplan analyse i Wadam, med den samme sjøtilstanden. De resulterende bøyemomentene lå relativt nære bøyemomentene fra tidsrealisasjonene, som indikerer at tverrsnittskraftene er hovedsaklig bølgedrevne. Det største forholdet mellom bøyemomenter fra tidsplan-, og frekvensplan analysene ble funnet til å være 1.17 og oppstod i tverrsnittet nærmest senterkraftet.

Den undersøkte metoden tilnærmer skroget som et uendelig stivt legeme og fremtidig arbeid inkluderer å se videre på effekten av elastisitet i skroget.

Stikkord: Flytende havvindturbiner, Fornybar energi, Sesam pakken, Lastoverføring, Potensialteori

TABLE OF CONTENTS

Preface	i
Acknowledgements	ii
Scope of work	iii
Abstract	vii
Sammendrag	viii
List of Figures	xiii
List of Tables	xv
Nomenclature	xvi
1 Introduction	1
1.1 Background	1
1.2 Objectives	1
1.3 Offshore wind power - current status and outlook	2
1.4 Lifes50+ and the OO-Star Wind Floater concept	3
1.5 Literature review	4
1.6 Thesis outline	5
2 Theoretical background	6
2.1 Floating wind turbine concepts	6
2.1.1 Ballast Stabilized Platforms	6
2.1.2 Buoyancy Stabilized Platforms	7
2.1.3 Mooring Stabilized Platform	7
2.2 Rigid body mechanics	7
2.3 Linear potential flow theory	8

2.3.1	Superposition of velocity potentials	9
2.3.2	Panel methods - solution of the potential flow problem	10
2.4	Hydrodynamic loads on FOWTs	10
2.4.1	Hydrodynamic pressure loads from Bernoulli's equation	11
2.4.2	Hydrodynamic loads in linear potential flow theory	11
2.4.3	The Morison equation	13
2.5	Aerodynamic loads on FOWTs	13
2.5.1	The Blade element momentum (BEM) model	13
2.5.2	Other important aerodynamic considerations	14
2.6	Wind turbine controller theory	14
2.7	Hydro-aero-servo-elastic coupling	16
2.8	Equation of motion for a floating body	16
2.8.1	Equation of motion according to linear potential flow theory	16
2.8.2	Equation of motion with nonlinearities	17
2.9	Statistical description of sea	17
2.9.1	Wave spectrum	18
2.9.2	Response spectrum	18
2.9.3	Response maxima	19
2.10	Limit state design	20
2.11	The Fast Fourier Transform algorithm	20
2.12	Computer software	21
3	Lifes50+ 10 MW OO-Star design	24
3.1	Substructure properties	25
3.2	Tower properties	28
3.3	Top mass properties	28
3.4	Mooring system properties	29
4	Method and computer implementation	31
4.1	Method overview	33
4.2	GeniE	34
4.2.1	T*.FEM panel model	34
4.2.2	.pln section model	35
4.2.3	Mass-, compartment- and structure models	35
4.2.4	Morison model	38
4.3	HydroD	39

4.3.1	Compartment filling fractions	40
4.3.2	Panel model for Wasim	41
4.4	Wadam	41
4.5	Wasim	41
4.5.1	Surface mesh	42
4.5.2	Prescribed motions, forces and waves	42
4.6	Sima	43
5	Model and method verification	46
5.1	Model verification	46
5.1.1	Hydrodynamic analysis of substructure	46
5.1.2	Sima model	49
5.1.3	Model compitability	49
5.2	Method verification	52
5.2.1	Prescribed wave elevation	53
5.2.2	Force resultant in heave	53
5.2.3	Prescribed motion - tower base bending moment	54
5.2.4	Pressure mapping	55
5.2.5	Prescribed forces	57
6	Fully coupled ULS analysis	63
6.1	ULS analysis, set up	63
6.1.1	Surface mesh sensitivity analysis	64
6.1.2	Time step sensitivity analysis	67
6.2	Sectional bending moments from time domain analysis	68
6.3	Frequency domain comparison	69
7	Conclusion	72
8	Further work	74
	Bibliography	76
	Appendix	80
A	<i>SIMA.timeseries.m</i> by Erin Bachynski Polić	80
B	<i>bpass.m</i> by Halvor Lie	81
C	Correct gravity and buoyancy implementation in Sima	81
D	.wnd input file for TurbSim turbulent wind generation	82

E	Buoyancy correction force in Sima	84
E.1	Estimation of vertical pretension at fairlead	84
E.2	<i>buoyancy_correction.m</i>	85
F	Applying prescribed data from Sima in Wasim analysis	85
F.1	Wave.txt	87
F.2	forces.frc	88
F.3	Motion.txt	89

LIST OF FIGURES

1.1	Lifes50+ 10 MW OO-Star	3
2.1	Floating offshore wind turbine concepts	6
2.2	Freely floating rigid body	8
2.3	Power curve for a variable speed, variable pitch wind turbine	15
2.4	TurbSim turbulent wind illustration	23
3.1	Lifes50+ 10MW OO-Star with coordinate system definition	25
3.2	Technical drawings of the Lifes50+ 10 MW OO-Star substructure	27
3.3	Lifes50+ 10 MW OO-Star mooring system	29
4.1	Sesam workflow	32
4.2	GeniE panel model of Lifes50+ OO-Star substructure	34
4.3	GeniE .pln section model of Lifes50+ OO-Star substructure	35
4.4	Mass/structural/compartment models of the Lifes50+ 10 MW OO-Star	36
4.5	Beam elements in structural model	37
4.6	Support points on structural model	38
4.7	Lifes50+ OO-Star Morison model	39
4.8	HydroD model of the 10 MW Lifes50+ OO-Star substructure	40
4.9	Compartments from compartment model	40
4.10	.pln panel model	41
4.11	Surface mesh in HydroD	42
4.12	Fully coupled analysis model in Sima	43
4.13	Illustration of wind turbine model in Sima	44
5.1	Lifes50+ 10MW OO-Star added mass from Wadam	47
5.2	Lifes50+ 10MW OO-Star wave radiation damping from Wadam	48
5.3	Panel model sensitivity	48
5.4	Equilibrium z-coordinate of floater from static analysis in Sima	49

5.5	FFT analysis of heave motion response with regular incoming waves	50
5.6	Unfiltered and filtered heave motion from Sima	51
5.7	RAO comparison between Wadam and Sima for surge, heave and pitch	51
5.8	Wave elevation comparison between Sima and Wasim	53
5.9	Heave resultant force from Wasim	54
5.10	Simplified models used for verification of prescribed motion	55
5.11	Tower base M_y fore-aft bending moment comparison between Sima and Wasim . .	55
5.12	Structural model for bottom slab	56
5.13	Pressure contours in Xtract from ULS seastate	57
5.14	Load cross section at (0 m, 0 m, 10.5 m)	58
5.15	Prescribed forces at tower base vs cross sectional loads from Wasim	59
5.16	Load cross section in vicinity of fairlead	60
5.17	Prescribed forces at fairlead vs cross sectional loads from Wasim	61
6.1	Load cross sections used in fully coupled ULS analyses	64
6.2	HydroD surface mesh sensitivity	65
6.3	Surface mesh sensitivity, "Area 1"	66
6.4	Surface mesh sensitivity, "Area 2"	66
6.5	Surface mesh used for ULS analysis	67
6.6	Time step sensitivity	68
6.7	Data plots from Wadam frequency domain analysis	69
A1	Static mooring line configuration	84
A2	Prescribed motion, point forces and wave elevation specification in HydroD for Wasim analysis	86
A3	"Export results to Wasim" option in Sima	87

LIST OF TABLES

3.1	Lifes50+ 10MW OO-Star platform parameters, including ballast	26
3.2	Tower properties from the Lifes50+ OO-Star design (YU et al. 2018)	28
3.3	Lifes50+ 10 MW OO-Star, RNA properties	29
3.4	Lifes50+ 10 MW OO-Star, mooring system properties	30
4.1	Material properties for mass-, and structural model in HydroD	36
4.2	Mass properties from GeniE model	37
4.3	Support points for structural model	38
4.4	Morison model for the 10 MW OO-Star	39
4.5	Compartment filling fractions from HydroD	41
4.6	Finite element representation of lines in Sima model	43
5.1	ULS condition	52
5.2	Mass properties for simplified top mass representation	54
6.1	Seed combinations used for ULS analysis	63
6.2	HydroD load cross sections used in ULS analysis	64
6.3	Mesh properties for mesh refinement of "Area 1"	65
6.4	Bending moments M_y when refining mesh "Area 1"	65
6.5	Mesh properties for mesh refinement of "Area 2"	66
6.6	Bending moments M_y when refining mesh "Area 2"	66
6.7	Time step sensitivity analysis	67
6.8	Maximum bending moments M_y for 10 ULS realisations	68
6.9	Static bending moments in pontoons	68
6.10	Bending moments, time domain vs frequency domain	70

NOMENCLATURE

α	Phase angle of excitation force
β	Phase angle of motion response relative to excitation force
∇	Vector differential operator
$\boldsymbol{\eta}_0$	Motion response amplitude array
$\boldsymbol{\eta}, \dot{\boldsymbol{\eta}}, \ddot{\boldsymbol{\eta}}$	Rigid body motion-, velocity- and acceleration response vectors respectively
$\tilde{\boldsymbol{\eta}}$	Complex response array
$\tilde{\boldsymbol{F}}_{\text{exc}}$	Complex excitation force per unit wave amplitude array
\boldsymbol{A}_∞	Infinite-frequency added mass matrix
\boldsymbol{A}	Added mass matrix
\boldsymbol{B}	Linear wave radiation damping matrix
$\boldsymbol{F}_{\text{exc}}$	Excitation force array
$\boldsymbol{F}_{0,\text{exc}}$	Excitation force amplitude array
\boldsymbol{h}	Retardation function matrix
$\boldsymbol{i}, \boldsymbol{j}, \boldsymbol{k}$	Unit normals in x-, y- and z-direction respectively
\boldsymbol{K}	Stiffness matrix
\boldsymbol{M}	Structural mass matrix
$\boldsymbol{M}_{\text{exc}}$	Excitation moment array
\boldsymbol{n}	Unit normal vector
\boldsymbol{r}	Moment arm
ϵ	Wave steepness
$\eta_1, \eta_2, \dots, \eta_6$	Surge-, sway-, heave-, roll-, pitch- and yaw motion respectively
$\hat{f}(\omega)$	Frequency domain representation of mathematical function f
λ	Wave length
\boldsymbol{V}	Kinematic velocity field
$\mathcal{F}, \mathcal{F}^{-1}$	Fourier transform and inverse Fourier transform respectively
ω	Angular wave frequency
ϕ	Velocity potential
ϕ_0	Incident wave velocity potential

ϕ_7	Velocity of scattered wave field due to presence of body
ϕ_D	Diffraction velocity potential
$\phi_j, j = 1, 2, \dots, 6$	Radiation velocity potential for the j^{th} rigid body motion
ϕ_R	Radiation velocity potential
ρ	Density of sea water
ζ_a	Wave amplitude
A_{wp}	Water plane area
C_D	Drag coefficient
E	Youngs modulus
$f(t)$	Time domain representation of mathematical function f
f_s	Sampling frequency
$F_{k,j}^{\text{rad}}$	Radiation load in k -direction due to oscillation in j^{th} degree of freedom
G	Shear modulus
g	Acceleration of gravity
I	Second moment of area
J	Polar moment of inertia
k	Wave number
p	Fluid pressure
p	Kinematic fluid pressure
p_a	Atmospheric pressure
S_B	Instantaneous wetted body surface
S_{0B}	Mean wetted surface
u	Kinematic velocity in x-direction
v	Kinematic velocity in y-direction
V_D	Displaced volume
w	Kinematic velocity in z-direction
z_B	Centre of buoyancy
z_G	Centre of gravity
BEM	Boundary element methods OR Blade element momentum theory
BVP	Boundary value problem
CM	Centre of mass
COB	Centre of buoyancy
COG	Centre of gravity
DFT	Discrete Fourier transform
DOF	Degree of freedom

FE	Finite element
FEA	Finite element analysis
FFT	Fast Fourier transform
FOWT	Floating offshore wind turbines
FWT	Floating wind turbines
IEA	International Energy Agency
LCOE	Levelized Cost of Energy
MSL	Mean sea level
RAO	Response amplitude operator
RNA	Rotor nacelle assembly
TLP	Tension leg platform
ULS	Ultimate limit state

1

INTRODUCTION

1.1 Background

One of the greatest challenges facing mankind today is a successful transition from fossil fuels to renewable energy resources. It is a large consensus amongst scientists today that humans are contributing to climate change that is not natural and has large negative consequences for the environment. The world also has an increasing energy demand and the energy transition towards renewables is therefore more urgent than ever. This fact is also reflected in EU's renewable energy directive that has established a binding target of 40% energy by renewables by 2030 for the EU (EUROPEAN COMMISSION 2021).

The energy potential in offshore wind is enormous. IEA (2019) have estimated that offshore wind power has the potential to meet the world's total electricity demand 11 times over in 2040. It is evident that offshore wind has the potential to play a very important role in the energy transition ahead.

Most of the installed capacity of offshore wind per 2021 comes from bottom-fixed turbines. Bottom-fixed turbines are profitable, but have a depth limitation of approximately 50 meters. For deeper waters, bottom-fixed offshore wind turbines are no longer economically feasible (ARAPOGIANNI, ATHANASIA ET. AL. 2013). A large part of the potential in offshore wind is located at depths where bottom-fixed turbines are no longer an option. Furthermore, wind is stronger and steadier further offshore. These are the main motivational factors for now looking more into the development of floating offshore wind turbines.

The development of floating offshore wind turbine technology has introduced several new engineering challenges. One of these challenges is the transfer of loads to a structural model for the substructure. This is the main motivation for looking further into the method that this thesis investigates.

1.2 Objectives

Large volume structures of floating wind turbine do not have a well-defined methodology for transfer of loads to a structural model of the hull. The overall objective for this thesis is to investigate a method of combining fully coupled analysis with linear potential theory time domain

analysis, aiming at solving this issue. Motions, waves, forces at the mooring lines and the fairleads from coupled Sima analysis are used as prescribed data for time domain potential flow analysis in Wasim. The hydrostatic and hydrodynamic pressure distribution on the floater are obtained from Wasim. These pressures together with prescribed forces and motions are used on a structural model to obtain cross sectional loads or for finite element analysis (FEA).

1.3 Offshore wind power - current status and outlook

The cumulative offshore wind capacity at the end of 2020 was 35.3 GW (GLOBAL WIND ENERGY COUNCIL 2021a, p. 21). Out of this capacity, the installed cumulative capacity of floating offshore wind power was 73.33 MW (GLOBAL WIND ENERGY COUNCIL 2021a, p. 20). In comparison, the cumulative installed capacity of total wind power was approximately 743 GW (GLOBAL WIND ENERGY COUNCIL 2021b). The amount of installed offshore wind therefore still accounts for a very small fraction of the total cumulative installed wind power. The same can especially be said about floating offshore wind which only accounts for approximately 0.01% of the total installed wind power capacity and 0.21% of offshore installed wind power capacity, based on the aforementioned numbers.

Floating offshore wind is a technology in its early stages and the technology is only taking its first steps towards commercialization (DNV 2020). Many floating offshore wind turbine concepts have emerged over the years but only a couple have actually been demonstrated due to high costs and resources needed. The first multi-megawatt FOWT demonstrator was the Hywind Spar Demo, installed outside Karmøy of the west coast of Norway in 2009 (SKAARE et al. 2015). The Hywind Demo is a 2.3 MW spar type concept, owned by Equinor and initially developed by Hydro before a merger was realized between Equinor and parts of Norsk Hydro (BRETON and MOE 2009; EQUINOR 2017). The second large floating system was the WindFloat concept developed by Principle Power in partnership with EDP and Repsol. The WindFloat concept is of the semisubmersible type and a demonstrator of this concept was first installed off the Portuguese coast in 2011 with a 2 MW Vestas turbine (CASTRO-SANTOS and DIAZ-CASAS 2016; ENERGIAS DE PORTUGAL 2018). Other demonstrators in the MW class includes Ideol's FloatGen and Hibiki demonstrators located offshore Le Croisic in France and Kutakyushu in Japan respectively (IDEOL 2021).

Other concepts that have been tested are the TetraSpar demonstrator outside Karmøy, the SeaTwirl S1 offshore Sweden, and the Eolink 1/10th prototype (EOLINK 2021; SEATWIRL 2021; STIESDAL 2021). Demonstrators are also planned for the future such as the SeaTwirl S2 and Dr. techn. Olav Olsen's 11 MW OO Star wind floater (DURAKOVIC 2021a; SEATWIRL 2021).

In 2021, there are three floating offshore wind farms in the world - Hywind Scotland, WindFloat Atlantic and the Kincardine Offshore Wind farm. Hywind Scotland is a 30 MW pilot park approximately 15 miles off the coast of Peterhead, near Aberdeen that was launched in 2017 (WHITFIELD 2020). Hywind Scotland is based on the Hywind demo after successful demonstration of the concept. The WindFloat Atlantic farm is based on the WindFloat concept and consists of three 8.4 MW turbines off the coast of Viana do Castelo on the west coast of Portugal (ENERGIAS DE PORTUGAL 2018). The Kincardine Offshore Wind farm is located off the coast of Aberdeenshire in Scotland and is the largest operating floating wind farm with five 9.5 MW turbines and one 2 MW turbine. The Kincardine wind farm became fully operating in 2021 and uses the WindFloat floater concept (DURAKOVIC 2021b). In 2021, construction of the Hywind Tampen wind farm was also started. Hywind Tampen will become the largest floating wind farm in the world with 11 wind turbines, delivering a total of 88 MW power (EQUINOR 2021).

The International Energy Agency has estimated that the technical potential for offshore wind worldwide is more than 120 000 GW (IEA 2019). A large portion of this potential is only unlocked with further development of floating offshore wind. As is obvious from the aforementioned, many companies have recognized this potential and are now looking into getting involved in this new technology. Only the future can tell how much of the potential of floating offshore wind will be fulfilled, but predictions look promising for those involved. Among several optimistic speculations,

DNV has estimated that floating wind will reach a total capacity of 250 GW by 2050 (DNV 2020).

1.4 Lifes50+ and the OO-Star Wind Floater concept

The investigations in this thesis are centered around Dr. techn. Olav Olsen's OO-Star Wind Floater concept. The OO-Star is a semi-submersible concept that consists of a star-shaped base pontoon, which connects a central column and three outer columns. The floater is made out of post-tensioned concrete and stationkeeping is provided by catenary mooring lines connected to the three outer columns (YU et al. 2018).

An optimized substructure design of a 10 MW OO-Star has been published in the Lifes50+ project (YU et al. 2018). Lifes50+ is a European Horizon 2020-founded programme led by SINTEF Ocean. The objective of the Lifes50+ project has been to mature floating substructure design, increase scientific and industrial knowledge and to develop better design methodologies and procedures in order to ultimately reduce the LCOE (Levelized Cost of Energy) for large floating offshore wind farms (LIFES50+ 2021).

The 10 MW OO-Star design published by YU et al. (2018) in the Lifes50+ project is used in the work presented in this thesis. An illustration of the OO-Star concept is seen in Figure 1.1.

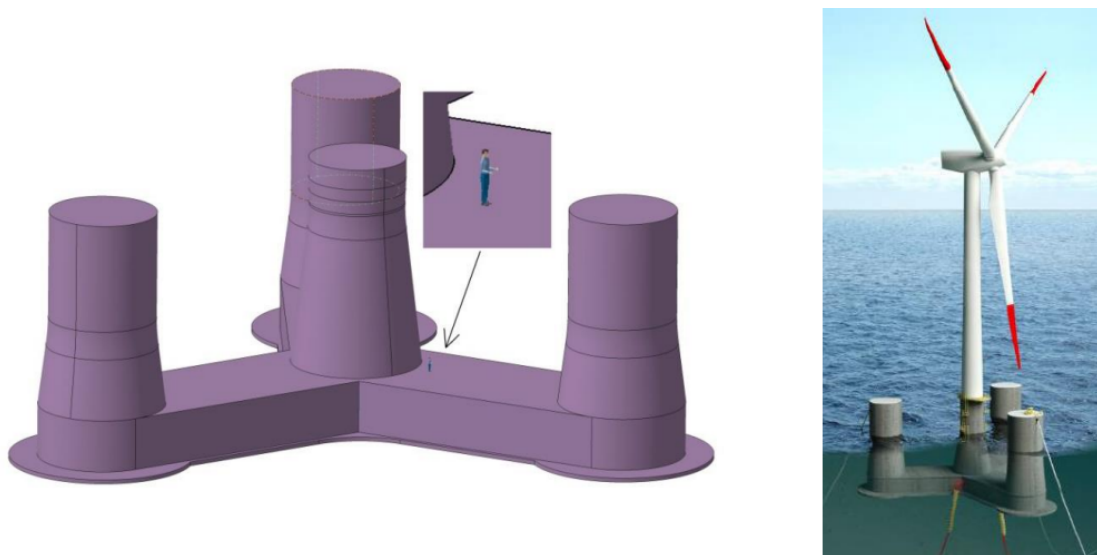


FIGURE 1.1: Lifes50+ OO-Star Wind Floater Semi 10 MW structure

Source: (YU et al. 2018)

1.5 Literature review

The loads to stress transfer for FOWT hull design is an open challenge and many approaches exist (ALEXANDRE et al. 2018). A substructure of a FOWT can either be modelled as a rigid body or as a flexible body. The latter should be considered if the effect of elasticity in the hull is of importance. The effect of flexibility will typically be increased for larger wind turbines (BORG, A. M. HANSEN et al. 2016). The rigid body approach is usually accepted for FOWTs with up to 5 MW capacity. For larger FOWTs, the flexibility in the hull will typically need to be taken into account. This means that reliable methods for the inclusion of hull flexibility have to be developed and improved in a time where FOWT dimensions are getting larger and larger (BORG, BREDMOSE et al. 2017).

ALEXANDRE et al. (2018) presents at least three methods for doing a loads to stress transfer of FOWT platforms. Two of the methods involve splitting the hull into sections, where properties from hydrodynamic analysis are assigned to each section in a coupled analysis. The first method is to do a hydrodynamic analysis of the substructure represented as one body. Hydrodynamic properties for each section are found by integrating panel pressures from the panels associated with each section. The other method is similar, but in this method, hydrodynamic loads are computed taking coupled terms in the radiation force into account. The latter method captures hydro-elastic coupling, but is computationally demanding. The first method is faster and takes elasticity in the hull into account, but it does not take hydro-elastic coupling into account.

SVENDSEN (2016) has implemented the first method mentioned above. Svendsen did a master thesis on the effect of elasticity in the hull of a tension leg platform (TLP) turbine by making an equivalent beam element model in Riflex. Radiation and diffraction pressures were found in Wamit by using a panel model and dividing the structure in sections. The total radiation and diffraction pressures on each section were then found by integrating loads over each section with the use of an algorithm that associates the panels in the panel model with the sections. The total hydrodynamic loads from the radiation and diffraction pressures for each section were then transferred to the Riflex beam model by using Simo-bodies. Time-domain analysis could then be carried out with the flexible TLP beam element model together with hydrodynamic coefficients from the Wamit analysis. The investigations done by SVENDSEN (2016) showed that flexibility gave larger natural periods compared to a equivalent rigid body. The nacelle motion, tower base bending moment and tension at the top of each tendon also increased when running wind-wave environments.

GUIGNIER et al. (2016) have done a similar analysis as SVENDSEN (2016), but also taken the hydrodynamic interaction between sections into account. This is the first method from ALEXANDRE et al. (2018) presented above. The diffraction radiation calculations were done using the software Aqwa. Time domain global analyses were afterwards done with a finite element model in OrcaFlex where hull compartments are linked via beam elements.

HAN et al. (2018) have done structural analysis of a FOWT substructure using a rigid body approach. Hydrodynamic coefficients for the FOWT substructure were first sent to a time domain coupled analysis solver for the full wind turbine system. The wave, substructure motions and auxiliary forces were subsequently sent back to a floater representation in a Rankine source solver. This Rankine source solver was used to compute the hydrodynamic pressure distribution on the floater and the hydrodynamic pressure and prescribed forces were mapped to a structural model for structural analysis. A similar method is also presented by ALEXANDRE et al. (2018). This is the same approach as this thesis work is investigating.

1.6 Thesis outline

The following is an outline for this thesis.

Chapter 2 Provides the theory used throughout the thesis where emphasis is put on rigid body mechanics and linear potential flow theory.

Chapter 3 Contains a detailed description of the 10 MW OO-Star design as presented in Lifes50+ by YU et al. (2018). This includes the substructure, mooring system, tower and RNA.

Chapter 4 Contains a detailed description on the computer modelling that was done and how the computer software was used.

Chapter 5 Describes all the model- and method verification that was used in order to ensure that the investigated method worked as intended and that the method gives reliable results.

Chapter 6 Contains results from a full ULS analysis using the method of investigation in order to obtain cross sectional loads in the OO-Star floater. These cross sectional loads are compared with the cross sectional loads at the same positions from a frequency domain analysis with the same ULS seastate.

Chapter 7 Gives concluding remarks regarding the method of investigation and the results from chapter 6.

Chapter 8 Contains suggestions for further work.

2

THEORETICAL BACKGROUND

2.1 Floating wind turbine concepts

Floating offshore wind turbine designs can roughly be categorized into three different types - buoyancy stabilized design, mooring stabilized design and ballast stabilized design (UZUNOGLU et al. 2016). In practice, a FOWT design is often a combination of these main types of design. This section will briefly explain these three different concepts. An illustration of the different types of designs together with some examples of real life designs can be seen in Figure 2.1.

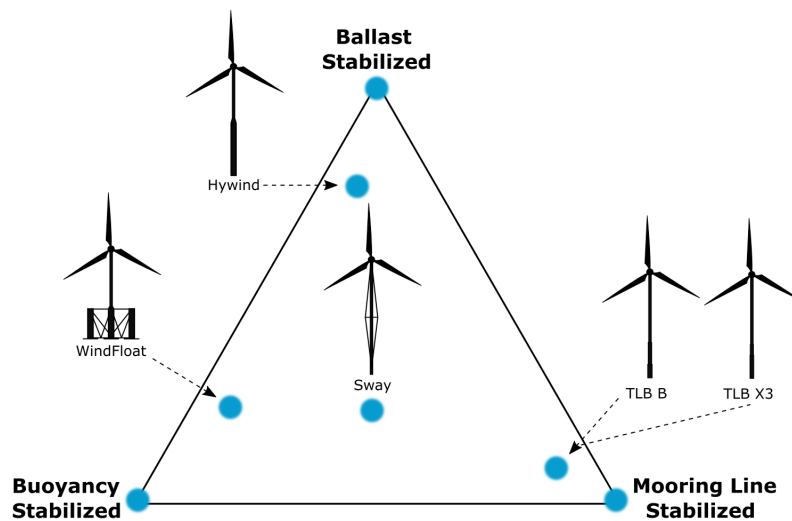


FIGURE 2.1: FOWT concepts illustration with some selected designs

Source: (BJERKSETER and ÅGOTNES 2013)

2.1.1 Ballast Stabilized Platforms

Spar-buoys are examples of the ballast stabilized concept. The spar-buoy is made up of a long vertical floating cylinder. Heavy ballast is placed towards the bottom part of the floater, hence

the name ballast stabilized. This is shifting the centre of gravity below the centre of buoyancy and this ensures uprighting moment for rotational motions. The heavy ballast also ensures large moment of inertia for the rotational motions. Station keeping is provided by catenary mooring (UZUNOGLU et al. 2016). This can be either anchor chains, steel cables and/or fiber ropes.

Restoring force in heave is provided by the change in buoyancy, so-called hydrostatic stiffness. Since the floater is slender, this change in buoyancy is small, and the spar-type is therefore characterized by small stiffness in heave (UZUNOGLU et al. 2016).

Advantages of the spar-buoy are that hydrodynamic forces and motions are small. The motions are also slow. The shape of the spar is also very simple and this may make the production of these concepts relatively simple and economical. Disadvantages are that large water depth is required both for installation and operation (IRENA 2016).

2.1.2 Buoyancy Stabilized Platforms

Buoyancy stabilized platforms are typically semisubmersibles. Semisubmersibles rely on large second moment of area of the waterplane which implies a lot of hydrostatic stiffness. The main contributions to the second moment of area is typically the outer columns, while the pontoons connecting them provides additional buoyancy. The substructure is kept in position by catenary or taut mooring.

An advantage of semi-submersibles is the installation procedure. The semisubmersible can float with a relatively small draft due to the flexibility in the amount of ballast and the large amount of hydrodynamic stability even with little or no ballast. This means that the structure can be installed and towed out at relatively shallow waters. The semisubmersible can also be operated at lower water depths than e.g. the spar-buoy. Disadvantages of this concept are the relatively large motions, complex fabrication and a tendency for larger material usage (IRENA 2016).

2.1.3 Mooring Stabilized Platform

Mooring Stabilized Platforms are typically TLPs. The stability of this type of structure is provided by mooring lines. These mooring lines are pretensioned, meaning that the floater structure in equilibrium position has an excess of buoyancy. This implies that the mooring lines have a tension force in its equilibrium condition. The TLP has high stiffness in roll-, pitch and heave motion and has a behaviour similar to fixed structures in these modes. This also implies that the natural frequencies in these rigid body modes are relatively high (UZUNOGLU et al. 2016).

The major benefit of the TLP concept is the rigidity provided by the mooring lines which makes motions small. The TLP also has relatively small steel weight and is flexible with respect to water depth. Another benefit is that this concept has a small footprint area compared to e.g. a catenary system. Disadvantages are installation and maintenance complexity (UZUNOGLU et al. 2016). Keeping a TLP stable during transport and installation is a challenge and special purpose vessel may be required (IRENA 2016).

2.2 Rigid body mechanics

A rigid body is defined as a body where no points move relatively to each other (LARSEN et al. 2019, p. 94). Many marine structures such as ships are typically treated as rigid bodies. No structure is infinitely stiff, so modelling a structure as a rigid body will always be an idealisation. The rigid body approximation is however in many cases good.

A rigid floating body has six rigid body modes - three translations and three rotations. This is illustrated in Figure 2.2. The three translational rigid body modes are called surge, sway and heave and are defined as translations in x-, y- and z-direction respectively. The three rotational

rigid body modes are called roll-, pitch- and yaw and are defined as rotations about the x-, y- and z-axis respectively. The motion in surge, sway, heave, roll, pitch and yaw are denoted $\eta_1, \eta_2, \dots, \eta_6$ respectively and they are collected in a motion vector $\boldsymbol{\eta}$ given according to Equation 2.1. The velocity and acceleration vectors are denoted $\dot{\boldsymbol{\eta}}$ and $\ddot{\boldsymbol{\eta}}$.

$$\boldsymbol{\eta} = [\eta_1 \quad \eta_2 \quad \dots \quad \eta_6]^T \quad (2.1)$$

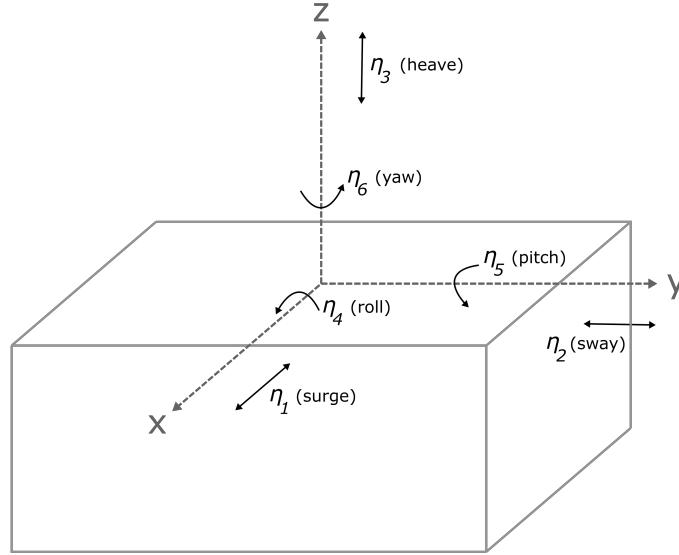


FIGURE 2.2: Freely floating rigid body

When treating a structure as a rigid body, the position on every point on the rigid body is known if the six rigid body motions $\eta_1 \dots \eta_6$ are known. For small motions, the motion of any point \mathbf{s} is given by Equation 2.2, where x, y and z are the coordinates of the point where the motion is obtained (LARSEN et al. 2019, p. 94). Velocity and acceleration are found by taking the derivative and the double derivative respectively.

$$\mathbf{s}(x, y, z) = [\eta_1 \quad \eta_2 \quad \eta_3] + [\eta_4 \quad \eta_5 \quad \eta_6] \times [x \quad y \quad z] \quad (2.2)$$

2.3 Linear potential flow theory

This section covers the basics of linear potential flow theory which is thoroughly explained in several textbooks such as CHAKRABARTI (1987).

When using potential flow theory, the flow velocity is defined as the gradient of a scalar, called the velocity potential ϕ . The flow velocity field can then be given according to Equation 2.3, where u, v and w are the velocity magnitude in x-, y- and z-direction respectively.

$$\mathbf{V} = \mathbf{i} \frac{\partial \phi}{\partial x} + \mathbf{j} \frac{\partial \phi}{\partial y} + \mathbf{k} \frac{\partial \phi}{\partial z} = \mathbf{i}u + \mathbf{j}v + \mathbf{k}w \quad (2.3)$$

The total pressure in the fluid relative to the atmospheric pressure p_a can be expressed according to Bernoulli's equation which is given in Equation 2.4. ρ is the fluid density which is typically 1025 kg/m^3 for seawater, g is the acceleration of gravity and is typically taken as 9.81 m/s^2 , ∇ is the vector differential operator and z is the z -coordinate.

$$p - p_a = -\rho \left(\frac{\partial \phi}{\partial t} + \frac{1}{2} |\nabla \phi|^2 + gz \right) \quad (2.4)$$

According to Bernoulli's equation, the fluid pressure p can be expressed as a function of the velocity potential. This means that the four unknowns u , v , w and p effectively are reduced to one unknown - the velocity potential ϕ , if potential flow theory is used.

Some important assumptions are made in order to fully describe the velocity field with a velocity potential ϕ :

1. Irrotational flow.
2. Inviscid fluid.

In practice, the assumption of incompressible fluid is also often used even though potential flow can be used to describe compressible fluids as well.

Potential flow theory can be both linear and non-linear. When finding the velocity potential, a boundary value problem (BVP) is solved. The perturbation method is typically used where the unknowns are expanded in powers of the wave steepness, which is defined as $\epsilon = k\zeta_a$. k is the wave number and is given by $k = \frac{2\pi}{\lambda}$, where λ is the wave length. The boundary conditions in the BVP are Taylor expanded and the power series is inserted in the boundary conditions. When using linear potential flow theory, only the first order terms are kept, meaning terms that are proportional to ϵ . The superposition principle is now valid for the unknown potential since all the governing equations in the BVP are linear. More in-depth explanations of this BVP linearisation can be found in many books on hydrodynamics such as CHAKRABARTI (1987, p. 244).

2.3.1 Superposition of velocity potentials

Since the superposition principle is valid within linear potential flow theory, the hydrodynamic problem is often divided into two separate sub-problems. These sub-problems are:

- (A) **The diffraction problem.** The forces and moments on the body when the body is fixed in incident regular waves. These loads are called excitation loads and consist of the Froude-Kriloff forces and the diffraction forces.
- (B) **The radiation problem.** The forces and moments on the body when the body is forced to oscillate in initially still water without the presence of waves. The solution of this problem provides the added mass-, damping- and restoring forces and moments.

Solution of the diffraction problem and the radiation problem yields velocity potentials that are superposed in order to get the total velocity potential. This can be expressed in Equation 2.5, where ϕ_D is the diffraction velocity potential and ϕ_R is the radiation velocity potential.

$$\phi = \phi_D + \phi_R \quad (2.5)$$

The diffraction problem

The diffraction velocity potential ϕ_D in Equation 2.5 can be further split into subproblems. The diffraction potential can be expressed according to Equation 2.6. ϕ_0 is the incident wave velocity potential and ϕ_τ is the potential of the scattered wave field due to the presence of the body.

$$\phi_D = \phi_0 + \phi_\tau \quad (2.6)$$

The radiation problem

The radiation velocity potential can also be split into subproblems. The radiation potential can be expressed according to Equation 2.7. ϕ_j is the radiation velocity potential for the j^{th} rigid body motion. The velocity potentials ϕ_j , $j = 1, 2, \dots, 6$ in Equation 2.7 are typically found using numerical panel methods.

$$\phi_R = \sum_{j=1}^6 \phi_j \quad (2.7)$$

2.3.2 Panel methods - solution of the potential flow problem

Panel methods are numerical methods for obtaining the radiation and diffraction potential flow generated in the vicinity of bodies with arbitrary shape (CHAKRABARTI 2005, p. 160). Panel methods are the most common techniques used to analyze the linear steady state response of large-volume structures in regular waves (FALTINSEN 1993, p. 102). Panel methods are also well established for the second-order potential flow problem (CHAKRABARTI 2005, p. 161). The first numerical panel method solution for potential flow around an arbitrary body moving in an infinite fluid was developed by HESS and SMITH (1962).

Panel methods are also commonly called boundary element methods (BEM) and there exist multiple different types of panel methods (FALTINSEN 1993, p. 102). Common for all panel methods is that they transform the the three-dimensional Laplace equation over the whole fluid volume, into a surface integral equation over the solution domain boundaries using Green's theorem. The integral is solved numerically by dividing the boundary, such as a e.g. the submerged part of a semisubmersible, into small elements. These elements typically consist of potential sources, sinks, dipoles or a combination, and each element has to fulfill the Laplace equation with appropriate boundary conditions. This results in a set of integral equations from which the individual velocity potentials are found (JOURNEE and MASSIE 2000). The total velocity potential will then be the superposition of these velocity potentials.

Panel methods are based on potential flow theory and the methods are therefore consistent with the assumptions and simplifications that potential flow theory uses. This means that the theory will not yield satisfactorily results when viscous effects are important. The effect of flow separation is not taken into account and the method is therefore not applicable to structures such as risers or tethers. The method can only predict wave radiation damping, so panel methods will give inaccurate results for cases with a large amount of viscous damping such as rolling motions of a ship (FALTINSEN 1993, p. 102).

2.4 Hydrodynamic loads on FOWTs

A typical procedure for evaluating the hydrodynamic loads on large marine structures is to find excitation forces and radiation forces from linear potential flow theory and subsequently add non-linear excitation forces such as drag forces from the Morison equation if these are of importance. The hydrodynamic loads from linear potential flow theory is covered in detail by CHAKRABARTI (1987).

When finding the hydrodynamic loads given from linear potential flow theory, the diffraction and radiation velocity potentials are first found with panel methods, as described in Section 2.3.2. The hydrodynamic loads are then found by integrating the fluid pressure over the mean wetted body surface. The fluid pressure is given by Bernoulli's equation.

2.4.1 Hydrodynamic pressure loads from Bernoulli's equation

The total pressure forces on a submerged body can be found by integrating the pressure given by Bernoulli over the instantaneous wetted body surface, S_B . Bernoulli's equation was introduced in Equation 2.4 and the total pressure is seen to consist of three terms. These are:

1. $-\rho \frac{\partial \phi}{\partial t}$, the dynamic fluid pressure.
2. $-\rho \frac{1}{2} |\nabla \phi|^2$, quadratic pressure that contributes to second-order forces.
3. $-\rho g z$, hydrostatic pressure, providing hydrostatic buoyancy and restoring forces.

When integrating the hydrodynamic pressure given by Bernoulli in linear wave theory, the second order term in Bernoulli is neglected and pressure is integrated over the mean wetted surface of the submerged body in order to be consistent with the linearisation used in the BVP.

2.4.2 Hydrodynamic loads in linear potential flow theory

Excitation loads

The loads resulting from the diffraction problem are called the "Excitation loads". The excitation forces and moments are found from integrating the dynamic diffraction potential pressure over the mean wetted surface, S_{0B} , of the fixed body. This can be expressed according to Equation 2.8 for the forces in surge-, sway- and heave and Equation 2.9 for the roll-, pitch- and yaw moments. \mathbf{n} and \mathbf{r} are the unit normal vector on the structure and the moment arm respectively, at each position along the structure when integrating.

As explained at the start of Section 2.3.1, the diffraction loads can be split into Froude-Kriloff forces and diffraction forces. The Froude-Kriloff forces are found by integrating the undisturbed incident wave potential, while the diffraction loads are the pressure load resulting from the scattered wave potential due to the presence of the body.

$$\begin{aligned} \mathbf{F}_{\text{exc}} &= -\rho \int \int_{S_{0B}} \frac{\partial \phi_D}{\partial t} \mathbf{n} dS_{0B} = \underbrace{-\rho \int \int_{S_{0B}} \frac{\partial \phi_0}{\partial t} \mathbf{n} dS_{0B}}_{\text{Froude-Kriloff force}} - \underbrace{\rho \int \int_{S_{0B}} \frac{\partial \phi_7}{\partial t} \mathbf{n} dS_{0B}}_{\text{Diffraction force}} \quad (2.8) \\ \mathbf{M}_{\text{exc}} &= -\rho \int \int_{S_{0B}} \frac{\partial \phi_D}{\partial t} (\mathbf{r} \times \mathbf{n}) dS_{0B} = \underbrace{-\rho \int \int_{S_{0B}} \frac{\partial \phi_0}{\partial t} (\mathbf{r} \times \mathbf{n}) dS_{0B}}_{\text{Froude-Kriloff moment}} - \underbrace{\rho \int \int_{S_{0B}} \frac{\partial \phi_7}{\partial t} (\mathbf{r} \times \mathbf{n}) dS_{0B}}_{\text{Diffraction moment}} \quad (2.9) \end{aligned}$$

Added mass-, damping- and hydrostatic restoring loads

Added mass-, damping- and restoring loads are loads resulting from the radiation problem in linear potential flow theory. The added mass-, damping- and restoring loads are proportional to the body acceleration, velocity and displacement respectively. This means that the total radiation load in k -direction due to radiation in the j^{th} degree of freedom can be expressed according to Equation 2.10. $A_{k,j}$ will be the added mass force in k -direction due to oscillation in the j^{th} degree of freedom and the same goes for $B_{j,k}$ and $C_{j,k}$. This means that there will be a total of 36 added mass-, damping- and restoring force coefficients.

$$F_{k,j}^{\text{rad}} = -A_{k,j} \ddot{\eta}_j - B_{j,k} \dot{\eta}_j - C_{j,k} \eta_j \quad (2.10)$$

The restoring force is the force resulting from the change in buoyancy on the body when the body translates or rotates in any of its degrees of freedom. Within linear theory, the restoring forces will

be proportional to the body motion. The non-zero stiffness coefficients for a freely floating body which is symmetric around the x-z plane are given in general form according to Equation 2.11 through Equation 2.15 (FALTINSEN 2005, p. 235). These coefficients are found from integrating the hydrostatic pressure over the additional submerged part that is caused by the motion of the body. A_{wp} is the water plane area, V_D is the displaced volume, z_B is the center of buoyancy and z_G is the center of gravity.

$$C_{33} = \rho g A_{wp} \quad (2.11)$$

$$C_{35} = -\rho g \int \int_{A_{wp}} x dx dy \quad (2.12)$$

$$C_{44} = \rho g V_D (z_B - z_G) + \rho g \int \int_{A_{wp}} y^2 dx dy \quad (2.13)$$

$$C_{53} = C_{35} \quad (2.14)$$

$$C_{55} = \rho g V_D (z_B - z_G) + \rho g \int \int_{A_{wp}} x^2 dx dy \quad (2.15)$$

The hydrostatic restoring coefficients represent a static force contribution due to additional buoyancy when the body translates or rotates in any degree of freedom. The hydrostatic stiffness components are therefore frequency independent. This is also clearly seen in the expressions in Equation 2.11 throughout Equation 2.15.

The resulting forces and moments when integrating the linear dynamic radiation pressure over the mean wetted body surface are given in Equation 2.16 and Equation 2.17 respectively, for oscillation in degree of freedom j . ϕ_j is the velocity potential due to an oscillation in degree of freedom j and \mathbf{n} is the unit normal on the structure at every integration point. \mathbf{r} is the moment arm at each position along the structure when integrating. The resulting forces will in general have a phase that is different from the incoming wave. A sinusoid or a cosine with arbitrary phase can always be expressed as a sum of a sine and a cosine with different amplitudes. This implies that these forces can be expressed as one component in phase with the body acceleration and one component in phase with the body velocity. The force component in phase with body acceleration is called the added mass force while the force component in phase with velocity is called the wave radiation damping force.

\mathbf{F}_j will now be a vector containing the force in surge, sway and heave from oscillation in degree of freedom j . \mathbf{M}_j will be a vector containing moments in roll, pitch and yaw from oscillation in degree of freedom j . This means that Equation 2.16 will provide the added mass and wave radiation damping terms A_{1j} , A_{2j} , A_{3j} , B_{1j} , B_{2j} and B_{3j} . Equation 2.17 will provide A_{4j} , A_{5j} , A_{6j} , B_{4j} , B_{5j} and B_{6j} .

$$\mathbf{F}_j^{A,B} = -\rho \int_{S_{0B}} \frac{\partial \phi_j}{\partial t} \mathbf{n} dS_{0B} = - \begin{bmatrix} A_{1j} \\ A_{2j} \\ A_{3j} \end{bmatrix} \ddot{\eta}_j - \begin{bmatrix} B_{1j} \\ B_{2j} \\ B_{3j} \end{bmatrix} \dot{\eta}_j \quad j = 1, 2, 3, 4, 5, 6 \quad (2.16)$$

$$\mathbf{M}_j^{A,B} = -\rho \int_{S_{0B}} \frac{\partial \phi_j}{\partial t} (\mathbf{r} \times \mathbf{n}) dS_{0B} = - \begin{bmatrix} A_{4j} \\ A_{5j} \\ A_{6j} \end{bmatrix} \ddot{\eta}_j - \begin{bmatrix} B_{4j} \\ B_{5j} \\ B_{6j} \end{bmatrix} \dot{\eta}_j \quad j = 1, 2, 3, 4, 5, 6 \quad (2.17)$$

The total wave radiation force can be expressed on matrix form according to Equation 2.18, where \mathbf{A} , \mathbf{B} and \mathbf{C} are (6×6) matrices. The resulting wave radiation matrix \mathbf{F}^{rad} will be of dimension (6×1) . Since added mass and wave radiation damping coefficients are frequency dependent, \mathbf{A} and \mathbf{B} will be written as $\mathbf{A}(\omega)$ and $\mathbf{B}(\omega)$ throughout this thesis.

$$\mathbf{F}^{\text{rad}} = -\mathbf{A}(\omega) \ddot{\boldsymbol{\eta}} - \mathbf{B}(\omega) \dot{\boldsymbol{\eta}} - \mathbf{C} \boldsymbol{\eta} \quad (2.18)$$

2.4.3 The Morison equation

Morison's equation was first introduced by Morison, O'Brien, Johnson and Schaaf in 1950 and gave the excitation force exerted by surface waves on vertical cylindrical, bottom-fixed, rigid piles that extends from the bottom through the free surface (MORISON et al. 1950). The excitation force when using Morison's equation consist of one drag load contribution and one inertia load contribution that are added linearly together. Morison's equation is typically used for small structures relative to the water wave length (CHAKRABARTI 1987, p. 168).

The original Morison equation presented by MORISON et al. (1950) can be modified in the case of a moving vertical cylinder in current. The horizontal hydrodynamic force on a cylinder strip of length dz is then given according to Equation 2.19 (CHAKRABARTI 1987, p. 189). u and a_1 are the horizontal undisturbed fluid velocity and acceleration at the midpoint of the strip, u_c is the current velocity, C_M and C_D are the empirical mass and drag coefficients, D is the cylinder diameter, ρ is the density of sea water and $\dot{\eta}_1$ is the body motion.

$$dF = \underbrace{\frac{1}{2}\rho C_D D dz (u_c + u - \dot{\eta}_1) |u_c + u - \dot{\eta}_1|}_{\text{Drag load, } F_D} + \underbrace{\rho C_M \frac{\pi D^2}{4} dz a_1 - \rho (C_M - 1) \frac{\pi D^2}{4} dz \dot{\eta}_1}_{\text{Inertial load, } F_I} \quad (2.19)$$

The Morison equation is not restricted to circular members and can be used for slender members with different cross sections and orientation. C_M and C_D are different for different cross sections and they are also a function of several other parameters effecting the flow, such as surface roughness and Reynolds number. Values for C_M and C_D for different cross sections and fluid regimes, relevant for offshore structures, are given in multiple books such as CHAKRABARTI (1987) and FALTINSEN (1993).

The inertial load term in Morison's equation is covered by the potential flow theory, but not the drag term. A normal approach when handling hydrodynamic loads when drag loads are of importance is therefore to use linear potential flow theory and subsequently add the drag load term from Morison's equation.

2.5 Aerodynamic loads on FOWTs

Aerodynamic loads are important to take into consideration for offshore wind turbines. Integrating aerodynamic loads on the blade over the whole rotor gives a thrust force and torque that is important for motions and structural response. The thrust force will lead to significant surge- and pitch motions while torque contributes most to roll motion. Inhomogenous flow fields over the blades and wind forces flowing in at an angle will also cause additional motions in sway, yaw, pitch and roll (SVENDSEN 2016).

Another important aspect that is important to be aware of in the design of FOWTs is the so-called 1-p and 3-p frequencies which are the rotational rotor frequency and blade-passing frequency respectively (SVENDSEN 2016). It is important when designing FOWTs that natural frequencies are outside these excitation frequencies.

2.5.1 The Blade element momentum (BEM) model

The Blade element momentum (BEM) theory is one out of many methods for computation of aerodynamic loads on wind turbine blades. The blade element momentum theory is used in many computer codes such as Sima (SINTEF OCEAN 2022a, p. 113).

The BEM method uses a combination of momentum theory for an ideal turbine with wake rotation, and foil theory. In the momentum theory, the wind field is modelled as a streamtube, and thrust-

and torque contributions from annular infinitesimal elements are integrated over the turbine rotor area. This theory is covered in detail by MANWELL et al. (2009) and BURTON et al. (2011).

The momentum theory is highly idealized and several corrections are used in order to have a realistic model for aerodynamic loads on a wind turbine. The corrections used in Sima are (SINTEF OCEAN 2022a, p. 114):

1. **Prandtl correction.** Takes into account air flowing around the tip of the turbine blade from the lower to upper sides. This leads to aerodynamic losses.
2. **Glauert correction.** Is a correction factor which extends the theory for induction factors greater than 0.5, where the BEM theory is not valid.
3. **Dynamic inflow/wake.** Takes into account that the flow field around the turbine blades takes some time to react to changes.
4. **Dynamic stall.** Takes sudden attachment and re-attachment of flow into account.
5. **Skewed inflow.** Takes rotor tilt or a yaw angle between the rotor and incoming wind into account.

More theory on these corrections is found in multiple sources such as M. O. HANSEN (2015) and SINTEF OCEAN (2022a).

2.5.2 Other important aerodynamic considerations

In addition to aerodynamic loads on the turbine rotor, several other aerodynamic effects are important to take into account. One of these is drag forces on the tower. Drag forces are occurring due to skin friction from the wind on the tower and pressure loss due to flow separation, and will in some cases be important to take into consideration (SVENDSEN 2016).

Another important consideration to take into account is the concept of "tower shadow". Tower shadow is a term used in order to describe the influence of the tower on the incoming wind. The tower will influence the wind upstream of the turbine in the same way as a pile in a water stream will influence the flow upstream. As each blade passes through a region of modified flow, a thrust variation will occur. This will happen at the 3-p frequency and this effect can lead to fatigue damage or resonance effects. For upwind turbines, a potential flow model can be used to model tower shadow (BACHYNSKI-POLIĆ 2021a). This is used in Sima (SINTEF OCEAN 2022a).

2.6 Wind turbine controller theory

A wind turbine controller is required to ensure that the turbine operates as intended. The job of the wind turbine controller can be split into two (BURTON et al. 2011):

- (A) **Supervisory control.** The supervisory control switches between operational states of the wind turbine such as:
 - Standby
 - Start-up
 - Power production
 - Shut-down
 - Stopped with fault
- (B) **Operational control.** The operational control is used during normal operation and consist of.

- Blade pitch regulation.
- Generator torque regulation
- Yaw motors regulation.

There are several objectives for a control system. The controller in many cases seeks to maximize the energy capture as well as ensuring power quality control. Among others, the controller also ensures drive-train load alleviation and avoidance of enhancing structural loads (BACHYNSKI-POLIĆ 2021c).

The typical operating regions for a variable speed, variable pitch wind turbine can be seen in Figure 2.3. In region I, the wind turbine is not operational. This is because the possible power output is so low that it is not worth producing power. Power producing in region I would only cause unnecessary fatigue damage etc. on the turbine and the rest of the structure.

In region II, the turbine starts producing power. This happens at the cut-in speed. The goal in region II is to maximize the power output. The rotor speed is then seen to be non-zero and is increasing as the incoming wind speed is increasing. The same can be said about the captured power. Both the available power in wind and the power captured are proportional to the wind speed cubed, but the power captured curve is lower. The reason for this is that it is impossible to extract all the theoretical available power in wind due to aerodynamic losses such as tip losses on the blades and dynamic stall. There will also be some losses in the energy conversion from rotational energy of the rotor to electrical energy from the generator.

In region III, the turbine has reached its rated power. This happens at the rated speed. The rated power is the maximum power output that the wind turbine is designed for and larger power output is therefore not wanted. The pitch controller is used actively above the rated wind speed in an effort to keep the power output at the rated power. In the case of extreme weather and sufficiently large incoming wind, the turbine shuts down in order to preserve the integrity of the structure. This wind speed is known as the cut-out speed. The turbine is then in idling condition.

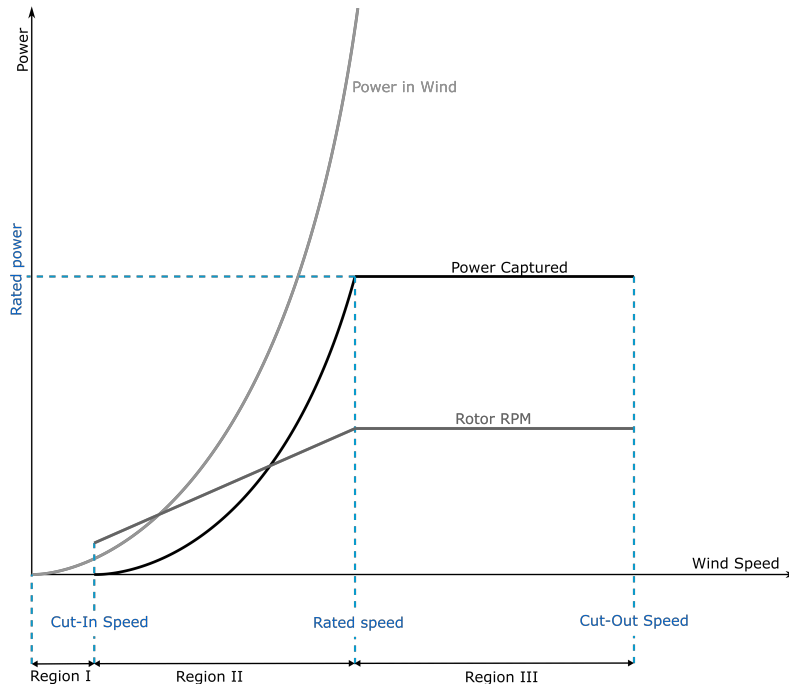


FIGURE 2.3: Power curve for a variable speed, variable pitch wind turbine

Source: (BACHYNSKI-POLIĆ and GAO 2021)

2.7 Hydro-aero-servo-elastic coupling

For a model of a FOWT to give realistic results it must take into account the coupling between hydrodynamic loads, aerodynamic loads, controller theory and elasticity.

For an elastic body, hydrodynamic loads will cause an elastic deformation. This will again change the load on the structure, meaning that there is a dependency between the load and the structural response. A structural model coupled with a hydrodynamic load model is called a hydro-elastic model. The same dependency will occur between aerodynamic loads and structural response for an elastic structure. A structural model coupled with an aerodynamic model is called an aero-elastic model. If an aerodynamic model, a hydrodynamic model, a structural model and a controller theory are combined we have a hydro-aero-servo-elastic model that takes the dependency of all these effects into account (SVENDSEN 2016). Sima is a software developed by DNV that uses hydro-aero-servo-elastic analyses. Sima is explained in further detail in Section 4.6.

2.8 Equation of motion for a floating body

The equation of motion for a freely floating body is given according to Newton's 2nd law. If the equation of motion only contains linear terms, calculations in frequency domain can be done. This reduces the computational cost dramatically. If nonlinear terms are needed in the equation of motion, a time stepping procedure has to be carried out.

2.8.1 Equation of motion according to linear potential flow theory

Section 2.4.2 introduced the wave loads given from linear potential flow theory. In many engineering problems, the hydrodynamic loads from linear potential flow theory is sufficient to yield useful results for a floating structure (CHAKRABARTI 1987, p. 329). The dynamic equilibrium equation of a freely floating rigid body six degrees of freedom system can be expressed according to Equation 2.20 when using linear potential flow theory.

$$[\mathbf{M} + \mathbf{A}(\omega)] \ddot{\boldsymbol{\eta}} + \mathbf{B}(\omega) \dot{\boldsymbol{\eta}} + \mathbf{C}\boldsymbol{\eta} = \mathbf{F}_{\text{exc}}(\omega) \quad (2.20)$$

The displacement response amplitude operator (RAO) is defined as the complex amplitude of the body motion in response to an incident wave of unit amplitude (NEWMAN 2018, p. 321). The modulus of the RAO gives the amplitude of response while the argument of the RAO gives the phase angle of the response relative to the excitation force.

The response amplitude operator can be found under the assumption of linear wave theory. The dynamic equilibrium equation will then be linear and the excitation loads from regular waves will be harmonic and proportional to the wave amplitude.

When expressing the RAO it is convenient to solve the dynamic equilibrium equation on complex form. The excitation load and response in all six degrees of freedom can be expressed in matrix form according to Equation 2.21 and Equation 2.22 respectively. $\tilde{\mathbf{F}}_{\text{exc}}$ is the complex excitation force per unit wave amplitude and $\tilde{\boldsymbol{\eta}}$ is the complex response. $\mathbf{F}_{\mathbf{0},\text{exc}}$ is the excitation force amplitude array and $\boldsymbol{\eta}_{\mathbf{0}}$ is the motion response amplitude array. These are arrays of dimension (6×1) . α is the phase angle of the excitation force and β is the phase angle of the motion response relative to the excitation force.

$$\mathbf{F}_{\text{exc}}(t) = \Re(\tilde{\mathbf{F}}_{\text{exc}} \zeta_a e^{i\omega t}) = |\tilde{\mathbf{F}}_{\text{exc}}| \zeta_a \cos(\omega t + \arg(\tilde{\mathbf{F}})) = \mathbf{F}_{\mathbf{0},\text{exc}} \cos(\omega t + \alpha) \quad (2.21)$$

$$\boldsymbol{\eta}(t) = \Re(\tilde{\boldsymbol{\eta}} e^{i(\omega t + \alpha)}) = |\tilde{\boldsymbol{\eta}}| \cos(\omega t + \alpha + \arg(\tilde{\boldsymbol{\eta}})) = \boldsymbol{\eta}_{\mathbf{0}} \cos(\omega t + \alpha + \beta) \quad (2.22)$$

The resulting complex amplitude body motion per wave amplitude, the RAO, is found by inserting Equation 2.21 and Equation 2.22 into the dynamic equilibrium equation. This resulting RAO will be of dimension (6×1) - one RAO per rigid body motion.

$$\mathbf{RAO}(\omega) = \frac{\tilde{\eta}}{\zeta_a} = [-\omega^2 (\mathbf{M} + \mathbf{A}(\omega)) + i\omega\mathbf{B}(\omega) + \mathbf{K}]^{-1} \tilde{\mathbf{F}}_{\text{exc}}(\omega) \quad (2.23)$$

The steady state response will be harmonic with the same frequency as the excitation, and proportional to the wave amplitude. The steady state response amplitude can then be found by multiplying the modulus of the RAO with the wave amplitude, while the phase is found from the argument of the RAO. The response amplitude operator is only a function of frequency. This means that the total response can be found based on one calculation with the excitation frequency ω as input. This is called frequency domain calculation.

Also other responses than the motion will, when using linear wave theory, be proportional to the wave amplitude. Responses normalized on the wave amplitude are typically called transfer functions and are frequently used in ocean engineering.

It is also important to mention that the equation of motion in Equation 2.20 can be extended with more terms, but the same considerations only holds if these terms are linear. In many cases nonlinear loads such as drag loads are linearised to make frequency domain analysis possible.

2.8.2 Equation of motion with nonlinearities

In many cases, a rigid body can not be accurately described with the assumptions introduced in linear wave theory due to nonlinearities. Examples are nonlinear drag loads, nonlinear viscous damping, nonlinear mooring line force (CHAKRABARTI 1987, p. 330), and nonlinear aerodynamic loads. These nonlinearities therefore have to be used in the equation of motion in addition to the loads from the linear wave theory.

Computations in frequency domain are not possible in the case of nonlinearities unless they are replaced by linear approximations. Direct time-integration scheme with the equation of motion then has to be used such as the constant average acceleration method (CHAKRABARTI 1987, p. 330). The governing rigid-body time domain equation of motion in these cases is called the Cummins equation and is given according to Equation 2.24 (CUMMINS et al. 1962).

$$(\mathbf{M} + \mathbf{A}_\infty)\ddot{\mathbf{x}} + \mathbf{D}_1\dot{\mathbf{x}} + \mathbf{K}\mathbf{x} + \int_0^t \mathbf{h}(t - \tau)\dot{\mathbf{x}}(\tau)d\tau = \mathbf{q}(t, \mathbf{x}, \dot{\mathbf{x}}, \ddot{\mathbf{x}}) \quad (2.24)$$

\mathbf{A}_∞ is the infinite-frequency added mass matrix, \mathbf{D}_1 is the linear viscous damping matrix, \mathbf{q} is the external load vector and \mathbf{h} is a vector of so-called retardation functions.

The retardation function is used in time domain in order to take frequency dependent added mass and damping into account. This retardation function is calculated from frequency-dependent added mass or potential damping coefficients and is used in a convolution term in the time domain equation of motion. This convolution term represents the memory effect in the wave radiation forces, meaning that the pressure field around the body will take some time to die out even after the body has stopped oscillating.

2.9 Statistical description of sea

Waves are treated with statistics in marine engineering. The properties of waves are typically assumed to be stationary for a period typically lasting a few hours, where three hours is a normal choice. The sea surface is modelled as a sum of an infinite number of harmonics with different

frequencies and random phase angles, where the phase angles are given from a normal distribution. The resulting sea surface elevation when modelled in this way will follow a Gaussian distribution.

2.9.1 Wave spectrum

A sea state is typically described by a variance wave spectrum $S(\omega)$. The wave spectrum represents the distribution of wave energy over the frequencies of wave components. If Gaussian sea surface elevation and stationarity is assumed, then all statistical characteristics are determined by the wave spectrum (HOLTHUIJSEN 2007, p. 36).

A wave spectrum is typically given as a function of H_s and T_p . T_p is the period corresponding to the peak of the spectrum and H_s is the significant wave height. The significant wave height is by definition the mean of the 1/3 largest waves in the sea state (HOLTHUIJSEN 2007, p. 28).

The statistical properties of the wave elevation can be expressed in terms of the spectral moments, which are given according to Equation 2.25. m_n is called the ' n^{th} -order moment' (HOLTHUIJSEN 2007, p. 57).

$$m_n = \int_0^{\infty} f^n S(f) df \quad (2.25)$$

There exist several wave spectra used for the treatment of waves. Examples are the Pierson-Moskowitz spectrum, Jonswap spectrum, Gamma spectrum, ISSC spectrum, Ochi-Hubble spectrum and Torsethaugen spectrum (DNV 2022b).

The Jonswap (JOint North Sea WAve Project) spectrum was developed in a international project as an effort to standardize wave spectra for the Southeast part of the Nort Sea (K. HASSELMANN et al. 1973; WAFO GROUP 2022). The Jonswap spectrum can be given in general form according to Equation 2.26 (SINTEF OCEAN 2022b; WAFO GROUP 2022).

$$S_{\zeta}(\omega) = \frac{\alpha g^2}{\omega^5} \exp\left(-\beta \left(\frac{\omega_p}{\omega}\right)^4\right) \gamma^{\exp\left(\frac{(\omega/\omega_p-1)^2}{2\sigma^2}\right)} \quad (2.26)$$

α , γ , β and σ are called the spectral-, peakedness-, form- and spectral parameters respectively. α and γ may typically be expressed as a function of H_s and T_p , while β and σ are typically taken as constants.

A more detailed elaboration on the Jonswap spectrum together with values and expressions for α , γ , β and σ can be found in multiple resources such as SINTEF OCEAN (2022b), WAFO GROUP (2022) and K. HASSELMANN et al. (1973) to mention a few.

2.9.2 Response spectrum

Any random process derived from a Gaussian process will also be a Gaussian process if the relationship is linear (HOFFMAN and KARST 1975). This is applicable for linear wave theory since the wave elevation is assumed to be Gaussian. One important consequence of this is that is possible to transform the input wave elevation spectrum to the spectrum for other responses. Such output variables might be cross sectional forces or motions.

The transformation between the spectra involves the transfer function (HOLTHUIJSEN 2007, p. 52). The transfer function for motions (typically called the RAO) was derived for a linear system in Section 2.8, but the same principle applies to other variables as well.

The input-output spectrum relation as given by NEWLAND (2012, p. 72) is seen in Equation 2.27.

$$S_y(\omega) = |H_{yx}(\omega)|^2 S_x(\omega) \quad (2.27)$$

As explained in Section 2.9.1, all short term statistical properties of the wave elevation are given by the wave spectrum $S(\omega)$. The same logic applies for the spectrum of other quantities such as cross sectional loads, meaning that statistical quantities of these response variables can be calculated from spectral moments.

2.9.3 Response maxima

The Rice distribution was first introduced by RICE (1944, 1945) and gives the distribution of maxima from a normally distributed process. The Rice distribution can be used for the response maxima in a short term seastate within linear wave theory.

$$F_{X_{\max}}(x) = \Phi\left(\frac{x}{\epsilon\sigma_x}\right) - \sqrt{1-\epsilon^2}\Phi\left(\frac{1-\epsilon^2}{\epsilon}\frac{x}{\sigma_x}\right)e^{-\frac{1}{2}\left(\frac{x}{\sigma_x}\right)^2} \quad (2.28)$$

σ_x is the standard deviation of the process. ϵ is the spectral width parameter which is given according to Equation 2.29.

$$\epsilon = \left[1 - \frac{m_2^2}{m_0 m_4}\right]^{1/2} \quad (2.29)$$

If we have a perfectly narrow banded process, $\epsilon = 0$, and Equation 2.28 reduces to the Rayleigh distribution

$$F_s(x) = 1 - e^{-\left(\frac{x^2}{2\sigma_x^2}\right)} \quad (2.30)$$

It can be deduced that the most probable largest response X_{\max} occurring within a time interval can be approximated according to Equation 2.31 if the initial maxima distribution is a Rice distribution.

$$X_{\max} = \sqrt{2}\sigma_x \left[\ln\left(\sqrt{1-\epsilon^2}N_c\right)\right]^{1/2} \quad (2.31)$$

Equation 2.31 reduces to Equation 2.32 if the process is perfectly narrow banded, i.e. $\epsilon = 0$.

$$X_{\max} = \sqrt{2}\sigma_x \sqrt{\ln N_s} \quad (2.32)$$

N_c is the number of response maxima. N_c is equal to the number of zero-upcrossings N_s if the process is perfectly narrow banded. The number of zero-upcrossings can be calculated as

$$N_s = \frac{D_s}{T_x} \quad (2.33)$$

D_s is the duration of the short term seastate and T_x is the mean-zero-upcrossing period.

DEWAR and H. C. LONGUET-HIGGINS (1952) have derived an asymptotic expression for the expected value of X_{\max} , denoted \bar{X}_{\max} , as N_c increases. This expression is given in Equation 2.34. The expression is given under the assumption of a perfectly narrow banded process, i.e. the initial distribution of maxima is a Rayleigh distribution (CARTWRIGHT and M. S. LONGUET-HIGGINS 1956). DEWAR and H. C. LONGUET-HIGGINS (1952) also showed that this expression is accurate within 3% if N_c is greater than 50. σ_X is the standard deviation of the response variable X , which can be estimated as the 0th moment of the spectrum of X .

$$\bar{X}_{\max} = \sigma_X \left[\sqrt{2 \ln N_c} + \frac{0.57722}{\sqrt{2 \ln N_c}} \right] \quad (2.34)$$

2.10 Limit state design

The concepts of load effects and resistance are important in limit state design. Load effect is the structural response to external loads acting on the structure, while the load capacity is the load level that the structure can withstand. Partial safety factors are also applied to the load effects and capacities in order to account for uncertainties, e.g. in material properties.

A limit state is defined as a condition beyond which the structure no longer fulfills its design criteria (BRITISH STANDARD et al. 2002). The basic principle of limit state design is to ascertain that the structure does not reach any of its limit states. Four types of limit states are typically considered (PAIK and THAYAMBALLI 2003, p. 2):

- Serviceability limit state (SLS)
- Ultimate limit state (ULS)
- Fatigue limit state (FLS)
- Accidental limit state (ALS)

SLS represents failure states for normal operations due to causes such as large vibrations, damage caused by corrosion, unacceptable deformations which effects the use of structural elements and/or equipment, noise etc (PAIK and THAYAMBALLI 2003, p. 2).

ULS typically represents collapse of the structure due to causes such as insufficient structural capacity, insufficient stability or loss of equilibrium (PAIK and THAYAMBALLI 2003, p. 3).

FLS represents loss of structural integrity of the structure due to accumulated damage under repeated cyclic loading. In most cases, FLS represents uncontrolled crack propagation due to cyclic loading (PAIK and THAYAMBALLI 2003, p. 3).

ALS represents excessive structural damage due to accidents. Examples of accidents can be ship collisions, explosions and fire.

2.11 The Fast Fourier Transform algorithm

The basic idea behind the Fourier transform is that a piecewise continuous and integrable function f can be represented as a superposition of sinusoidal oscillations of all possible frequencies (KREYSZIG 2006, p. 520). The Fourier transform can be used to find the frequency composition in a function f . The harmonics making up the function f are called Fourier components. The frequency composition of a function is typically presented in a frequency spectrum.

The Fourier transform also has an inverse called the inverse Fourier transform. The Fourier transform and the inverse Fourier transform are given according to Equation 2.35 and Equation 2.36 respectively. The Fourier transform operator and inverse Fourier transform operator are commonly written as \mathcal{F} and \mathcal{F}^{-1} respectively, and the Fourier transform of the function f is commonly written as \hat{f} . The Fourier transform maps the input function $f(t)$ to another function $\hat{f}(\omega)$ that is a function of frequency and the Fourier transform is therefore commonly called the frequency domain representation of $f(t)$, while $f(t)$ is called the time domain representation.

$$\mathcal{F}(f(x)) = \hat{f}(\omega) = \frac{1}{\sqrt{2\pi}} \int_{-\infty}^{\infty} f(x)e^{-i\omega x} dx \quad (2.35)$$

$$\mathcal{F}^{-1}(\hat{f}(\omega)) = f(x) = \frac{1}{\sqrt{2\pi}} \int_{-\infty}^{\infty} \hat{f}(\omega)e^{i\omega x} d\omega \quad (2.36)$$

If the waveform is sampled, the discrete version of the Fourier transform - the discrete Fourier transform (DFT), has to be used (COCHRAN et al. 1967). The DFT and the inverse DFT are defined according to Equation 2.37 and Equation 2.38 respectively (KREYSZIG 2006, p. 525). $f(x_r)$ is the value of sample r and N is the total number of sample points. The Fourier transform is here a function of k which is related to frequency as $f = \frac{k f_s}{N}$. The frequency resolution from FFT is therefore $f_s \cdot \frac{1}{N}$.

$$\hat{f}(k) = \sum_{r=0}^{N-1} f(x_r) e^{-i(2\pi kr/N)} \quad k = 0, \dots, N-1 \quad (2.37)$$

$$f(x_r) = \sum_{k=0}^{N-1} \hat{f}(k) e^{-i(2\pi kr/N)} \quad r = 0, \dots, N-1 \quad (2.38)$$

The fast Fourier transform (FFT) is an algorithm to calculate the DFT which is much faster than the direct approach (NEWLAND 2012, p. 150). The FFT is an efficient algorithm for calculating the DFT of a series of data samples which was first presented by COOLEY and TUKEY (1965). The FFT facilitates signal analysis and filter simulation by means of digital computers and greatly reduced the computational cost of calculating the DFT compared to algorithms that previously existed (COCHRAN et al. 1967).

It can be shown that the largest possible frequency that can be analysed with the discrete Fourier transform is equal to one half of the sampling ratio, $f_s/2$. This frequency is called the Nyquist frequency (NEWLAND 2012, p. 120).

2.12 Computer software

A large part of the work done in this study was centered around use of the software suite Sesam which is a Software package for marine applications developed by DNV. This section will give a brief introduction to the most used software tools and their capabilities. The different software user manuals should be read for more details.

GeniE A software tool for concept design and analysis of offshore structures. GeniE can be used for modelling beams, stiffened plates and shells. Explicit loads can be applied as point-, line-, surface- and wind loads with automatic load transfer. After the model has been generated, the model can be transferred to other DNV software such as Sestra for structural analysis or Wadam for hydrodynamic analysis. The DNV software tools Sestra, Wajac and Splice are directly integrated in GeniE and general result representation together with code checking of members and tubular joints can be carried out (DNV 2022c).

HydroD A software used for hydrodynamic and hydrostatic analysis. The hydrostatic analysis and environment modelling is done directly by HydroD. This can typically be stability analysis, maximum KG analysis and strength analysis. Hydrodynamic stability analysis is done by running the linear frequency domain software Wadam or the non-linear time domain software Wasim in the background (DNV 2022c).

Wadam Analysis program for calculation of wave-structure interaction for fixed and floating structures of arbitrary shape (DNV 2022c). Wadam performs hydrodynamic analysis in the frequency domain. Wadam has the possibility to include several second order effects such a sum frequency loads, difference frequency loads, drift forces, wave drift damping coefficients steady drift forces, second-order rigid body motions and second-order free surface elevations. Wadam can also include Morison loads and the effect of small current or forward speed. Results are presented as complex transfer functions (DNV 2022c).

Wadam uses panel methods as explained in Section 2.3.2. Wadam typically uses a Green's function based panel model. The elementary solution in this panel method satisfies the free surface boundary. This is in opposition to a Rankine panel method, that is used by Wasim. This means that the integral equation to be solved only has unknowns on the hull. As a consequence, only the hull needs to be discretized into elements when using this type of panel method.

Wasim Analysis program for wave-structure interaction for fixed and floating structures. Wasim is based on time domain potential theory, but can also perform frequency domain calculations by the use of Fourier transform. Wasim has the possibility to account for drag effects with the use of the Morison formulation and can handle forward speeds as long as the vessel is not planing. Wasim can also include several non-linear effects such as hydrostatic and Froude-Krylov pressure on exact wetted surface, exact treatment of inertia and gravity, quadratic Bernoulli terms, Quadratic roll and pitch damping and non-linear waves (DNV 2022c,e).

Wasim uses a Rankine panel method. The elementary solution in the Rankine panel method does not satisfy the free surface condition, and as a consequence, the integral equation to be solved will have unknowns on both the hull and the free surface. This means that both the hull and free surface have to be discretized into elements. The equation system to be solved is therefore larger and more computationally demanding. A benefit to Rankine panel methods is that different free surface conditions can be handled since the free surface condition is not in the elementary solution directly (DNV 2022e).

Cross sectional loads are found in Wasim using so-called "LoadCrossSections" in HydroD. Cross sectional loads in a load cross section are found by integrating the forces on the model contributing to the reaction forces in the section. Wasim always integrates loads from $+\infty$ for both x -, y - and z axis. The loads from a load cross section is given in a body fixed coordinate system with user specified origo.

Sima Software tool for simulation of marine operations, mooring analyses and floating offshore wind turbines. Sima uses coupled aero-hydro-servo-elastic analyses and can also include several nonlinear effects such as drag forces-, aerodynamic loads and nonlinear restoring. Calculations are therefore carried out in time-domain (DNV 2022c).

Sima can model physical problems with great detail. Environment modelling includes current and wind profiles, wave and wind spectra, several seafloor properties and location specific data to mention a few. Floating structures can be modelled with added mass and potential damping, 1st and 2nd order wave excitation and additional viscous force elements can also be included to capture Morison forces. Sima calculates retardation functions from added mass and damping which are needed in order to take frequency-dependent added mass and damping into account when doing calculations in time-domain.

Sima combines the software tools Riflex and Simo. Riflex is a non-linear finite element software for slender marine structures and Simo is a simulator for marine operations. Both Riflex and Simo have integrated aerodynamics, but for the model used in this investigation, the Riflex implementation was used. The aerodynamic model implemented in Riflex is based on the blade element momentum theory (MANWELL et al. 2010). Dynamic stall and dynamic wake effects are taken into account with the Øye models (M. HANSEN 2015), Glauert's correction is used for high induction factors outside the validity range of the BEM theory and Prandtl's correction is used for hub and tip losses (SILVA DE SOUZA and BACHYNSKI 2020).

Elements in Riflex can either be bar elements or beam elements. The bar element has 6 translational degrees of freedom and is formulated using a total Lagrangian description. The beam element has 3 translational and 3 rotational degrees of freedom and is formulated using the concept of co-rotated reference. More theory on the element formulations in Riflex can be found in SINTEF OCEAN (2022a).

TurbSim Stochastic, full-field, turbulent-wind simulator. TurbSim creates a series of discrete two-dimensional rectangular grids containing windspeed vectors in all three dimensions. Together, these rectangular windspeed grids creates a time series of fully turbulent wind. This is illustrated in Figure 2.4. TurbSim provides several user defined input options for the turbulent wind to generate such as the grid size, number of grid points, reference wind speed and corresponding height, turbulence type, turbulence intensity and turbulence model. These user defined options are defined in a .inp file which is given as input to TurbSim when running the program (JONKMAN and KILCHER 2022). An example of such a input file can be found in the Appendix in Section D.

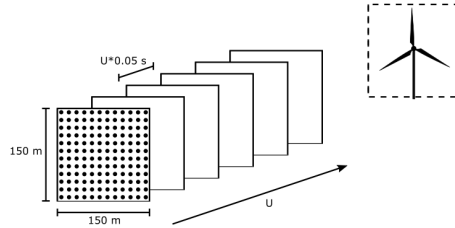


FIGURE 2.4: TurbSim turbulent wind illustration

Source: (BACHYNSKI-POLIĆ 2021b)

TurbSim interpolates the generated windspeed grids in both time and space using Taylor’s frozen turbulence hypothesis. TurbSim can create input files for codes such as Sima, FAST and MSC.ADAMS. TurbSim produces time series by using inverse Fourier transform with velocity components and spatial coherence in frequency domain. These velocity components and the spatial coherence are defined through spectra. This assumes stationarity and as a consequence, TurbSim superimpose coherent turbulent structures onto the stationary time series (JONKMAN and KILCHER 2022).

Xtract Is DNV’s postprocessor for presentation, animation and reporting of results. Results from static and dynamic structural analysis and hydrodynamic analysis can be investigated as well as model properties. The program offers easy user interaction through rotation, zooming and panning (DNV 2021).

Postresp A Postprocessor for Statistical Response Calculations. Postresp can postprocess general responses given as transfer functions and spectra in frequency domain, or time series in time domain. Postresp can also be used as a stand alone program for frequency domain calculations (DNV 2022b).

3

LIFES50+ 10 MW OO-STAR DESIGN

The following chapter presents the design for the 10 MW OO-Star as presented by YU et al. (2018) in the Lifes50+ published report. A selection of drawings personally provided to the author by Dr. techn. Olav Olsen are also included.

The substructure design published by YU et al. (2018) is a slightly simplified version of the actual 10 MW OO-Star substructure used in the Lifes50+ project. More detailed drawings were provided to the author for computer modelling, but these will not be published here due to confidentiality considerations. Some drawings of the 10 MW OO-star design were however handed out by Dr. techn. Olav Olsen to the author with permission to use in this report. These drawings shows additional details in the OO-Star which is not included in Lifes50+, but they have been stripped for many of the measurements. A selection of these are used in this chapter. This includes Figure 3.1, Figure 3.2b, Figure 3.2c and Figure 3.2d. These drawings have been included to give information that is not presented by YU et al. (2018), such as the compartment layout.

An illustration of the 10MW OO-Star with tower and RNA together with the definition of the coordinate system used for the model is seen in Figure 3.1. As seen from the figure, the coordinate system is defined in the middle of the central column at the mean surface level. Zero degree waves and wind are defined as propagating in positive x-direction.

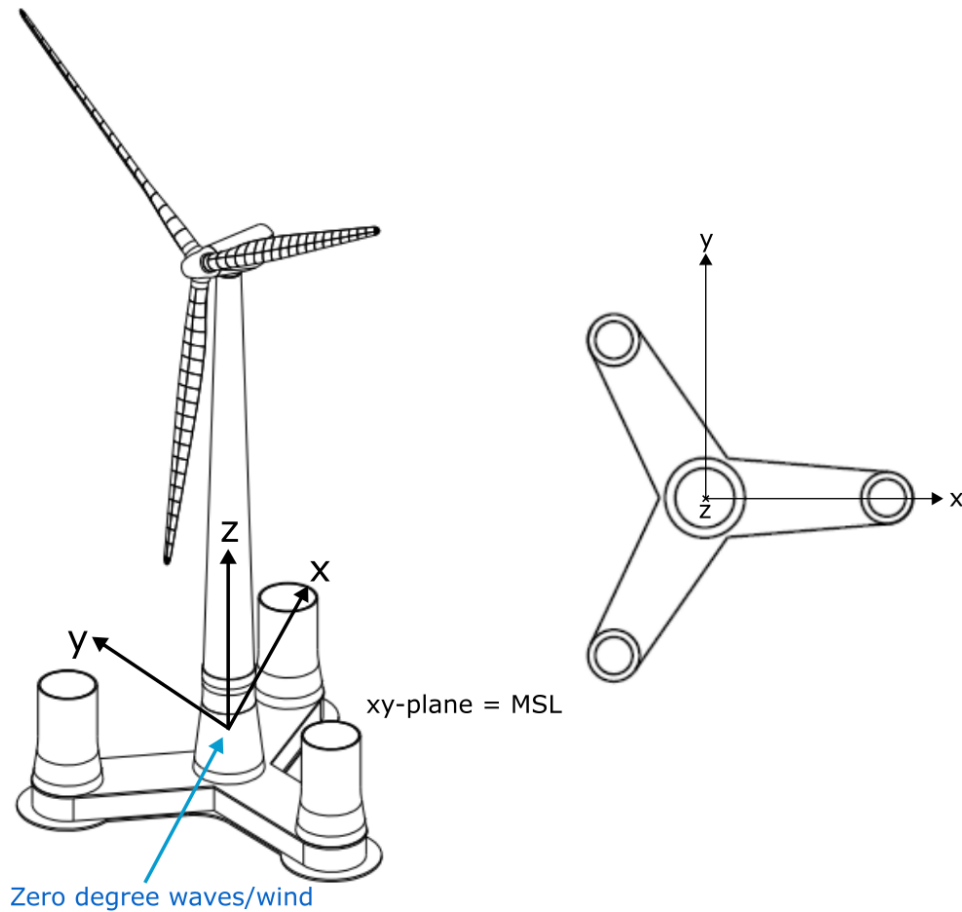


FIGURE 3.1: Lifes50+ 10MW OO-Star with coordinate system definition

3.1 Substructure properties

This section will introduce the OO-Star substructure properties. As stated in the beginning of this chapter, the substructure design published in Lifes50+ is slightly simplified. Detailed drawings of the "true" OO-Star design are included in this section, but these drawings are stripped of details needed to reproduce the exact substructure design. Some of the drawings included in the Lifes50+ report have been deliberately excluded due to inconsistencies between the simplified OO-Star design and the "true" OO-Star design used in this project.

Figure 3.2b shows an illustration of the OO-Star substructure. Figure 3.2a shows some of the main dimensions. The floater consists of a submerged star-shaped pontoon. The structure is made of post-tensioned concrete. Four columns piercing the water are connected to the pontoon - one central column and three outer columns. All the columns consist of both tapered parts and cylindrical parts. The substructure has a bottom slab with heave plates at the keel and an upper slab between the columns and the upper side of the pontoon walls. The draft of the substructure is 22 meters.

The distance between the central column and the outer columns is 37 meters. The width between the pontoon walls is 16 meters at the cross-section closest to the central column and 15.8 meters at the center point of the outer columns. This means that the pontoons are slightly tapered. The height from keel level to the upper side of the pontoon walls is 7 meters.

The central column has a diameter of 16.2 meters at the top slab. The central column diameter is 12.05 meters at the tower base which is 33 meters above the keel. The outer columns have a diameter of 15.8 meters at the top slab. The outer column diameter at the top of the outer column is 15.8 meters. This is at 31.5 meter from keel level.

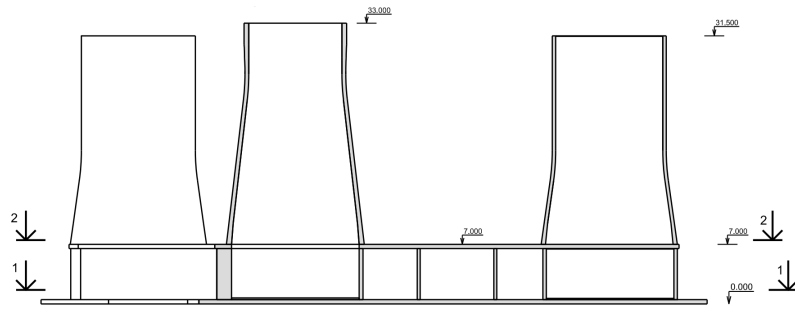
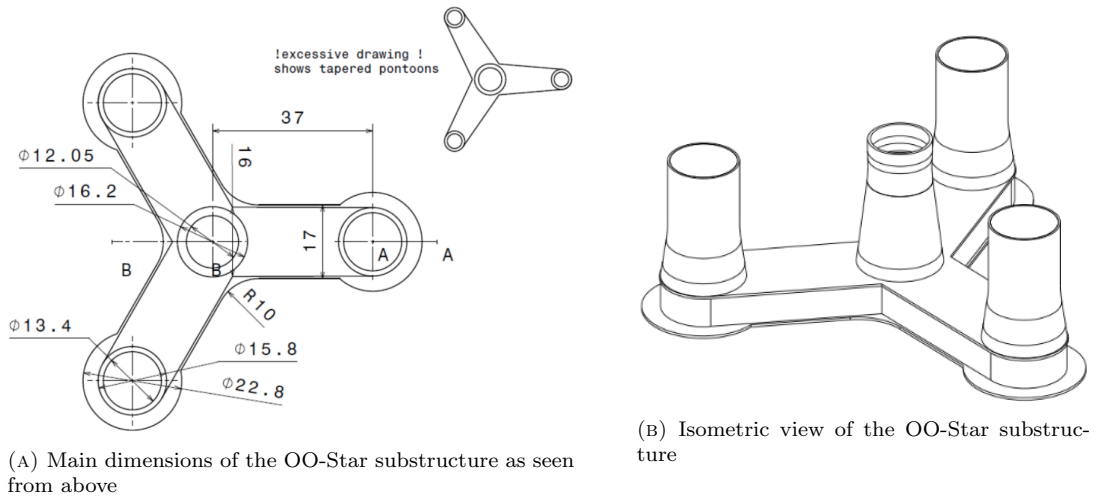
The bottom slab has a width of 17 meters and has a curvature radius of 10 meters in the corner points where the pontoon walls meet. Circular heave plates with a diameter of 22.8 meters is located below the outer columns. The purpose of the heave plates is to increase the added mass of the floater in heave in order to move the heave natural frequency out of the wave frequencies.

The compartment layout of the OO-Star substructure can be seen in Figure 3.2c and Figure 3.2d. There are a total of 12 compartments. Three of the compartments are located in the outer columns between the bottom slab and the top slab and there are also three compartments in all three pontoons. The central shaft is empty.

Some essential platform properties of the 10MW OO-Star concept including ballast are listed in Table 3.1 (YU et al. 2018).

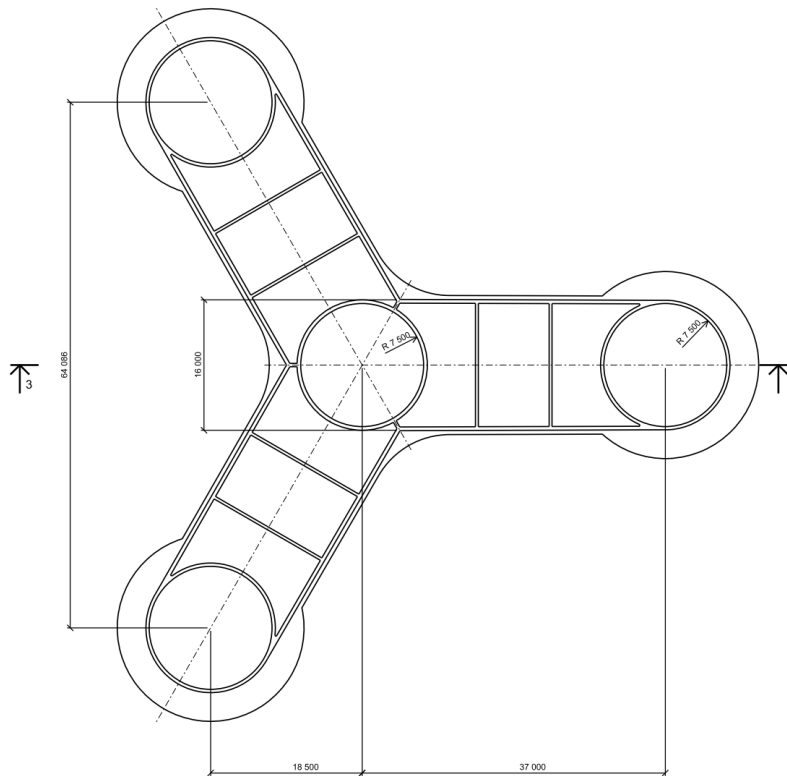
TABLE 3.1: Lifes50+ OO-Star 10MW floater platform parameters, including ballast

Property	Unit	Value
Overall substructure mass (excl. tower, mooring)	kg	2.1709E+07
Centre of mass below mean sea level (MSL)	m	15.225
Substructure roll inertia about centre of mass (CM)	kg m ²	9.43E+09
Substructure pitch inertia about CM	kg m ²	9.43E+09
Substructure yaw inertia about CM	kg m ²	1.63E+10
Tower base interface above MSL	m	11.0
Draft at equilibrium position with moorings (no thrust)	m	22.0
Displaced water volume	m ³	2.3509E+04
Centre of buoyancy below MSL	m	14.236



SECTION 3-3

(c) xz cross section of the substructure for $y = 0$



SECTION 1-1 PONTON

(D) Section 1-1 from Figure 3.2c

FIGURE 3.2: Technical drawings of the Lifes50+ 10 MW OO-Star substructure

3.2 Tower properties

Tower properties are given in Table 2 in the Lifes50+ report (YU et al. 2018). This table is reproduced here as Table 3.2.

TABLE 3.2: Tower properties from the Lifes50+ OO-Star design (YU et al. 2018)

Section [-]	Lower elevation [m]	Upper elevation [m]	Outer diameter [m]	Wall thickness [m]	Cross sectional area [m ²]	Section mass [kg]
1	0.000	3.946	11.385	0.075	2.665	8.667E+04
2	3.946	7.892	11.154	0.074	2.576	8.378E+04
3	7.892	11.838	10.923	0.072	2.454	7.983E+04
4	11.838	15.785	10.692	0.070	2.336	7.598E+04
5	15.785	19.731	10.462	0.068	2.220	7.222E+04
6	19.731	23.677	10.231	0.066	2.108	6.855E+04
7	23.677	27.623	10.000	0.065	2.029	6.599E+04
8	27.623	31.569	9.769	0.063	1.921	6.248E+04
9	31.569	35.515	9.538	0.061	1.816	5.908E+04
10	35.515	39.462	9.308	0.059	1.714	5.576E+04
11	39.462	43.408	9.077	0.057	1.615	5.254E+04
12	43.408	47.354	8.846	0.056	1.546	5.030E+04
13	47.354	51.300	8.615	0.054	1.452	4.724E+04
14	51.300	55.246	8.385	0.052	1.361	4.428E+04
15	55.246	59.192	8.154	0.050	1.273	4.140E+04
16	59.192	63.138	7.923	0.048	1.188	3.863E+04
17	63.138	67.085	7.692	0.047	1.129	3.672E+04
18	67.085	71.031	7.462	0.045	1.048	3.410E+04
19	71.031	74.977	7.231	0.043	0.971	3.158E+04
20	74.977	78.923	7.000	0.041	0.896	2.916E+04
21	78.923	82.869	6.769	0.039	0.825	2.682E+04
22	82.869	86.815	6.538	0.038	0.776	2.524E+04
23	86.815	90.762	6.308	0.036	0.709	2.307E+04
24	90.762	94.708	6.077	0.034	0.645	2.099E+04
25	94.708	98.654	5.846	0.032	0.585	1.901E+04
26	98.654	102.600	5.615	0.030	0.526	1.712E+04
27	102.600	104.630	5.441	0.029	0.484	8.104E+03

3.3 Top mass properties

The rotor nacelle assembly (RNA) properties are based on Table 1 in the Lifes50+ report by (YU et al. 2018). These properties are seen in Table 3.3.

TABLE 3.3: Lifes50+ 10 MW OO-Star, RNA properties (YU et al. 2018)

Property	Unit	Value
Rotor mass	kg	230 717
Rotor centre of mass	m, m, m	-7.07, 0, 119
Nacelle mass	kg	446 006
Nacelle centre of mass	m, m, m	2.69, 0, 118.08
Nacelle, rotor and hub vertical centre of mass	m	118.39
Combined tower top masses	kg	676 723
Combined tower top masses centre of mass	m, m, m	-0.939, 0, 2.789
Roll moment of inertia of tower top masses around tower top	kg m ²	1.659E+08
Pitch moment of inertia of tower top masses around tower top	kg m ²	1.062E+08
Yaw moment of inertia of tower top masses around tower top	kg m ²	1.014E+08

3.4 Mooring system properties

The mooring system layout is illustrated in Figure 3.3. The mooring system consist of three chain catenary mooring lines separated with 120 degrees. The mooring lines consist of a clump weight with a equivalent mass in water of 50 tonnes. This clump mass separates the mooring lines in an upper line segment going from fairlead to the clump mass, and a lower line segment going from the clump mass and too the anchor. The upper line segment is 160 meters long, while the lower segment is 543 meters long. The anchor radius from platform centreline is 691 meters while fairlead is located at a radius of 44 meters from the platform centreline at a vertical position of 9.5 meters above MSL. The mooring system properties are given in table 10 in the Lifes50+ project (YU et al. 2018). This table is given as Table 3.4 in this report.

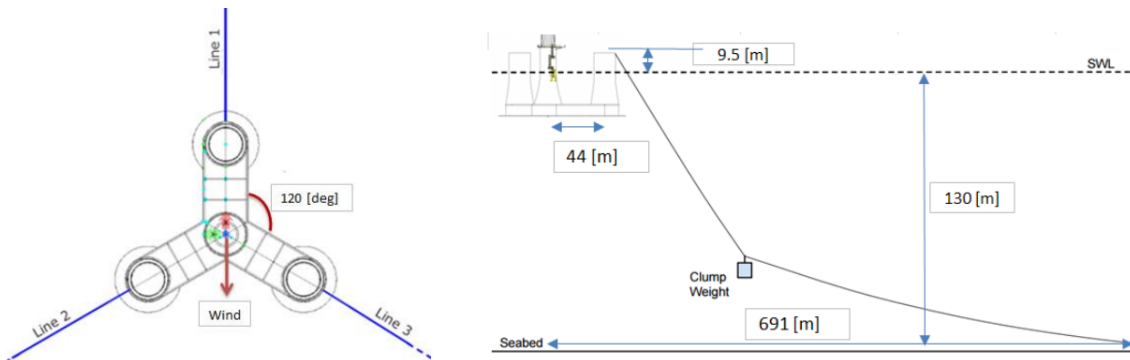


FIGURE 3.3: Lifes50+ 10 MW OO-Star mooring system

Source: (YU et al. 2018)

TABLE 3.4: Lifes50+ 10 MW OO-Star, mooring system properties (YU et al. 2018)

Property	Unit	Value
Number of lines	-	3
Angle between adjacent lines	deg	120
Equivalent total mass in water of the clump mass	kg	50000
Unstretched mooring line length, upper part	m	118
Unstretched mooring line length, lower part	m	585
Vertical position of fairleads above MSL	m	9.5
Radius to anchors from platform centreline	m	691
Anchor position below MSL	m	130
Radius to fairleads from platform centreline	m	44
Initial vertical position of clump mass below MSL	m	90.45
Initial radius to lump mass from centreline	m	148.6
Pre tension	N	1.67E+06
Soil stiffness	Pa/m	3.0E+06
Soil damping	PaS/m	3.0E+05
Equivalent mass per length in air	kg/m	375.38
Equivalent weight per length in water	N/m	3200.6
Extensional stiffness EA	N	1.5006E+06
Hydrodynamic added mass coefficient	-	0.8
Hydrodynamic drag coefficient	-	2.0
Effective hydraulic diameter of the chain	m	0.246
Physical chain diameter	m	0.137

4

METHOD AND COMPUTER IMPLEMENTATION

This thesis investigates a method of combining fully coupled analysis with linear potential theory time domain analysis for transfer of loads to a structural model. This chapter will explain this method in further detail and how computer implementation was used. Central to the work is the use of the Sesam software suite developed by DNV (DNV 2022c). An illustration of the Sesam workflow in this thesis work is seen in Figure 4.1. The subsequent sections will explain this workflow in greater detail.

All models presented are based on the 10 MW OO-Star design introduced in chapter 3. As explained in chapter 3, detailed drawings of the exact substructure design has been deliberately leaved out due to confidentiality consideration. The water depth for all models is, in accordance with the Lifes50+ project, 130 meters (YU et al. 2018).

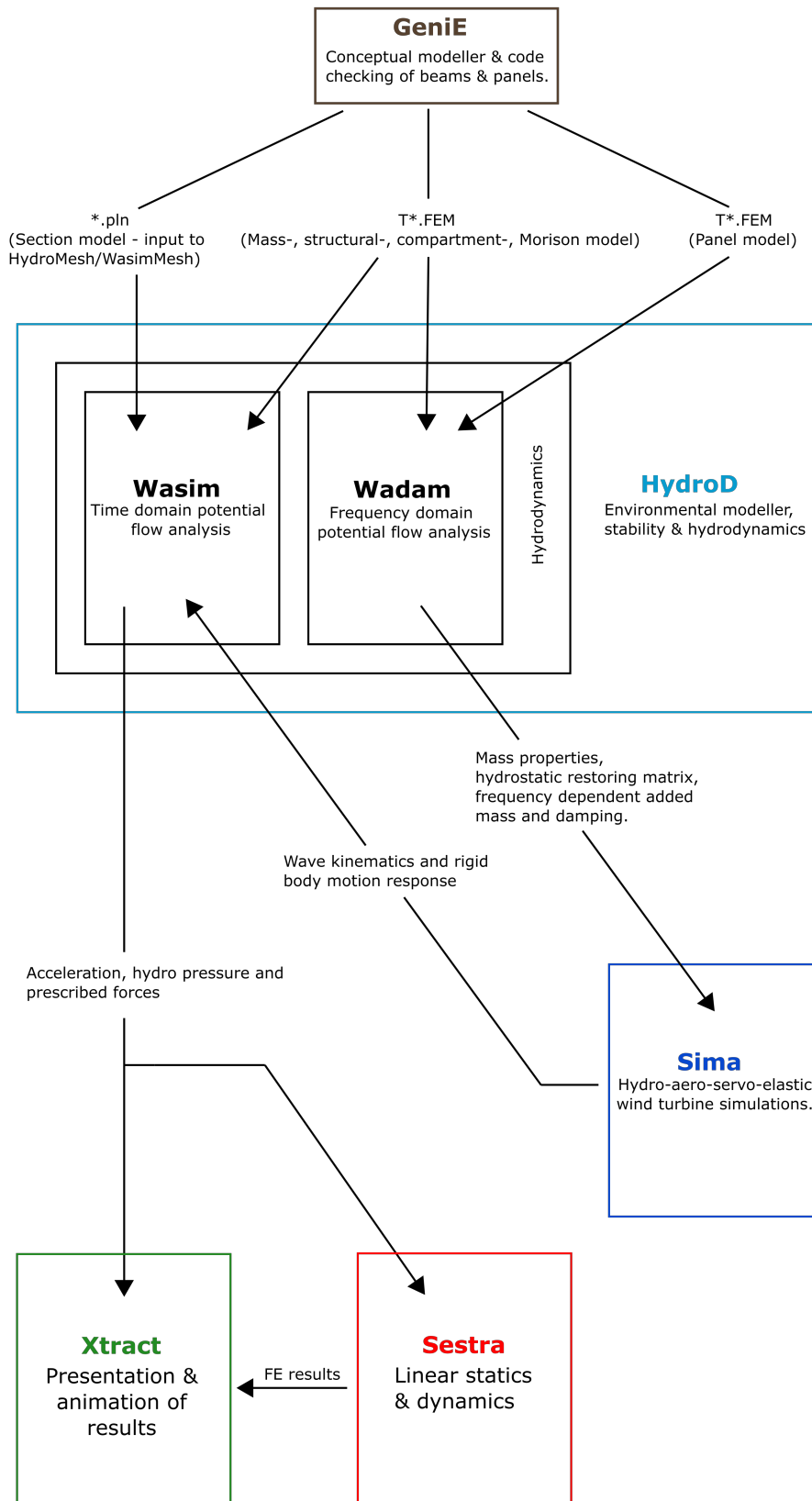


FIGURE 4.1: Sesam workflow

Source: (DNV 2022c)

4.1 Method overview

The investigated method combines fully coupled analysis with linear potential flow theory analysis. Sima was in this thesis work used for the fully coupled analysis part. Fully coupled means that the analyses takes hydro-aero-servo-elastic coupling into account, as described in Section 2.7. The whole system with mooring lines, floater substructure, tower and RNA is modelled in Sima and analyses can be run. From the Sima analysis one can obtain global floater motions, global floater loads and aerodynamic loads. Loads and displacements in tower cross sections and mooring lines can also be found since these are represented by finite elements. In order to get cross sectional loads on the floater, also the correct hydrodynamic pressure distribution has to be calculated in each time step of the calculation. This is most times not possible in Sima which models the body as a 6-degree of freedom (DOF) rigid body represented by (6×6) matrices with hydrodynamic coefficients.

The combination of coupled analysis and time domain potential flow analysis can be used to solve the issue of obtaining the structural response and cross sectional loads in the substructure. DNV's time domain potential flow analysis tool Wasim is used for this, in combination with Sima. The floater motions-, mooring line forces and wave elevation is then transferred from the coupled Sima analyses output to a floater representation in Wasim. Time domain potential flow analyses is then run in Wasim using the prescribed wave elevation, motions and forces, and the pressure distribution is calculated in each time step using panel methods, as explained in Section 2.3.2. The pressure distribution and prescribed forces can then be mapped to a structural model to obtain cross sectional loads or for FEA.

As mentioned, the substructure in Sima is modelled as a rigid body and the governing time domain equation of motion given in Equation 2.24 is solved. The mass matrix \mathbf{M} , the added mass matrix \mathbf{A} , the hydrostatic stiffness matrix \mathbf{C} , the wave radiation damping matrix $\mathbf{B}(\omega)$ and the excitation forces matrix $\mathbf{F}_{\text{exc}}(\omega)$ is input to the equation of motion. $\mathbf{A}(\omega)$, \mathbf{C} , $\mathbf{B}(\omega)$ and $\mathbf{F}_{\text{exc}}(\omega)$ are given according to linear potential flow theory and was found using DNVs frequency domain linear potential flow solver Wadam before being given as input to the floater in Sima.

When doing analysis in both of DNVs potential flow solvers, Wasim and Wadam, models are needed as input. A mass model and a panel model is the minimum requirement for running motion analysis. The mass model determines the mass properties of the structure and hence the mass matrix \mathbf{M} used in the equation of motion. The panel model models the outer surface of the model and is meshed with panels. When doing potential flow analysis, panel methods are used to solve for the pressure on each panel in the model. This is used to compute hydrodynamic pressure distribution on the body. The pressure distribution is also integrated in a frequency domain analysis to get hydrodynamic coefficients that is used in the equation of motion. Other input models can also be defined. A structural model is used to obtain the structural response, a Morison model can be used for capturing Morison loads and a compartment model can be used for defining compartments.

DNV's conceptual modeller GeniE was used to make the models needed for running analysis in Wasim and Wadam. GeniE is explained in further detail in Section 4.2. Panel-, mass-, Morison-, compartment- and structural models were made and these models are also explained further in the succeeding sections. The data files for these hydro models are typically called T-files since the naming convention of the files is *prefixT*.FEM*, where *prefix* is a arbitrary name and * is a unique number for each hydro model used to distinguish the different models. One exception for this is the section model which is used to make the Rankine panel model for time domain potential flow analysis in Wasim. The section model has the file extension *.pln* and is not assigned a unique

number as the T-files.

4.2 GeniE

GeniE was used to create input models for Wadam and Wasim analysis in HydroD. A *.FEM model is typically used as panel model in Wadam. This model is created and meshed directly in GeniE. The *.FEM panel model used in this project is introduced in Section 4.2.1.

As explained in Section 2.12 and Section 2.12, Wadam and Wasim uses two different types of methods for obtaining the hydrodynamic panel pressures on structures. One consequence of this is that *.FEM panel model format is not supported by Wasim. The basis for the Wasim Rankine panel model is a .pln section model that is created in GeniE. The panel model is created in HydroD using this section model. The section model of the OO-Star substructure created for this project is presented in Section 4.2.2. The resulting Rankine panel model created from this section model in HydroD is presented in Section 4.3.

Mass-, structure-, compartment- and Morison models were also made in GeniE. These models are made and meshed in GeniE and are exported as files of the T*.FEM format. These models are used in both Wadam and Wasim. The mass-, structure-, compartment- and Morison models used for this project work is presented in Section 4.2.3 and Section 4.2.4.

4.2.1 T*.FEM panel model

The T*.FEM panel model presented in this section was used as Greens function based panel model for HydroD and Wadam. A parametric panel model of The OO-Star was made as a JavaScript for input to GeniE. The GeniE model was meshed using the meshing commands in GeniE and directly exported as a T*.FEM file. A figure of the resulting meshed panel model can be seen in Figure 4.2. The default element size in the panel model was specified in the meshing commands to be 1 m. This element size is seen along the columns, while smaller elements are seen along the heaveplates and the skirt. A common rule of thumb is to require a minimum of six elements per wavelength. This implies that the smallest wavelength that can be analyzed with this mesh according to this rule is 6 m, which corresponds to a period of 1.96 s.

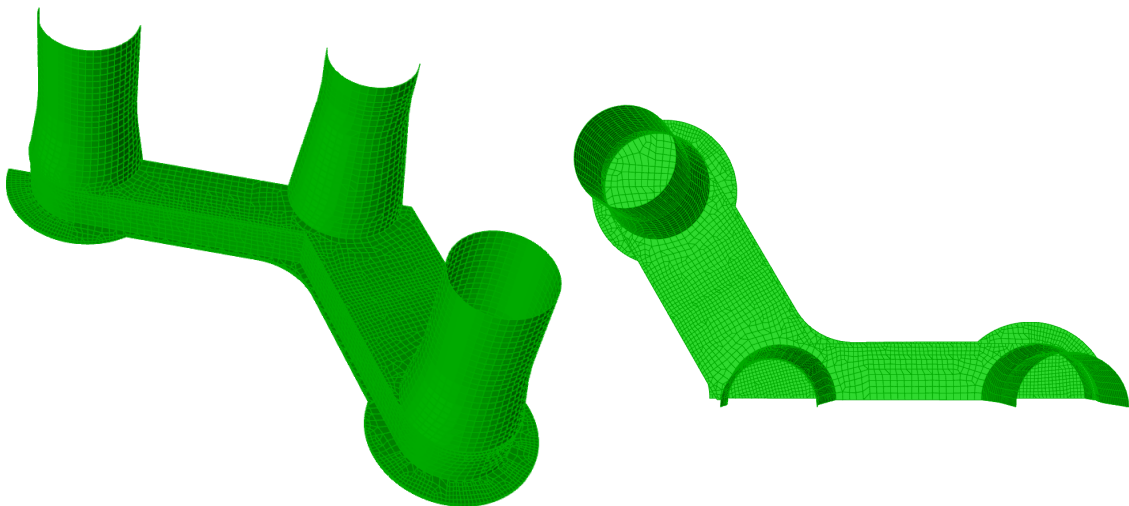


FIGURE 4.2: Panel model mesh of the 10 MW OO-Star generated in GeniE

4.2.2 .pln section model

Wasim uses, as mentioned in Section 2.12, a rankine panel method. The .pln section model is the basis for this Rankine model. A section model for the OO-Star substructure was made in GeniE by making user defined patches defined by GeniE sets. The patches are meshed in HydroD and the result is a panel model that can be used for Wasim. How the patches are defined will to a large degree determine how the resulting mesh will become. The same goes for the number of panels inside each patch, which is also user specified in HydroD. Quite a lot of time was therefore devoted to making the section model as good as possible. The resulting section model made from GeniE can be seen in Figure 4.3.

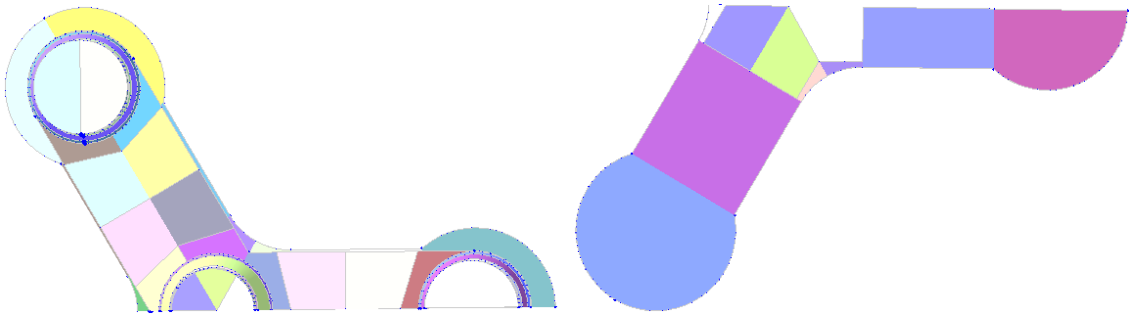


FIGURE 4.3: GeniE .pln section model of Lifes50+ OO-Star substructure

4.2.3 Mass-, compartment- and structure models

Mass-, structural- and compartment models were also made for analysis in HydroD. It is possible to make these models as three separate models, but in a lot of cases they can all be represented by the same T-file. The latter was done in this project.

The mass model models the mass of the model without compartments, while the compartment model is used to model the compartments. The compartments in the compartment model are assigned fluid properties and filling fractions. The mass model and the compartment model are used to compute the (6×6) mass matrix for motion analysis.

The structural model is used for finite element analysis in Sestra (DNV 2022d). When doing structural analysis, hydrodynamic- and hydrostatic pressure from the sea and compartments as well as any prescribed forces are mapped from the panel model to the structural model and FEA can be done. The structural model is also used when finding cross sectional loads in HydroD.

When analysing the structural response and cross sectional loads in the substructure it is not necessary to model the tower and top masses, but instead take the tower influence into account by applying the tower base force from Sima as a prescribed force in Wasim. Only models of the substructure is then needed in HydroD. The force applied at the tower base will, when using this method, take all forces along the tower into account. This means all dynamic forces such as the aerodynamic forces and static loads such as the weight of the tower and the top masses.

Investigations are done in this thesis using both models of the substructure alone, and substructure with tower and top mass representations. Two sets of models were therefore made. Figure 4.4a shows the mass/structural model for the substructure with tower and top mass, Figure 4.4b shows the mass/structural model for the substructure alone and Figure 4.4c shows compartments from the compartment model.

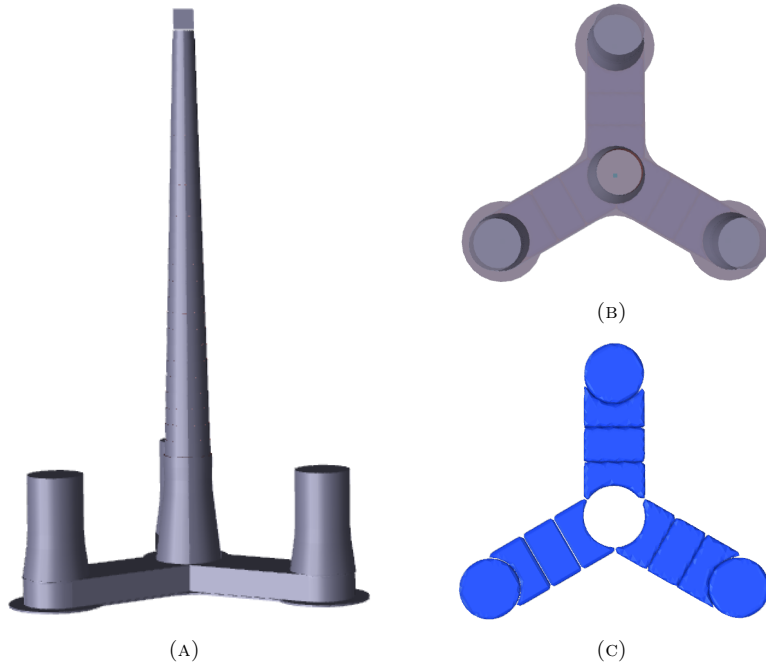


FIGURE 4.4: (A): Mass/compartiment/structural model of floater, tower and top masses. (B): Mass/compartiment/structural model of the substructure alone. (C): Compartments from compartment model

The materials used for the models are concrete and steel, which were used for the substructure and the tower respectively. The material densities used are seen in Table 4.1.

TABLE 4.1: Material properties for mass-, and structural model in HydroD

Material [-]	Density, ρ [kg/m ³]
Concrete	2276
Steel	8242.5

The top masses above the turbine tower were rather difficult to model in an exact way when making the models. Since it is mostly the Steiner contribution from the top masses that contributes to the rotational inertia, these top masses were modelled as a concentrated mass represented as a 5 m \times 5 m plate with COG at (0.939 m, 0 m, 118.39 m). The plate was given a weight of 676723 kg. These values for COG and mass were given based on Table 1 in the Lifes50+ report (YU et al. 2018).

The correct draft of 22 m was ensured by using automatic compartment filling in HydroD. Since the mass of the substructure floater was deviating from drawings provided by Dr. techn. Olav Olsen, the resulting filling fractions were also different from the filling fractions in these drawings. The result of the automatic filling can be found in Section 4.3.

Table 4.2 shows mass properties from the resulting mass and compartment models relative to the mass properties reported by YU et al. (2018). The mass properties of the substructure is seen to be deviating slightly from mass properties provided in Lifes50+. One reason for this can be modelling errors and certain assumptions when modelling based on the provided drawings. For a concrete structure of this size, the cumulative mass difference due to many relatively small differences can be significant. The OO-Star design used for the Lifes50+ project has also used different concrete material properties for different parts of the structure as well as different amounts of reinforcement. The design used in this project is using homogeneous concrete density throughout the whole structure given according to Table 4.1. This is believed to be the biggest contribution to the relative difference.

In order to use consistent models throughout the project, the new mass properties from the models were used in all models. The Sima model used in the project was therefore updated according to Table 4.2. This is further explained in Section 4.6.

TABLE 4.2: Mass properties from GeniE model

Property		This project	Lifes50+	Relative difference
Substructure (including ballast)	Mass	21765 tonnes	21709 tonnes	0.3 %
	COG (Rel. MSL)	(0 m, 0 m, -15.8 m)	(0 m, 0 m, -15.23 m)	(0.0 %, 0.0 %, 3.7 %)
	Roll inertia (Rel. COG)	1.4881E+10 kg m ²	1.4462E+10 kg m ²	2.9 %
	Pitch inertia (Rel. COG)	1.4904E+10 kg m ²	1.4462E+10 kg m ²	3.1 %
	Yaw inertia (Rel. COG)	1.6670E+10 kg m ²	1.6300E+10 kg m ²	2.3 %
Tower mass		1253 tonnes	1257 tonnes	-0.3 %
Top mass		677 tonnes	677 tonnes	0.0 %
Overall system (excl. mooring lines)	Mass	23695 tonnes	23643 tonnes	0.2 %
	COG (Rel. MSL)	(-0 m, 0 m, -8.5 m)	(-0.03 m, 0 m, -7.9 m)	(0.0 %, 0.0 %, 7.6 %)
	Roll inertia (Rel. Origo)	2.8443E+10 kg m ²	2.8193E+10 kg m ²	0.89 %
	Pitch inertia (Rel. Origo)	2.8466E+10 kg m ²	2.8134E+10 kg m ²	1.18 %
	Yaw inertia (Rel. Origo)	1.6698E+10 kg m ²	1.6402E+10 kg m ²	1.81 %

Prescribed forces in Wasim are applied applied to the structural model via beam elements. The program then recognise the closest beam node for every external force and apply the forces there. Beam elements were therefore created at the central column on the tower base and at the fairleads. The point forces applied at the tower base interface are applied at the centre point of the tower base, while ideally they should be evenly distributed over the cross section of the tower base. This was modelled by making a very stiff plate at the tower base cross section. The plate was assigned very large material stiffness in order to ensure that the load applied at the centre point were properly distributed over the cross section. An illustration in GeniE of the beam elements is seen in Figure 4.5 below.

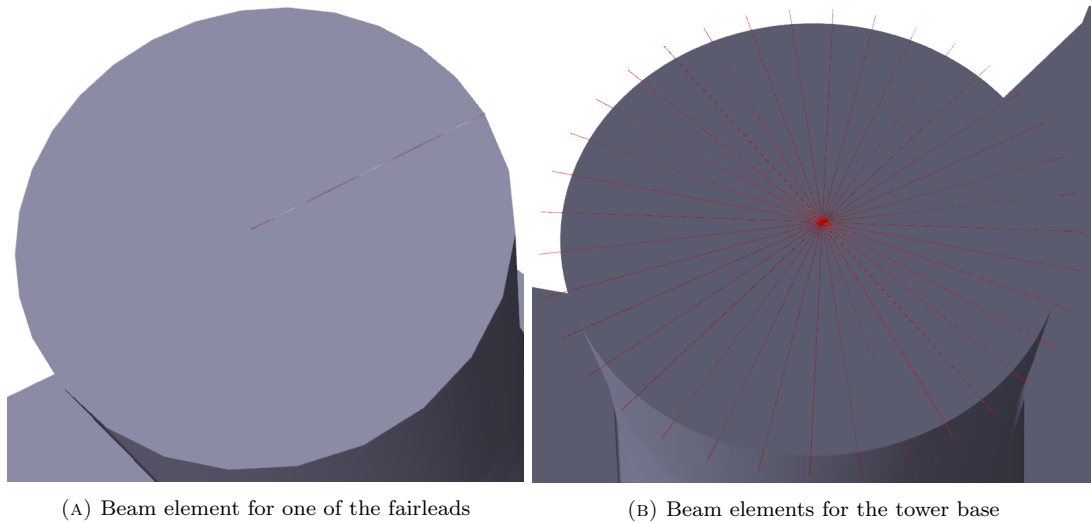


FIGURE 4.5: Beam elements used to map the prescribed forces in Wasim to the structural model

When doing structural analysis with a structural model, boundary conditions also need to be applied. If boundary conditions are not applied, the stiffness matrix will be singular and any finite element (FE) analysis will not be possible. Boundary conditions were applied as point supports in the xy-plane at the intersection between the bottom slab and the transverse bulkheads. The exact position and the boundary conditions of the three support points are found in Table 4.3. Figure 4.6 shows the support points on the structural model in GeniE.

TABLE 4.3: Support points for structural model

Support nr [-]	1	2	3
Position [m]	(23.0, 0.0, -21.5)	(-11.5, -19.9, -21.5)	(-11.5, 19.9, -21.5)
Support [-]	(Fixed, Fixed, Fixed, Free, Free, Free)	(Free, Free, Fixed, Free, Free, Free)	(Free, Fixed, Fixed, Free, Free, Free)

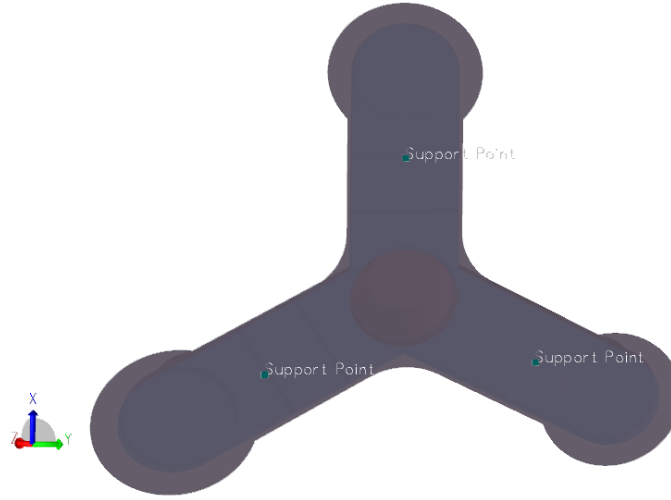


FIGURE 4.6: Support points on structural model

4.2.4 Morison model

A Morison model for HydroD was created in order to capture drag loads on the OO-Star substructure. The Morison model that was made for HydroD was made to be equivalent to the slender element formulation in the Sima model which had already been made by SINTEF Ocean. Sima and HydroD implements Morison loads slightly different, which explains why some of the drag coefficients represented in this section seems rather arbitrary.

A so-called dual model configuration was used in HydroD. This means that the Morison model and the panel model intersects (DNV 2022a). The inertia term of the Morison equation is already captured in the potential flow theory and should therefore not be included in the Morison model as well. The dimensions of the Morison beam elements were therefore scaled down with a factor of 1000, and drag coefficients scaled up with the same factor. The inertia term in the Morison equation will then be negligible.

Figure 4.7 shows an illustration of the Morison model that was used. The dimensions in the figure have been scaled up with a scaling factor of 100 for visualisation purposes. All the beam elements utilizes circular cross section. Table 4.4 shows the properties of the Morison model corresponding to Figure 4.7. The drag coefficients given in Table 4.4 are given in the local coordinate system of the elements and all the elements have local z-axis propagating from "End 1" to "End 2". The pontoons and heave plates have asymmetric drag properties. $C_{D,z}$ in Table 4.4 for the heave plates and the pontoons are the drag coefficient in global z-direction.

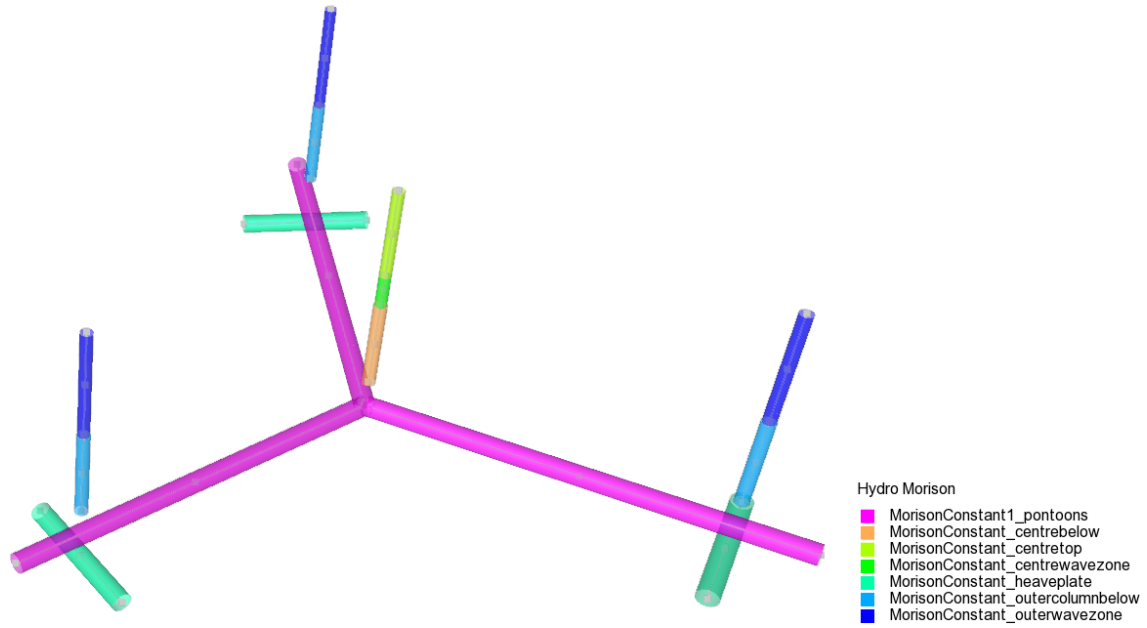


FIGURE 4.7: Illustration of the Morison model. Dimensions have been scaled for visualisation purposes.

TABLE 4.4: Morison model for the 10 MW OO-Star

Morison element type [-]	End 1 [m]	End 2 [m]	Outer diameter [m]	Cdy [m]	Cdz [m]
pontoons	(0.00, 0.00, -18.50)	(44.90, 0.00, -18.50), (-22.45, 38.89, -18.50), (-22.45, -38.89, -18.50)	0.0228	61.4	140.4
centrebelow	(0.00, 0.00, -15.00)	(0.00, 0.00, -4.00)	0.0149	400	400
centretop	(0.00, 0.00, 0.00)	(0.00, 0.00, 11.00)	0.0131	1500	1500
centrewavezone	(0.00, 0.00, -4.00)	(0.00, 0.00, 0.00)	0.0131	1500	1500
heaveplate	(37.00, -7.50, -21.75), (-12.01, -35.79, -21.75), (-25.00, 28.29, -21.75)	(37.00, 7.50, -21.75), (-24.99, -28.29, -21.75), (-12.01, 35.79, -21.75)	0.0228	0	2270
outercolumnbelow	(-18.50, -32.04, -15.00), (37.00, 0.00, -15.00), (-18.50, 32.04, -15.00)	(-18.50, -32.04, -4.00), (37.00, 0.00, -4.00), (-18.50, 32.04, -4.00)	0.0146	400	400
outerwavezone	(-18.50, -32.04, -4.00), (37.00, 0.00, -4.00), (-18.50, 32.04, -4.00)	(-18.50, -32.04, 9.50), (37.00, 0.00, 9.50), (-18.50, 32.04, 9.50)	0.0134	1500	1500

4.3 HydroD

HydroD was used for linear time domain potential flow analysis in Wasim and linear frequency domain analysis in Wadam. The mass/structure/compartiment-, section-, panel- and Morison model created from GeniE was imported into HydroD and the environment was modelled. Automatic compartment filling of the compartment model was done before running analysis in both Wadam and Wasim. A panel model mesh was also created from the .pln section model introduced in Section 4.2.2 together with a surface mesh for Wasim time domain potential flow analysis. The hull mesh from the section model with the waterline in ballasted condition are seen in Figure 4.8.

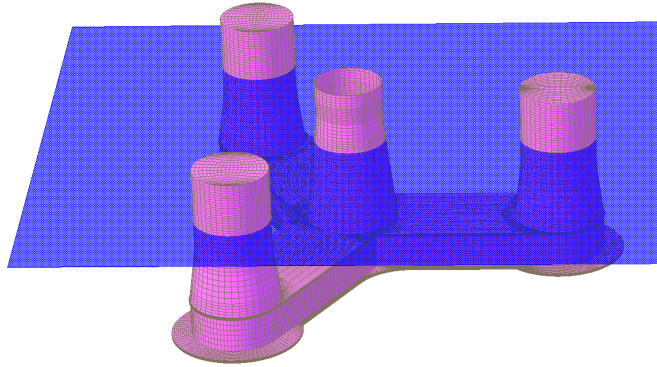


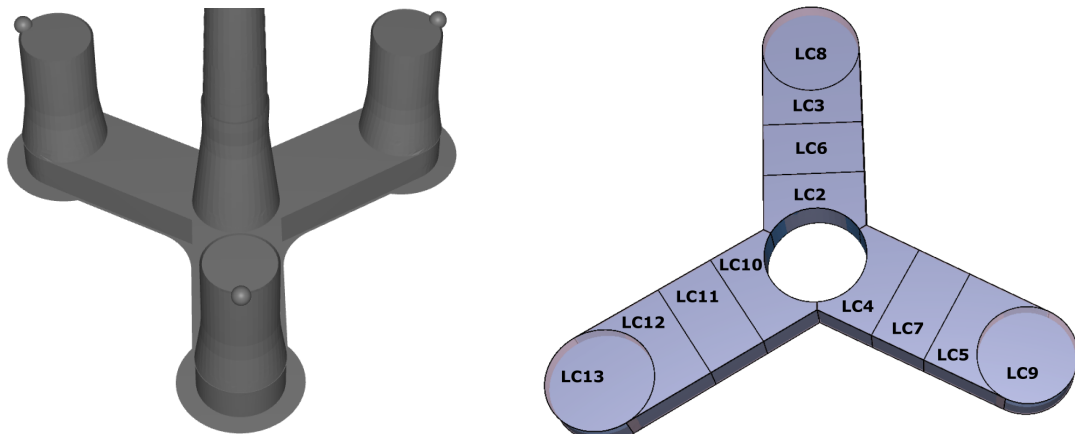
FIGURE 4.8: HydroD model of the 10 MW Lifes50+ OO-Star substructure

4.3.1 Compartment filling fractions

The compartment model used in this project work was introduced in Section 4.2.3. Automatic compartment filling was used in HydroD in order to ensure the design draft of 22 meters. Sea water with density 1025 kg/m^3 was used for the compartment filling.

The mass model in HydroD does not include mooring lines. Point masses were therefore defined in HydroD in order to account for the vertical pretension at the fairleads before using automatic compartment filling. The vertical pretension was estimated by calculating the mass of the mooring lines not resting on the ground, at the correct draft of 22 m. The calculations were done in a MatLab script, using the static mooring line configuration in Sima. This procedure is explained in the Appendix in Section E and the vertical pretension of one mooring line at fairlead was estimated to be $1.4654 \cdot 10^6 \text{ N}$. This implies that the three point masses applied at the fairleads were calculated as $\frac{1.4654 \cdot 10^6 \text{ N}}{9.81 \text{ m/s}^2} = 1.4937 \cdot 10^5 \text{ kg}$ each.

Figure 4.9a below shows the mass model of the 10 MW OO-Star structure with the three point masses representing the vertical pretension, while Figure 4.9b shows the compartments from the compartment model in HydroD. Table 4.5 below shows the resulting filling fractions at 22 meter draft.



(A) Point masses representing vertical mooring line pretension forces before using automatic compartment filling



(B) Compartments from compartment model in HydroD

FIGURE 4.9: Compartments from compartment model

TABLE 4.5: Compartment filling fractions from HydroD

Compartment	LC2	LC3	LC4	LC5	LC6	LC7	LC8	LC9	LC10	LC11	LC12	LC13
Filling fraction	100%	100%	100%	100%	100%	100%	60.00%	60.00%	100%	100%	100%	61.44%

4.3.2 Panel model for Wasim

Panel models used for Wasim analysis are made from .pln section models. The section model that was made in this project was introduced in Section 4.2.2. The Rankine panel model used for Wasim can be seen in Figure 4.10. The mesh density was adjusted visually and RAOs were compared with the *.FEM panel model in Section 4.2.1 in order to ensure that these models were consistent. This investigation is found in Section 5.1.3.

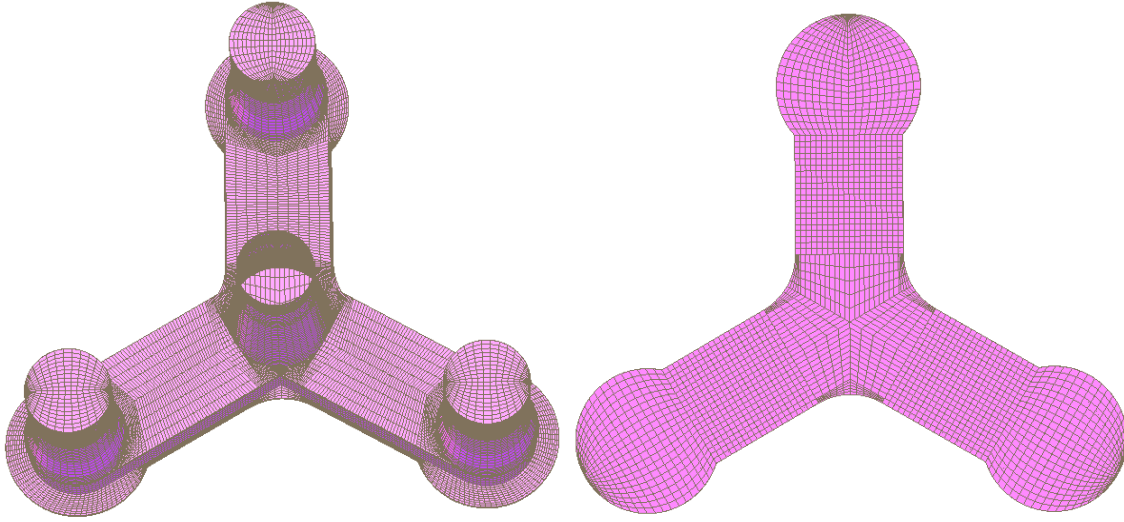


FIGURE 4.10: .pln panel model for use in Wasim

4.4 Wadam

Wadam is run from HydroD and was used to find the mass matrix \mathbf{M} , the hydrostatic stiffness matrix \mathbf{C} , frequency dependent added mass $\mathbf{A}(\omega)$, frequency dependent wave radiation damping $\mathbf{B}(\omega)$ and excitation forces $\mathbf{F}_{\text{exc}}(\omega)$ for the OO-Star substructure. This was given as input the floater representation in Sima in order to ensure that models in Sima and HydroD were compatible. Wadam was also used to plot RAOs for the HydroD models against RAOs from Sima in order to ensure compatibility between the models before transferring motion-, force- and wave data between them. The results from the the hydrodynamic analysis and the RAO analysis can be found in Section 5.1.1 and Section 5.1.3 respectively.

4.5 Wasim

Wasim was used for time domain potential flow analysis. The Rankine panel model for Wasim analysis was introduced in Section 4.3.2.

The Wasim analysis yields the hydrostatic and hydrodynamic pressure distribution on the the floater. Together with the prescribed forces and motions, cross sectional loads can be obtained. FEA can also be done in Sestra.

4.5.1 Surface mesh

As stated in Section 2.12, the surface also has to be meshed for Wasim analysis. The surface mesh was made in the program HydroMesh, which is run from HydroD. Figure 4.11 shows an example of such a surface mesh. According to DNV (2022e), the mesh size should be minimum one wavelength of the longest radiated or scattered wave. A radius of 5 times the vessel length was used in this project. The floater length is 78.3 m. This implies that the longest wave that can be analyzed with this mesh is $78.3 \text{ m} \times 10 = 783 \text{ m} = 783 \text{ m}$. In linear potential flow theory at infinite depth, this corresponds to a wave period of 22.4 s. The mesh will therefore cover most regular waves, which are in the range of 5 s - 20 s.

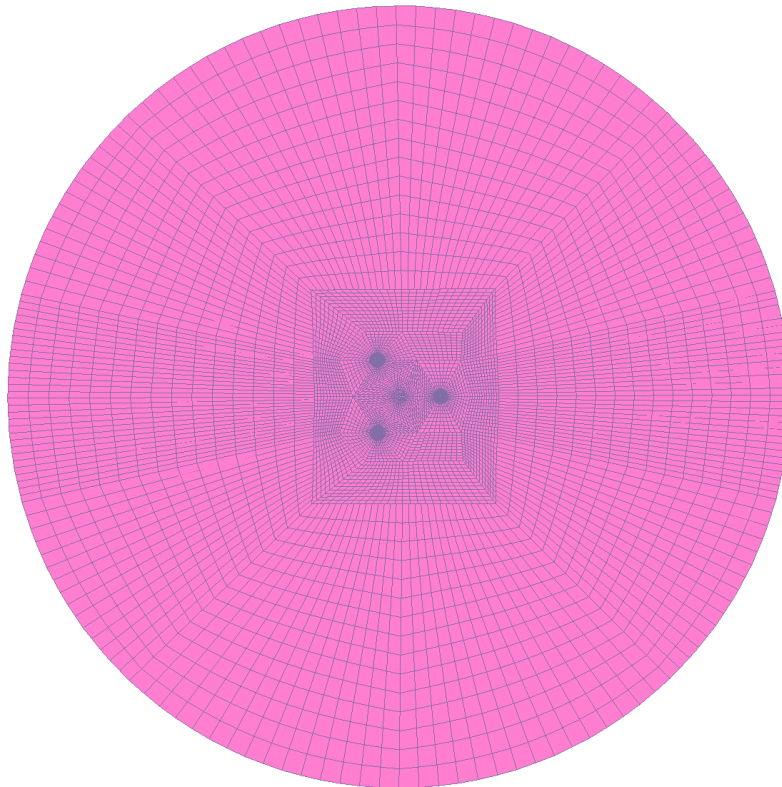


FIGURE 4.11: Surface mesh in HydroD

4.5.2 Prescribed motions, forces and waves

The method of investigation uses prescribed forces, motions and waves from Sima analysis. This prescribed data is given as input files in Wasim. How prescribed data is used in Wasim is explained in further detail in Section F.

The motion and forces are given as time series at specified positions. The prescribed wave can be given either as the time series of the wave elevation, or alternatively as a list of regular wave components. In any case, Wasim reproduces the wave elevation by superposing regular wave components. When giving the wave time series as input, Wasim uses a total of 1000 regular waves to reproduce the wave elevation. The lowest and largest frequencies in this set of regular waves can be specified in the text file. Default values are used if not. When specifying the wave elevation as a list of regular waves in Wave.txt, there are in principle not limitations to the number of

components (DNV 2022e).

4.6 Sima

Coupled analysis was done in Sima. Analysis is used to output forces in the tower base and the fairleads as well as motions and waves that is applied as prescribed data in Wasim. This prescribed data is given as input files in Wasim and files of the correct format can be outputted directly from Sima. A detailed explanation on how this is done can be found in the Appendix in Section F.

The Sima model used in this study was initially made by SINTEF Ocean. The model and environment are based on the 10 MW OO-Star presented in the Lifes50+ project by YU et al. (2018). Two snapshots of the model in Sima can be seen in Figure 4.12.

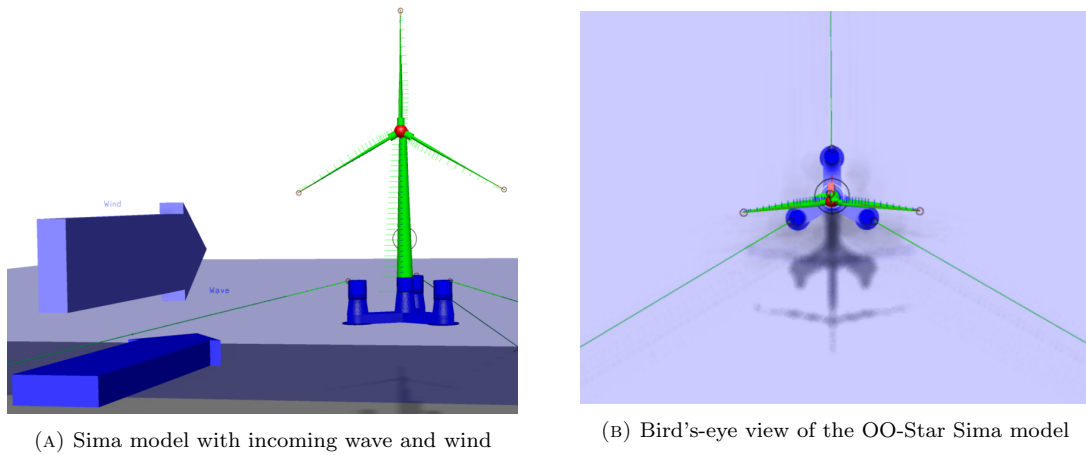


FIGURE 4.12: Fully coupled analysis model in Sima

The Sima model is made with a combination of Reflex lines using finite elements and rigid Simo bodies. A slender element formulation is used to take Morison loads into account. This slender element formulation is equivalent to the Morison model in Section 4.2.4.

An illustration of the Sima model is seen in Figure 4.13. Figure 4.13 is only an illustration and relative dimensions are not representative for the actual Sima model. The substructure and hub are modelled using rigid Simo bodies. Blade lines, blade eccentricities, tower, shaft, mooring lines and nacelle are modelled with Reflex lines. The eccentricity lines are connected to the shaft and models imperfections on the blades. The shaft is modelled with a two-segment line where one of the segments represents the lowspeed shaft and the other represents the high speed shaft. A nodal "Flex Joint" component is included between the segments, which models the generator torque.

The orange lines in Figure 4.13 represents master-slave connectivities in the model which are rigid body connections between supernodes. The line properties used in the model are summarized in Table 4.6.

TABLE 4.6: Finite element representation of lines in Sima model

Property	Element type	Nodal component
Mooring lines	Bar	Clump weight, 51025 kg
Tower	Beam	-
Blades	Beam	-
Eccentricity lines	Beam	-
Shaft	Beam	"Flex Joint", torque
Nacelle line	Beam	-

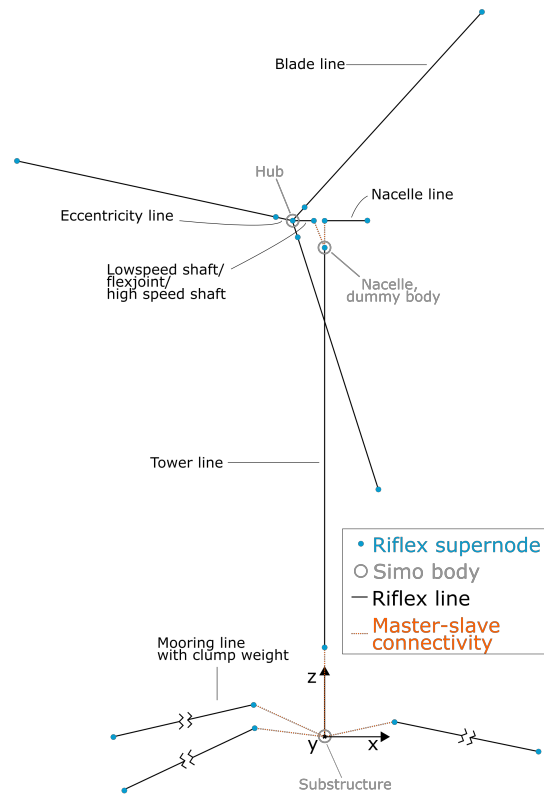


FIGURE 4.13: Illustration of wind turbine model in Sima

Source: (KVITTEM 2014)

As seen in Table 4.2, the mass model of the floater developed in this project was deviating slightly from the values reported in the Lifes50+ project. The floater data in Sima was therefore updated with the mass properties from the mass model created in this project in order to ensure compatibility between the models. The rigid body floater was also updated with hydrodynamic coefficients from a Wadam analysis in HydroD, using the panel model introduced in Section 4.3. The results from this Wadam analysis are introduced in Section 5.1.1. The tower and RNA were not changed in the initial Sima model from SINTEF.

Simas has some different possibilities in how buoyancy is correctly included for the wind turbine floater. How the correct floater buoyancy is included depends if the option "Gravity Included" is checked or unchecked in the floater Simo body settings in Sima. If the "Gravity Included" option is turned off in Sima, the program will automatically assume that the buoyancy force on the floater is equal to the mass of the floater. This means that the buoyancy force will be too small since the buoyancy force needs to carry the tower, RNA and mooring vertical pre tension at fairlead in addition to the substructure alone. This needs to be compensated for in Sima by applying a specified force in global z-direction that is equal to the mass (in Newtons) of the tower, RNA and vertical pretension at fairlead. The hydrostatic stiffness matrix for the substructure also has to be changed if this specified force is applied somewhere else than in the flotation centre since this gives additional restoring moment.

The missing buoyancy force in this case was compensated for in Sima by applying a specified force with a magnitude of $2.3342\text{E}+07$ N. This is equal to the mass of the tower, RNA and the total vertical pretension at fairlead. The tower mass and RNA mass were easily found directly in Sima by summing the mass from all the Riflex lines and Simo bodies that the tower and RNA are made up of. The vertical mooring line pretension was found by estimating the weight of the mooring line segments that were not resting on the ground in the equilibrium position of the wind turbine. The calculation of the buoyancy compensating force was done in a MatLab script which can be found in the Appendix in Section E. Section E in the appendix also contains a more detailed explanation on how the vertical pretension at fairlead from the mooring lines was estimated.

The compensating force was applied in local coordinates (0 m, 0 m, 0 m). This is the flotation centre and the hydrostatic restoring matrix from Wadam was therefore not modified before being given as input to Sima.

5

MODEL AND METHOD VERIFICATION

Before verifying the actual method of transferring data between Sima and Wasim, the models that were used needed to be verified. Section 5.1 in this chapter includes the model verification work that was done.

Several investigations were done in order to ensure that the method of transferring results between the fully coupled analysis and time domain potential flow analysis were done correctly. These investigations are included in Section 5.2. Different challenges that were encountered when doing these verifications are also discussed.

5.1 Model verification

5.1.1 Hydrodynamic analysis of substructure

The panel model created in GeniE was verified by interpreting results from the hydrodynamic analysis in Wadam, and comparing them with results with results presented by YU et al. (2018). A sensitivity analysis was also done in order to ensure convergence of results.

The linear potential flow problem was solved with Wadam through the HydroD interface at the equilibrium position of the floater in ballasted condition and with a waterdepth of 130 meters. The panel model used in HydroD was presented in Section 4.2.

Results for frequency-dependent added mass are seen in Figure 5.1. All added mass coefficients are seen to have asymptotic zero-frequency and infinite-frequency values. A_{35} , A_{45} and A_{56} are seen to be zero for all frequencies. A_{35} is zero due to cancellation effects between added mass force for negative values for x and positive values for x . Pitch radiation will not excite any added mass force in roll due to symmetry reasons and A_{45} is hence 0. A_{56} and A_{46} are expected to be zero since yaw oscillation is not expected to give any roll motion or pitch motion. A_{46} is seen to be non-zero and this is probably due to some numerical inaccuracies.

A_{44} and A_{55} are seen to be equal. A_{44} and A_{55} are not equivalent problems so they are not expected to be exactly the same. There is however a form of symmetry in the problems since there are an equal amount of working columns oscillating in both pitch and yaw and this explains why results seems to be very much alike. A_{11} and A_{22} are equal and this is somewhat expected since there are four "working columns" acting in both surge and sway oscillations. If A_{44} and A_{55} are

equal, and A_{11} and A_{22} are equal, then A_{24} and A_{15} have to be equal as well. A_{15} and A_{24} have however different sign, but this is only due to the coordinate system definition that has been used.

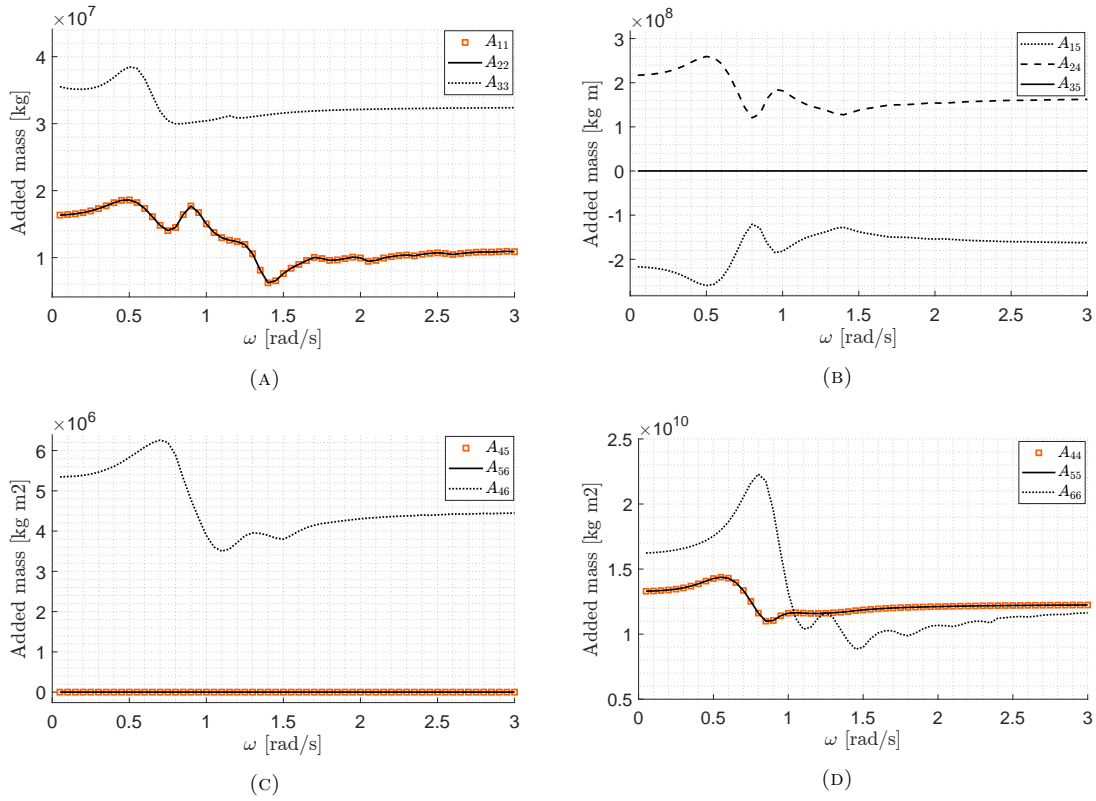


FIGURE 5.1: Lifes50+ 10MW OO-Star added mass from Wadam

Results for wave radiation damping are seen in Figure 5.2. Wave radiation damping is caused by the structure's ability to generate waves (FALTINSEN 2005, p. 10). All damping coefficients are approaching zero as ω approaches 0 and ∞ . For very low frequency oscillation and very high frequency oscillation the body cannot generate any free-surface waves and wave radiation damping is hence zero (FALTINSEN 1993, p. 44).

Many of the same considerations goes here as for the added mass results. As for A_{35} , B_{35} is zero due to cancellation effects in the loads between negative and positive values for x . B_{45} is zero due to symmetry. Yaw oscillations are expected to produce very little wave radiation damping from roll and pitch. B_{46} and B_{56} are therefore expected to be zero. B_{46} is seen to have some non-zero values. This is not expected and is likely due to numerical inaccuracies.

B_{22} and B_{11} are equal since the problems have an equal amount of columns producing wave radiation damping in the two cases. B_{44} and B_{55} are equal due to the same reasoning as for A_{44} and A_{55} described for the added mass discussion. This means that also B_{15} and B_{24} are expected to be the same. Again, these coefficients have opposite sign due to the coordinate system definition.

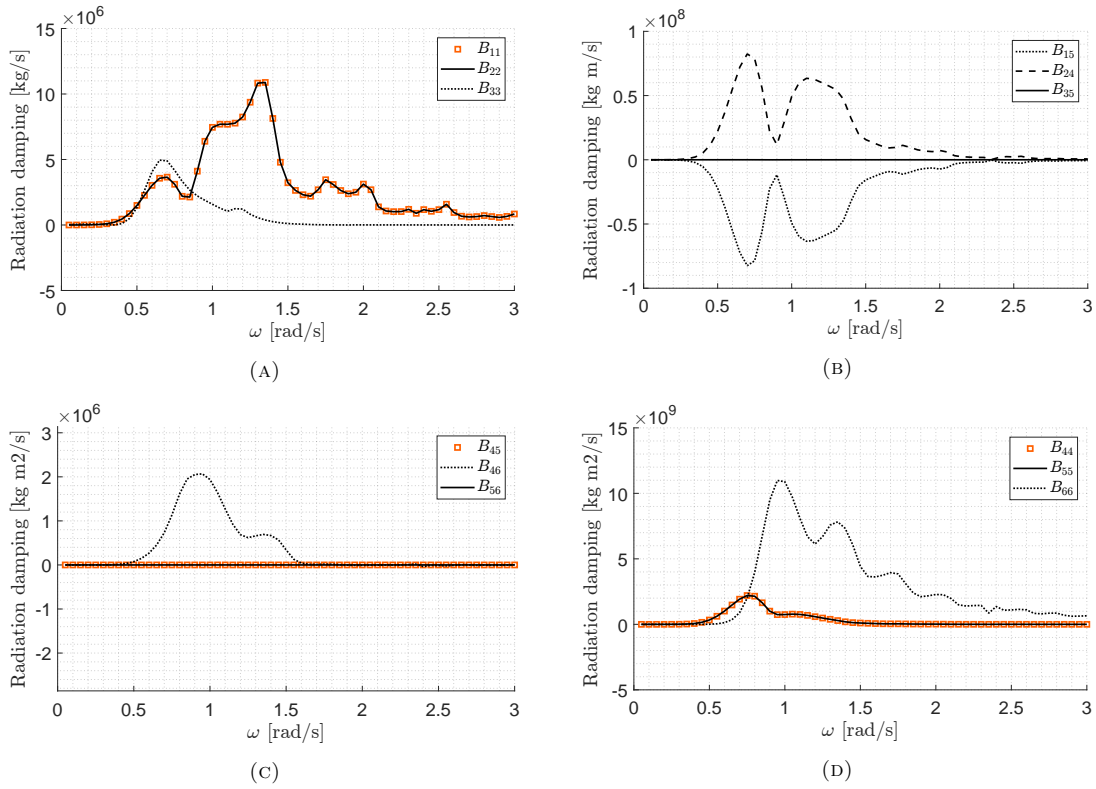


FIGURE 5.2: Lifes50+ 10MW OO-Star wave radiation damping from Wadam

Results for frequency-dependent added mass and damping in Wadam were compared to published results by YU et al. (2018). Solutions were seen to be very similar. This indicates that the panel model that was modelled in GeniE is correct in terms of geometry, and that the mesh is sufficiently fine enough to give accurate results. This is also supported by the fact that the volume displacement from Wadam is $2.357 \cdot 10^4 \text{ m}^3$ while the displaced water volume reported by YU et al. 2018 is $2.3509 \cdot 10^4 \text{ m}^3$ which is only a 0.28% relative difference.

Even though the initial mesh was believed to be sufficiently fine, some quick sensitivity analyses were done in order to check for convergence of results. Figure 5.3 shows the RAO for a default mesh size of 1.5 m, 1.25 m and 1.0 m. The only differences are seen to be the data points for the pitch RAO at the resonance frequency. The RAO at resonance is very sensitive to small mesh changes and the resonance frequency is nonetheless outside the regular wave frequencies. The results seem to have converged.

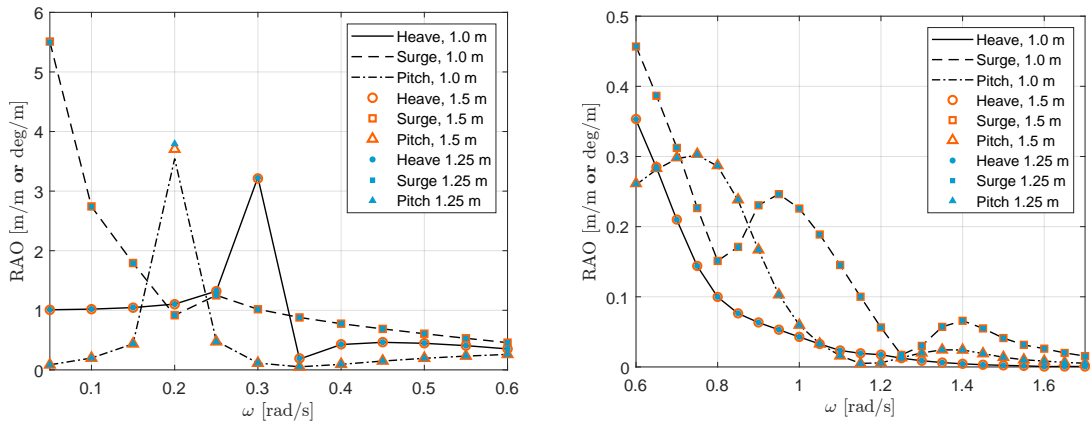


FIGURE 5.3: Panel model sensitivity for default mesh sizes of 1.5 m, 1.25 m and 1.0 m.

5.1.2 Sima model

The hydrodynamic results presented in Section 5.1.1 as well as mass-, hydrostatic stiffness and excitation force properties were given as input to the floater representation in Sima. As pointed out in Section 4.6, a buoyancy compensating force of $2.3342\text{E}+07$ N was also applied at the flotation centre to ensure the correct buoyancy of the substructure.

After applying the buoyancy correction force, a static analysis was done in Sima in order to check the equilibrium condition of the substructure. Ideally, the substructure equilibrium point should be close to (0 m, 0 m, 0 m). Figure 5.4 below shows the z-coordinate of the floater after completion of the static analysis. The floater is seen to move 0.45 cm in positive z-direction which is acceptable by good margin.

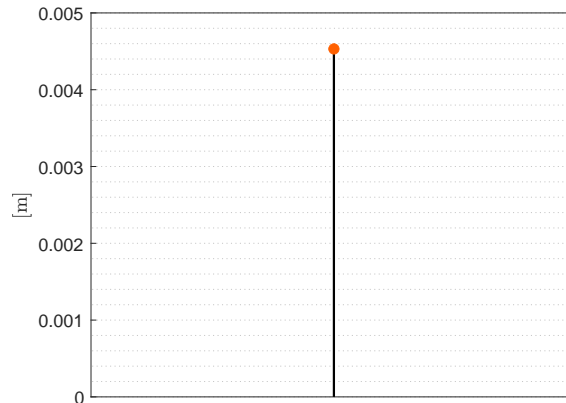


FIGURE 5.4: Equilibrium z-coordinate of floater from static analysis in Sima

Problems with slack in the mooring line laying in the xz-plane were at a later stage encountered when using the Sima model in a ULS condition, defined in Table 5.1. The mooring line modelling in Sima was investigated in order to see if any modelling errors could be found. No apparent modelling errors were found and all the properties of the mooring line system in the Sima model seemed to have the correct properties as reported by YU et al. (2018). The problem may either be due to some overlooked problem in the Sima modelling or suboptimal mooring system design. The problem was discussed with Dr. techn. Olav Olsen who had also encountered some problems with slack in previous investigations. No changes were therefore made to the mooring system.

5.1.3 Model compatibility

It is essential for the method to ensure compatibility between the fully coupled Sima model and the HydroD models if results are to be transferred between them.

RAOs obtained from Sima and Wadam were compared in order to ensure compatibility. RAOs from Wadam were given from the resulting .LIS file from frequency domain analysis with linearized drag. Analyses were done with both the Greens function based .FEM panel model and the Rankine source panel model, introduced in chapter 4. The distributed mass-, compartment-, and Morison models introduced in chapter 4 were also used.

The reason that both types of panel models were used in the RAO comparison is that the Rankine panel model for Wasim was verified against the .FEM panel model. The .FEM panel model was verified in Section 5.1.1 and RAOs from the Rankine panel model should therefore be sufficiently similar to the RAOs from the .FEM panel model. It made sense to do it this way since the .FEM panel model already had been made and verified during the project thesis work in the fall of 2021. Furthermore, GeniE offers much more flexibility when meshing the hull compared to HydroD. This made it easier to first verify a .FEM panel.

RAOs from Sima were obtained by analysing motion response of the floater when using regular

incoming waves. Incoming waves propagated in positive x-direction and were generated in Sima by using a time-series wave elevation as input. This time-series wave elevation was created with the MatLab script *SIMA.timeseries.m* provided by Prof. Erin Bachynski-Polić which can be found in the Appendix in Section A.

The motion response of the floater from Sima will not be a single harmonic with the same frequency as the incoming wave since Sima is non-linear. In order to overcome this, FFT was used on the motion responses. The frequency component at the same frequency as the waves was then filtered out of the response and the RAO was calculated as the amplitude of this frequency component. This was done for 40 regular incoming waves with frequencies ranging from 0.2 rad/s to 3.0 rad/s.

When using FFT on the motion response, a frequency component at the wave frequency is expected to appear as a peak in the frequency spectrum. The harmonic at that peak will then be the frequency component that is at the same frequency as the incoming wave and that was used for calculation of the RAO for that frequency.

The FFT analysis on one regular wave with a period of $T = 9.7$ s can be seen in Figure 5.5. The black curve shows the spectra of the total heave motion from Sima and the orange dots shows the frequency peaks found in this spectra. A MatLab script *bpass.m* created by Halvor Lie at Marintek was used to filter out the peak located at the wave frequency. Figure 5.5 also shows the FFT of the filtered signal in blue which will only appear as a spike at the wave frequency, since only this frequency is present. The script *bpass.m* can be found in the Appendix in Section B.

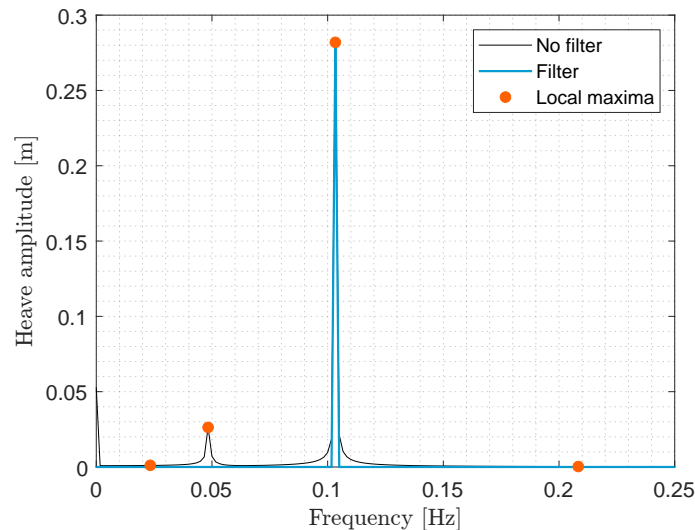
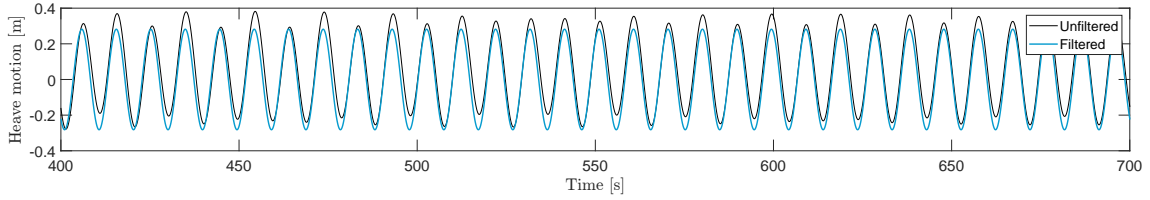


FIGURE 5.5: FFT analysis of heave motion response with incoming wave $T = 9.7$ s. Black = FFT on response from Sima, Blue = FFT on filtered response.

Figure 5.6 shows the unfiltered and filtered heave motion for the 9.7 s wave plotted against each other. The filtered heave motion is seen to be a single harmonic with the same frequency as the incoming wave, while the unfiltered signal has additional frequencies present. The two signals also have approximately the same mean value. This indicates that the Sima model is in equilibrium at 22 meters draft. This is also seen in the FFT plot in Figure 5.5 where the 0 Hz spectrum value represents the mean of the time series. This value is seen to be approximately 5.0 cm which corresponds well to the static equilibrium position from Sima in Section 4.6.


 FIGURE 5.6: Unfiltered and filtered heave motion from Sima. Wave period $T = 9.7$ s.

RAO curves were obtained directly from Wadam and with FFT from Sima with the procedure explained. RAOs for surge, pitch and heave were obtained. Waves and wind used throughout this thesis are defined with a direction of 0° and these motions are considered to be the most important.

RAO comparisons between Sima and Wadam are shown in Figure 5.7 for heave, surge and pitch respectively.

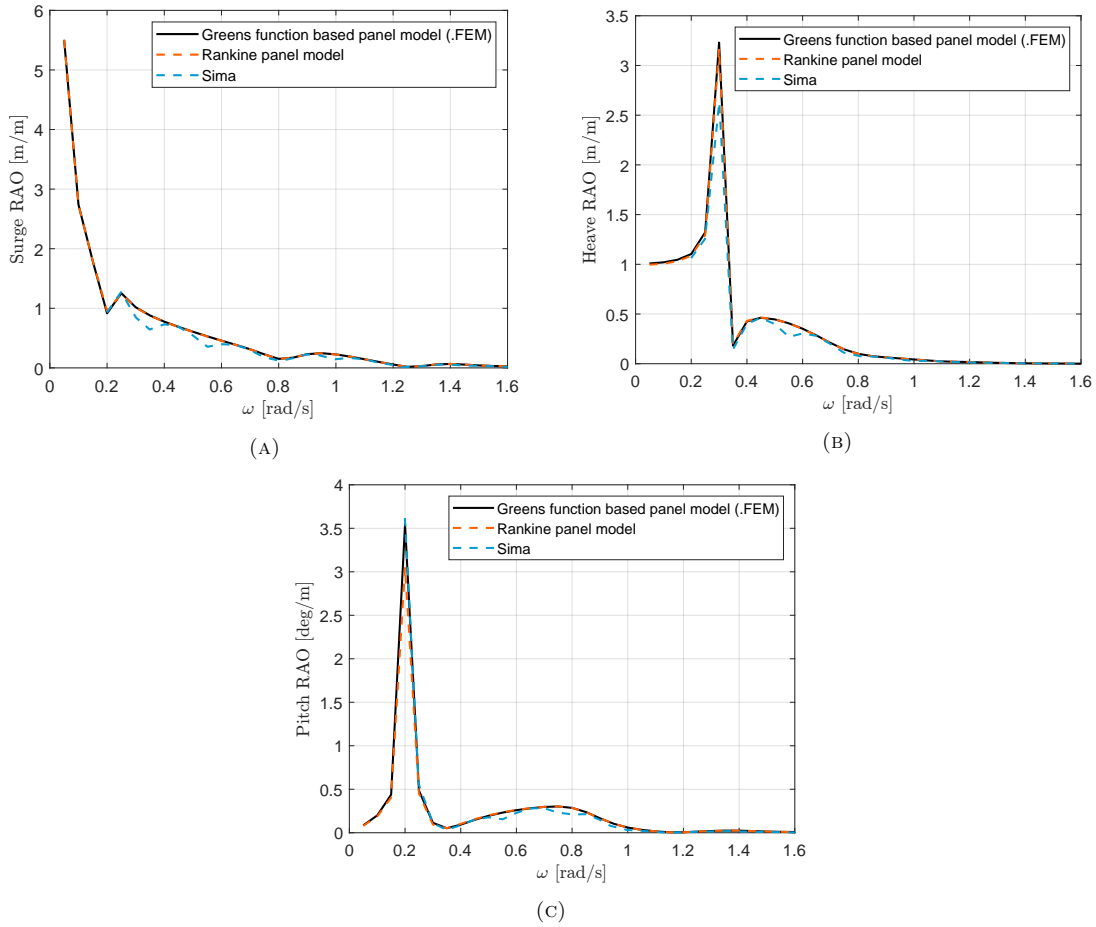


FIGURE 5.7: RAO comparison between Wadam and Sima for surge, heave and pitch

The RAOs from the .FEM panel model and the Rankine panel model are more or less the same, which is expected. A small difference can be spotted in the pitch RAO around the resonance peak, but this is outside the regular wave frequencies. The resonance peak RAOs are also very sensitive to small changes. As explained in Section 5.1.1, the hydrodynamic results for the .FEM panel model seems to yield satisfactory results. The Rankine panel model is therefore also believed to be good.

As seen from Figure 5.7, RAO results from Wadam and Sima shows good correspondence. The RAOs are seen to be very similar in magnitude for most angular frequencies. At resonance, the Sima response is lower for the heave motion. There are multiple explanations for this. The fully

coupled Sima model has additional viscous damping in the mooring lines as well as aerodynamic damping, which is not captured in the Wadam analysis. The Wadam analysis also uses linear drag. Furthermore, the motion amplitude at resonance is very sensitive and some differences can be expected due to this.

The heave RAOs from both Wadam and Sima have a resonance peak at $\omega = 0.3$ rad/s. This corresponds to a period of 20.94 s which is the natural period in heave reported by YU et al. (2018). The resonance peaks in the RAO plots for the heave motion are therefore as expected.

The surge RAOs from Wadam and Sima are also seen to be more or less equal for relatively large frequencies. The Wadam RAO is increasing exponentially for low frequencies, indicating that the natural frequency in surge is low. The natural frequency in surge reported in Lifes50+ by YU et al. (2018) is approximately 182 s which corresponds to a angular frequency of approximately 0.035 rad/s. The RAO is therefore expected to increase as the angular frequency goes towards 0 rad/s. As seen from the Sima surge RAO, the plot does not include as many frequencies as the Wadam RAO for small frequency values. Sima generates incoming waves with the use of Fourier transform and this was troublesome for the lowest frequencies. However, the Sima RAO is believed to follow the same trend as the Wadam RAO as the frequency decreases.

The pitch RAOs are also seen to follow the same trend, and values are more or less equal for frequencies above the peak frequency of the Wadam RAO. The Wadam peak frequency is occurring at 0.2 rad/s which corresponds to a natural period of 31.42 s. The natural period reported by YU et al. (2018) is 31.25 s so this corresponds well. It is not possible to conclude that the resonance peak from Sima is occurring at the same frequency as for Wadam, since the Sima RAO plot stops exactly at the Wadam peak frequency. The two RAO curves are however very similar and resonance frequencies are expected to occur at the same frequency.

It seems from the obtained RAO plots in Figure 5.7 that the HydroD models are compatible with the Sima model. Data for floater motion and auxiliary forces can therefore be transferred between the programs.

5.2 Method verification

A ULS case provided by Dr. techn. Olav Olsen was used for all verifications. This ULS condition is summarized in Table 5.1 and is characterized by irregular sea, turbulent wind and current. The turbine is in idling condition. The ULS condition is located at the 50-year contour line for Hs and Tp at the point of maximum Hs. The irregular waves used for the analysis are described by a JONSWAP spectrum characterized by $Hs = 10.9$ m and $Tp = 15.0$ s. The wind is defined by a Kaimal spectrum with a mean wind speed of 39.6 m/s at the hub located at 119 m. The wind profile is of the power law type, with a power law exponent of 0.11.

TABLE 5.1: ULS condition

Turbine state	Seeds [n]	Duration [min]	ULS								Comments	
			Waves			Current	Wind					
			Spectrum [-]	Hs [m]	Tp [s]	v_curr [m/s]	Spectrum [-]	U, hub [m/s]	I, u [%]	z, hub [m]		Exp [-]
Idling	10	180	JONSWAP	10.9	15.0	1.06	Kaimal	39.6	8.9	119.0	0.11	50-year sea state, maximum Hs

The basis of the method verification was the set up between fully coupled analysis in Sima with time domain potential flow analysis in Wasim. The waves, wind and current were specified directly with the properties in Table 5.1 under the environment definition in Sima. For the turbulent wind, the option "TurbSim Fluctuating Three Component" was used. This requires a .wnd- and .sum input file which were made by running TurbSim. An example of one of the .inp input files used for turbulent wind file generation can be found in the Appendix in Section D.

After analyses had been run in Sima, forces, motions and waves could be given as input to Wasim.

In the analysis, prescribed forces from the mooring lines on the fairleads and the towerbase forces were applied.

A motion data transfer verification was indirectly done in Section 5.2.3 by comparing the bending moment at the tower base from Sima and from HydroD. A verification that the forces had been correctly applied at correct positions was done by making load cross sections in the vicinity of the prescribed forces and investigating the results in Section 5.2.5. A verification was also done by looking at the force resultant in heave. This is included in Section 5.2.2.

It was also important to ensure that hydrodynamic and hydrostatic pressure were mapped correctly from the panel model to the structural model. This verification was done by visually looking at the pressure mapping in Xtract. The result from this investigation is found in Section 5.2.4.

5.2.1 Prescribed wave elevation

Verifying the wave elevation was done by comparing the input wave elevation from Sima with the output wave elevation from Wasim. The wave elevation is, as explained in Section 4.5.2, reproduced in Wasim using a set of regular waves. The wave time series can be given either as a time series or as a list of regular waves. As explained in Section 4.5.2, a complete list of such regular waves for the wave elevation can be given directly from Sima and be used as input to Wadam.

Figure 5.8 shows wave elevation plots from a 200 s time realisation for the ULS case in Table 5.1. The orange curve shows the wave elevation from Sima. The black dotted line shows the wave elevation when wave components given from Sima have been given as input, while the blue dotted curve shows the resulting wave elevation when the input wave elevation was given as a time series.

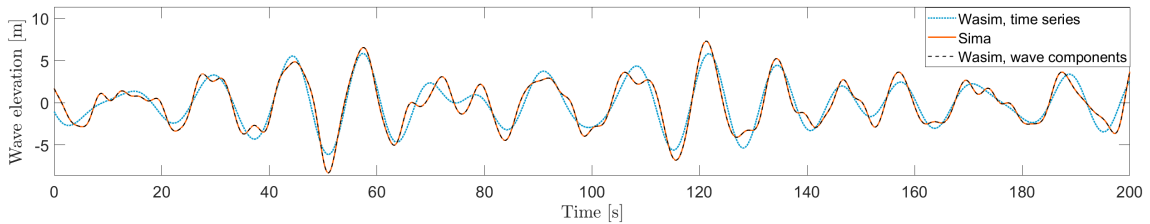


FIGURE 5.8: Wave elevation comparison between Sima and Wasim

As seen from Figure 5.8, Wasim reproduces the wave elevation poorly when time series from Sima is given as input. This method uses 1000 wave components, and was made using the default values for the frequency range of the wave components that is used. As explained in Section 4.5.2, this frequency range can be changed. It might be that Wasim could better reproduce the correct wave elevation if another frequency range is used. The wave time series when using all the wave components from the Sima analysis is seen to exactly reproduce the wave elevation, which is expected.

A benefit of inputting the wave as a time series is that less wave components are used. This implies that calculations are faster. This method can therefore be favourable if 1000 wave components are sufficient to reproduce the wave elevation. If the wave component output file from Sima is used, a sensitivity analysis is beneficial in order to investigate if any of the components can be removed without losing too much information about the wave elevation. This can potentially reduce the computational time a lot.

5.2.2 Force resultant in heave

The force resultant in heave from Wasim includes both static and dynamic loads. This includes hydrodynamic pressure forces from the waves and floater motion, prescribed forces, buoyancy and gravity. Since a floating structure should be in static equilibrium, all these forces should in principle fluctuate with a zero mean.

Figure 5.9 shows the resulting heave force for 350 s when running the ULS case in Table 5.1. The heave force in Figure 5.9 is seen to fluctuate around 0 N and the heave force time series seems reasonable. This indicates static balance and correctly applied forces.

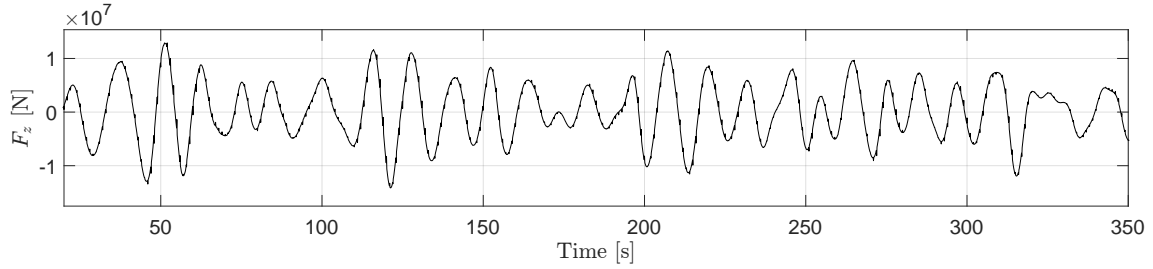


FIGURE 5.9: Heave resultant force from Wasim using correctly applied forces and hydrostatic balance

5.2.3 Prescribed motion - tower base bending moment

Point number 5 in the scope and research objectives defined at the start of this thesis states that the method to be investigated should be verified by comparing the loading at the tower interface between the fully coupled model in Sima and the structural model from Wasim. Cross sectional loads in Wasim are always integrated from positive values for x-, y- and z. The bending moment at the tower base will therefore only be calculated from the motion if no excitation forces are present above the tower base. It was therefore decided to use this as a verification of applying prescribed motion first and foremost.

The sea state defined in Table 5.1 was used in a Sima analysis and the motion, waves and fairlead forces from this analysis were given as input to Wasim. No wind or current was applied. HydroD models for the floater with tower and top mass representations were used.

As explained in Section 4.2.3, a (5 m × 5 m) plate was made for the top mass representation in the HydroD mass model with COG in (-0.939 m, 0 m, 118.39 m). This plate was assigned with a thickness of 11.89 meters and the same concrete material with density 2276 kg/m³ that was used for the substructure. This gives a total top mass of 676 723 kg which is the same total top mass as used in the Sima model and that is reported in Lifes50+ (YU et al. 2018). The mass and moment of inertia for this plate about its centre of gravity can be seen in Table 5.2.

TABLE 5.2: Mass properties for top mass representation in HydroD mass model and simplified Sima model

Mass	Centre of gravity	Ixx	Iyx	Iyy	Izx	Izy	Izz
[kg]	[m]	[kg m ²]	[kg m ²]	[kg m ²]	[kg m ²]	[kg m ²]	[kg m ²]
6.7672e+05	(0, 0, 0)	2.8197e+06	0.0	1.4098e+06	0	0	1.4098e+06

A simplified Sima model was made in order to have as equal as possible top mass representations in Sima and Wasim. The model was made by modifying the original Sima model and the top mass was made as a Simo body defined in the same COG and with the same mass properties as in Table 5.2. The Simo body was connected to the tower top with a rigid body master-slave connection. The tower stiffness was also increased by a factor of 10000 in order to get a very stiff tower in accordance with the rigid body representation in HydroD.

A snapshot from the simplified Sima model can be seen in Figure 5.10a below. The mass data in Table 5.2 were assigned to the Simo body represented as a red sphere, while the cubic Simo body seen on the images was only used as a "dummy body" with zero mass in order to be able to establish the rigid master-slave connectivity between the tower top and the sphere top mass Simo body.

Figure 5.10b shows model in HydroD and the defined load cross section used for collecting the cross sectional loads in the tower base from the Wasim analysis.

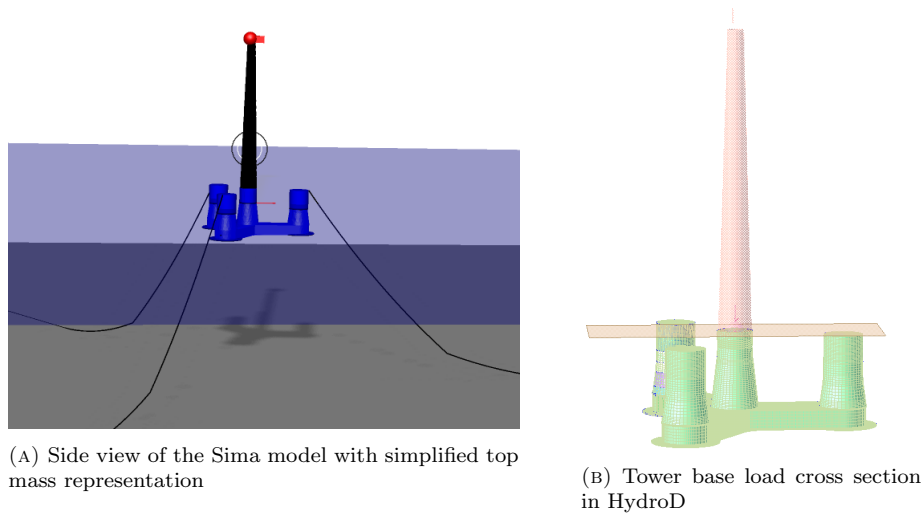


FIGURE 5.10: Simplified models used for verification of prescribed motion

Figure 5.11 shows the fore-aft M_y bending moment from Sima and Wasim. The solutions are seen to match more or less perfectly. This indicates that motions have been transferred correctly.

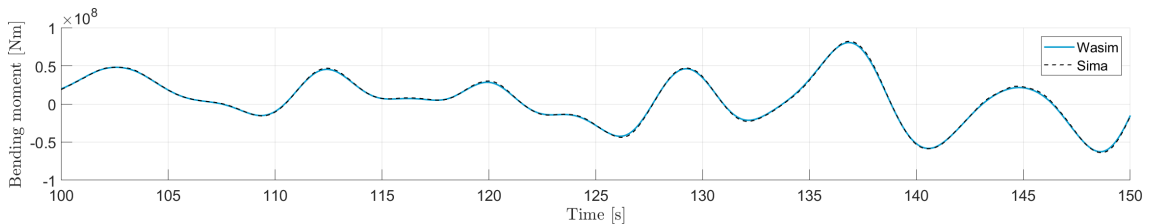


FIGURE 5.11: Tower base fore-aft bending moment comparison between Sima and Wasim

5.2.4 Pressure mapping

The way of verifying the pressure mapping was to run a realisation with the ULS case represented in Table 5.1 and look at the pressure distribution visually in Xtract. When doing Wasim analysis, pressures are found on each element on the panel model using numerical panel methods. These pressures are afterwards mapped to the structural model for structural analysis and for calculation of cross sectional loads. This pressure mapping has to work as intended for analyses to yield satisfactory results. HydroD can, to a certain degree, account for misalignment between panels in the panel model and plates in the structural model. The misalignment tolerance is specified as "Panel/plate out of plane tolerance" and "Panel to plate angular difference", which accounts for the distance and angular difference between panels and plates respectively.

Difficulties with pressure mapping were encountered at an early stage of the investigations. These difficulties were especially related to the base slab and roof slab representation in the structural model. The base slab of the real physical floater is one continuous slab with a thickness of 0.5 m. Plate elements are used in the GeniE modelling and the most physically correct way of modelling the bottom slab would be to model it as a single plate in the structural model. For this to work, the plate would need to receive hydrodynamic pressures from both the lower side and the upper side at certain positions. More specifically, this is along the skirt and on the heave plates outside the pontoon interface. This is illustrated as the red region in Figure 5.12b.

Contact was established with DNV Software support in order to check if it was possible to model the

heave plate in this manner. When defining a plate in GeniE, the wet surface has to be defined and this wet surface is defined on one side of the plate only. DNV therefore suggested a method of using the software tool Presel. Presel is used to combine so called "superelements" which are submodels that in total makes up the whole model. DNV's suggestion was to combine two superelements for the bottom slab - one part for the whole bottom slab with wet surface defined downwards in negative z-direction, and one "dummy heave plate" with wet surface defined upwards. The "normal" bottom slab structural model with wet surface defined outwards in negative z-direction and the dummy heave plate is illustrated in Figure 5.12a and Figure 5.12b respectively.

It was decided to try out the method of using Presel and two superelements was made and merged in the midpoint of the bottom slab. This is illustrated in Figure 5.12c. The same was also done for the top slab.

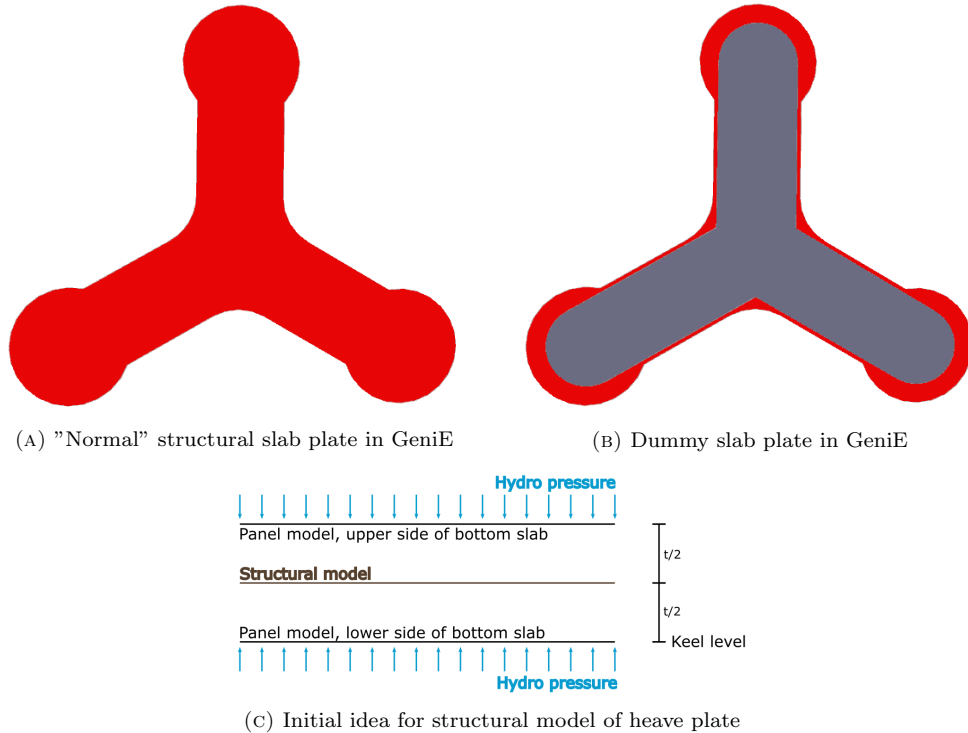


FIGURE 5.12: Structural model for bottom slab

The result when using Presel was a very poor pressure mapping, where there was several relatively large areas on the pressure contour plot where no hydrodynamic pressure had been mapped successfully on the top and bottom slab. Another problem with the method is that the pontoon walls have to be extended by $t/2$ both at the bottom- and top slab in order to have continuity between the slabs and the pontoons.

DNV Software Support reached out to the author at a later stage, stating that there was no way a bottom slab of this type could be modelled as one single plate for a structural model. According to DNV, the "pizza box" approach had to be used where the slab is made like a box with upper and lower plating connected with side walls.

After thinking about this problem and discussing with supervisor Prof. Zhen Gao and Dr. techn. Olav Olsen, it was decided to make the structural model with the "pizza box" approach explained above. In principle this means to model the structural model more in terms of outer geometry as for the panel model.

The default settings of 50 % "Panel/plate out of plane tolerance" and 30 degree "Panel to plate angular difference" were used and the pressure mapping was seen to be good, with only a few individual elements on the structural model not receiving hydrodynamic pressure. The pressure distribution from Xtract at one time instant from the ULS seastate in Table 5.1 is seen in Fig-

ure 5.13.

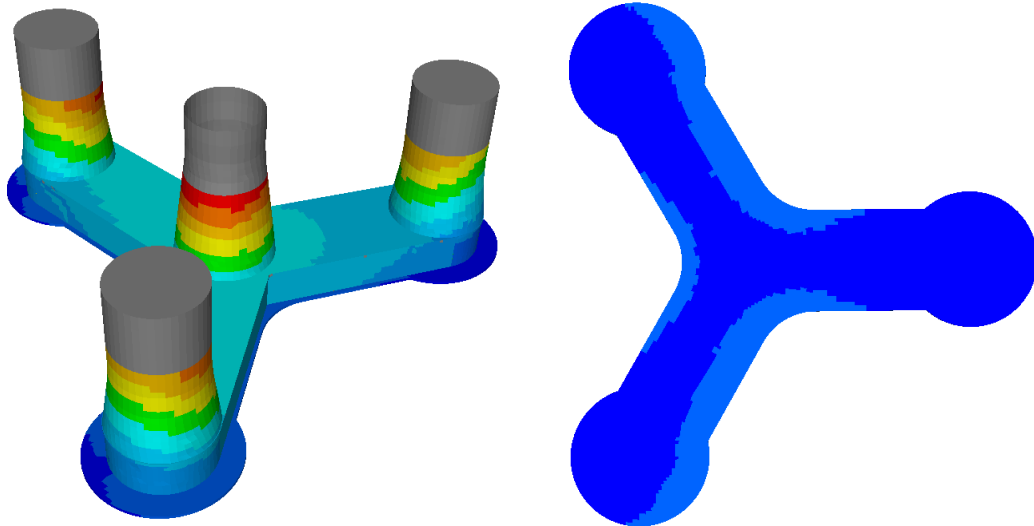


FIGURE 5.13: Pressure contours in Xtract from ULS seastate

It is important to be aware of the fact that this approach gives, in some regards, a nonphysical representation of the slab. This is especially in regards to the structural response. The slab is modelled using an upper and a lower part and they are connected with walls on the "thickness side". The result is that these two plates will have independent degrees of freedom after meshing. This means that the two plates will not necessarily deform together as one single plate, which would be closer to the actual behaviour of the slab.

The most important for the investigations done in this thesis is the pressure distribution on the floater and not the structural behaviour. The method gives the correct pressure distribution, and is therefore believed to yield acceptable results for the work done in this thesis.

5.2.5 Prescribed forces

Verifying that the prescribed forces were applied correctly in Wasim was done by investigating cross sectional reaction loads in sections in the vicinity of the applied prescribed forces from Sima. The reaction forces in these sections should be relatively similar to the applied forces if they are applied correctly at the correct position. The ULS case in Table 5.1 was also used for this verification. Motions, wave elevation and forces at the fairleads and the tower base from Sima were then given as prescribed data for Wasim.

First, a load cross section in position (0 m, 0 m, 10.5 m) was made for the central column which is close to the applied tower base forces at (0 m, 0 m, 11 m). The origo of the body fixed coordinate system from which loads are obtained was also specified as (0 m, 0 m, 10.5 m). A screenshot of the load cross section with the body fixed coordinate system for the forces are seen in Figure 5.14.

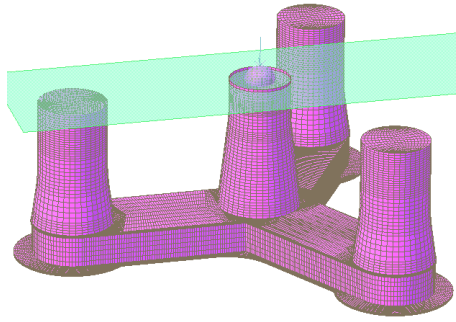
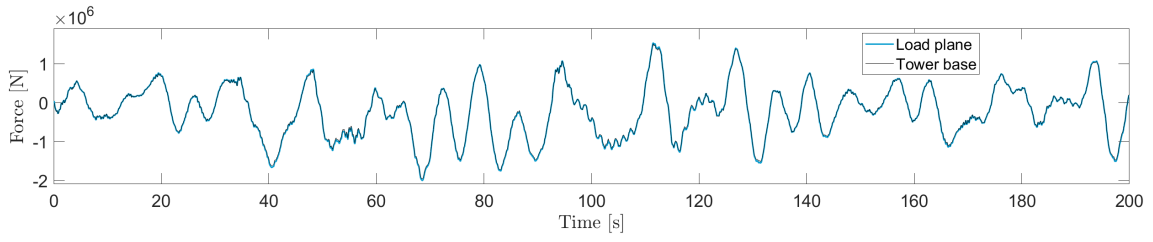
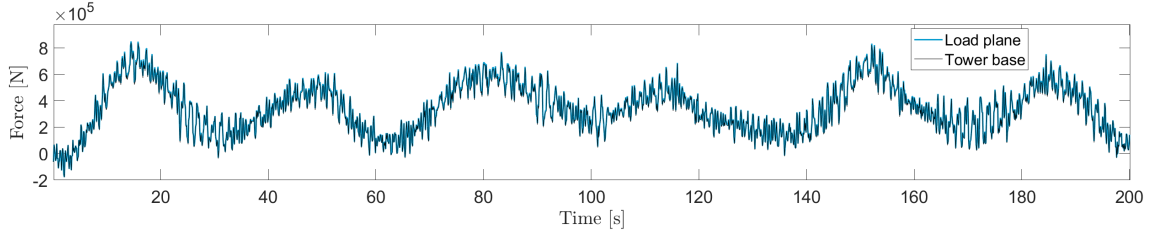


FIGURE 5.14: Load cross section at (0 m, 0 m, 10.5 m) with body fixed coordinate system

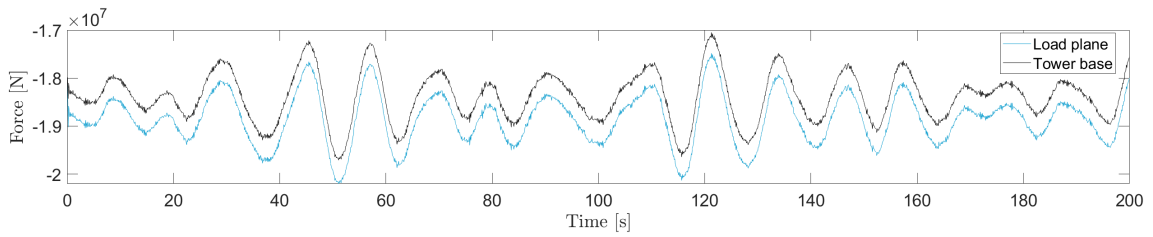
Figure 5.15 below shows the prescribed load in the tower base compared to the cross sectional loads in Wasim. The black curve is the prescribed tower base forces, while the blue curve is the loads found from the load cross section. The loads at the load cross section are internal reaction forces and are therefore of opposite sign to the applied forces at the tower base. The load cross section forces have therefore been multiplied with -1 for easier comparison in the plots. As is clearly seen, forces are almost exactly alike. Only the axial force F_z is deviating slightly, with a lower mean value, and this is due to the additional 0.5 meters of concrete that is contributing to the reaction force in the load cross section.



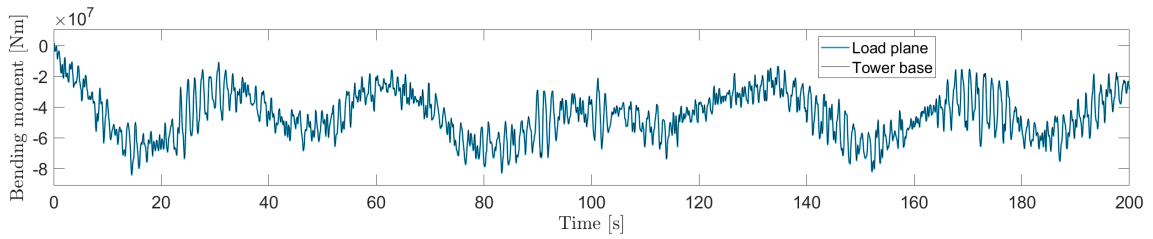
(A) F_x force in central column



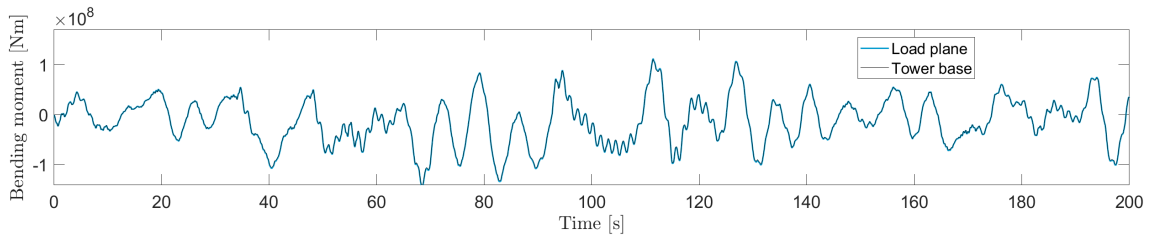
(B) F_y force in central column



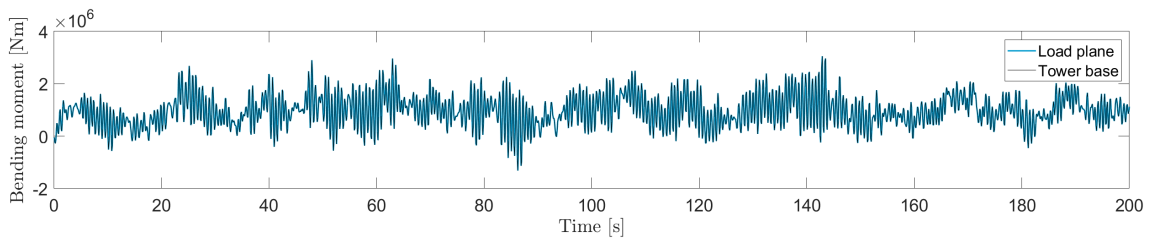
(C) Axial force, F_y force in central column



(D) M_x bending moment in central column



(E) M_y bending moment in central column



(F) M_z bending moment in central column

FIGURE 5.15: Prescribed forces at tower base vs cross sectional loads from Wasim

An effort was also done to check the applied forces at the fairleads. It was not possible to easily obtain cross sectional loads in the outer column in this case, which was the first idea. This was due to the fact that HydroD load cross sections use infinite planes. A xy load cross section in the outer column would therefore also include the central column and the remaining outer columns.

A yz load cross section was made close to the fairlead point on the pontoon going parallel with the x-axis. This load cross section can be seen in Figure 5.16. The point (43 m, 0 m, 0 m) in the waterline was chosen as the origo for the body fixed coordinate system that forces are given relative to.

When looking at the cross sectional load, the substructure was fixed and no waves were applied. The reason for this is that using waves and motions gives additional hydro pressure contributions on the cross sectional loads, and thus making it more difficult to conclude with a large degree of confidence that the forces were applied correctly.

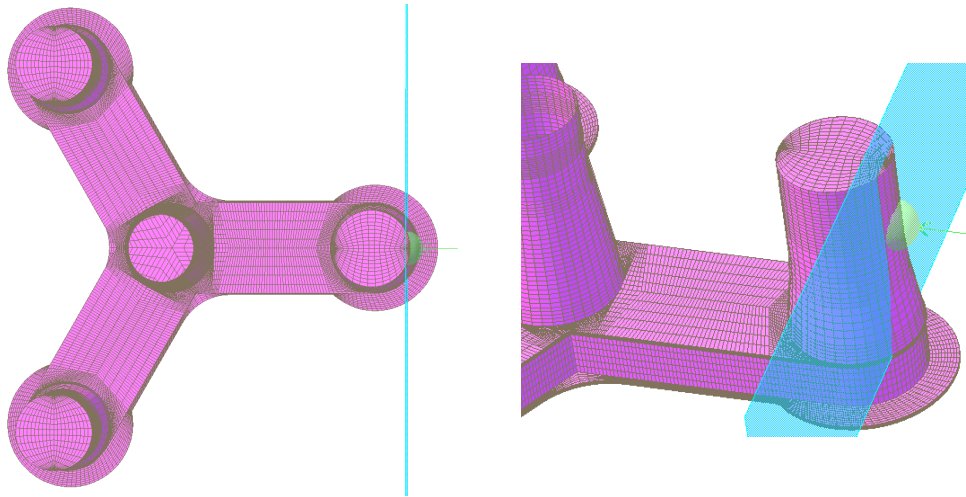


FIGURE 5.16: Load cross section in vicinity of fairlead

Figure 5.17 shows the applied fairlead forces and the reaction forces in the load cross section. Since bar elements are used for the mooring lines, there are no bending moments. The load cross section reaction forces have not been multiplied with -1 in this case, since this made it more difficult to interpret results.

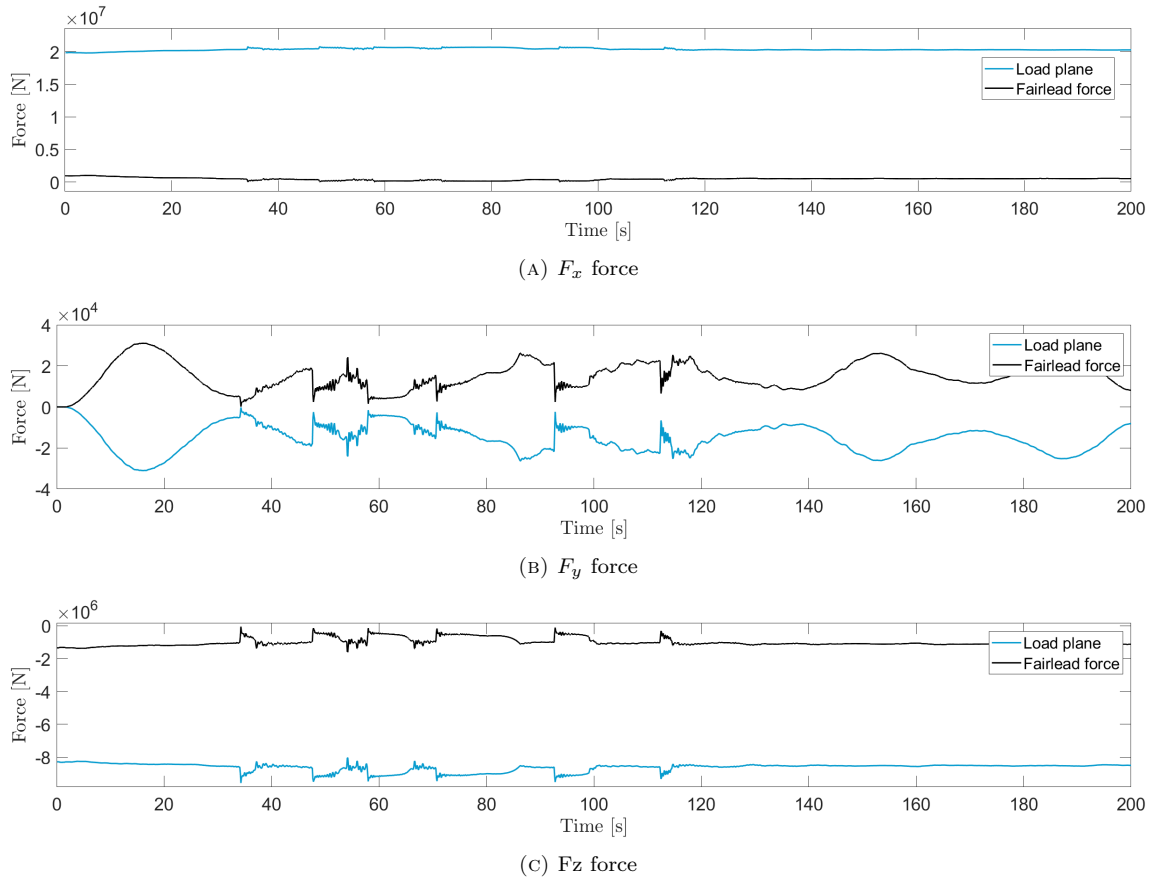


FIGURE 5.17: Prescribed forces at fairlead vs cross sectional loads from Wasim

As is seen from all the force plots in Figure 5.17, there are symmetry between each applied force component and the corresponding reaction forces. The forces in x-direction do not have the same absolute values and this is due to the additional force from the hydrostatic pressure on the column part on the outside of the load cross section. This pressure gives a force in negative x-direction, which means that the reaction forces acts in positive x-direction. The fairlead force is acting in positive x-direction and this means that the reaction forces from this force alone should act in negative direction. The largest contribution to the reaction force in x-direction in the load cross section is therefore the force from hydrostatic pressure.

The force in y-direction is symmetrical around $x = 0$. This makes sense as there is no contribution from hydrostatic pressure due to symmetry. The only contribution to the cross sectional load in y-direction is therefore the applied mooring line load. The cross sectional load is in opposite direction since it is a reaction force.

The same considerations goes for the F_z force as the F_x force. The curves are symmetrical, but their absolute values are different due to additional contributions from hydrostatic pressure for the cross sectional loads.

It is seen from Figure 5.17c that the F_z force goes to zero at several time instants. This is slack which should be avoided in mooring systems. This slack occurrence gives the high frequency spikes that can be seen for both the F_z and F_y components. This problem was discussed in more detail in Section 5.1.2.

It seems like the forces are applied correctly for both the tower bottom and the fairleads. For the tower bottom it is easy to see that the forces are the same but oppositely directed, which is expected when there is no other forces contributing to the cross sectional loads. The applied fairlead forces and the corresponding cross sectional forces are symmetric around a constant value of x , but does not have the same absolute value as for the tower base. This is due to the additional

contribution from hydrostatic pressure to the cross sectional loads. The symmetry in the applied forces and the cross sectional loads makes it reasonable to conclude that also the fairlead forces have been applied correctly.

6

FULLY COUPLED ULS ANALYSIS

Once the method of investigation had been verified, a full ULS analysis was run with the ULS condition defined in Table 5.1. The main objective for the ULS analysis was to evaluate the cross sectional loads along the pontoons and in the central column a distance from the tower base. Dr. techn. Olav Olsen also wanted to see the difference in cross sectional loads from fully coupled analysis and a frequency domain analysis. Cross sectional bending moments from time realisations using coupled analysis are therefore compared with bending moments obtained from a frequency domain analysis using short term statistics.

6.1 ULS analysis, set up

The basis for the ULS analysis was the setup between fully coupled analysis in Sima and time domain potential flow analysis in Wasim. Motions, waves and forces on the fairleads and at the tower base from coupled analysis were then given as input to the time domain potential flow analysis. The wave elevation and current were specified in Sima through the environment definition, and turbulent wind was specified by using files from TurbSim.

A total of 10 realisations with different wave and wind seeds were used in the analysis in order to capture the stochastic nature of such time realisations. These seeds were generated using a random number generator. The wave seed is specified under the environment definition in Sima, and the wind seeds are specified in TurbSim when generating the wind files. TurbSim uses two seeds to make wind files, given as "RandSeed1" and "RandSeed2". Table 6.1 below shows the 10 pairs of random seeds that were used.

TABLE 6.1: Seed combinations used for ULS analysis

Time realisation [-]	1	2	3	4	5	6	7	8	9	10	
Wave seed [-]	5060	6991	8910	9593	5473	1387	1493	2576	8408	2543	
Wind seeds [-]	RandSeed1	501485150	1703994003	62702384	-469927519	1475466973	655262270	-1985501102	-1135979321	-1163006424	-1267159781
	RandSeed2	1456975012	704575628	587089770	-1130752634	1027384052	-2108263712	-255588889	-1562766995	1581281055	902095550

A total of four load cross sections were defined in HydroD. Three of them were defined along the pontoon going parallel to the x-axis, while the last was defined a distance down from the tower base in the central column. The pontoon load cross sections were given as yz-planes, while the load cross section in the central columns was given as a xy-plane. The four load cross sections are

defined in Table 6.2. The cross sectional loads from each load cross section are given in the body fixed coordinate system with origo defined as the points given in Table 6.2. Figure 6.1 shows the visualisation of the load cross sections in HydroD.

TABLE 6.2: HydroD load cross sections used in ULS analysis

Load cross section [-]	1	2	3	4
Plane normal [m]	[1, 0, 0]	[1, 0, 0]	[1, 0, 0]	[0, 0, 1]
Body fixed coordinate system origo [m]	(10, 0, 0)	(17.5, 0, 0)	(25, 0, 0)	(0, 0, 10)

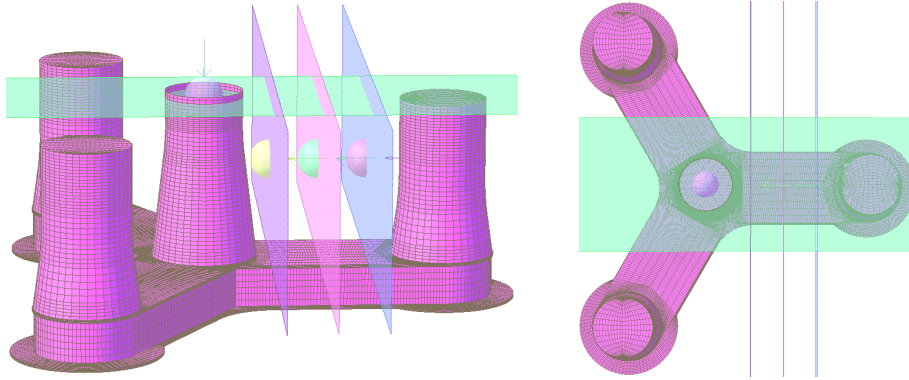


FIGURE 6.1: Load cross sections used in fully coupled ULS analyses

6.1.1 Surface mesh sensitivity analysis

As described in Section 4.5, Wasim uses a user defined surface mesh. Some sensitivity investigations was done on this surface mesh in order to figure out how fine mesh was needed in order for results to converge. The mesh in HydroMesh is more or less made by hand by drawing patches across the surface and assigning each patch a grid size. Actually quantifying the mesh was therefore a challenge.

The surface mesh created for Wasim was divided into two separate areas, where the first area is in the vicinity of the structure, and the second area is outside. The mesh was quantified by counting the numbers of panels inside each of these two areas. This is illustrated in Figure 6.2.

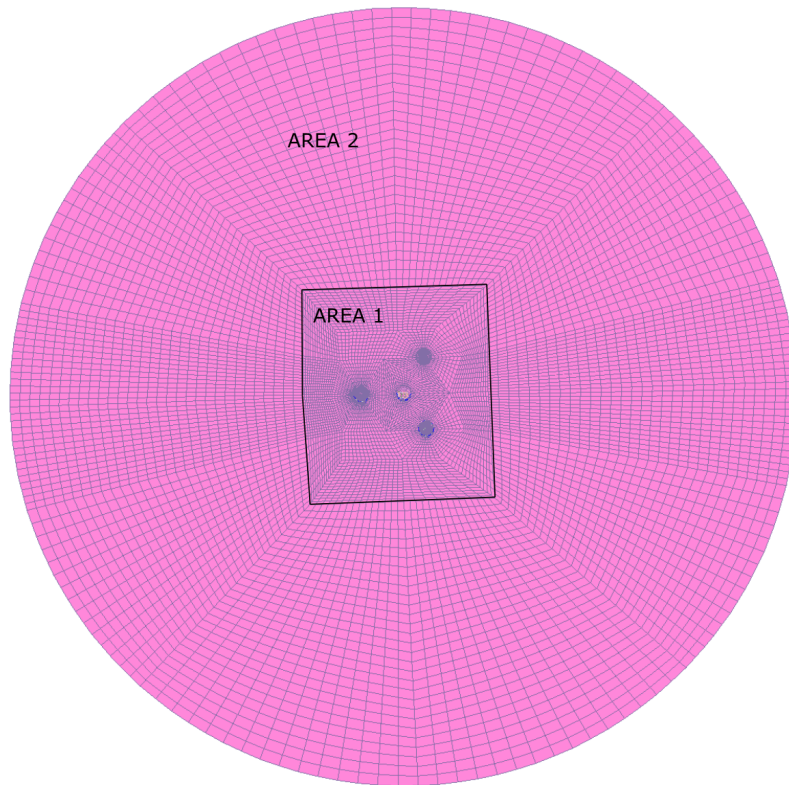


FIGURE 6.2: Surface mesh divided in one area close to the structure and one area outside

Since cross sectional forces are the main focus of this thesis, it was decided to investigate the bending moment in one of the pontoons when looking for convergence. A yz load cross section was defined for x-coordinate 18.5 m which is approximately in the middle of the pontoon going in x-direction. Origo of the cross sectional body fixed coordinate system was deined to be (18.5 m, 0 m, 0 m). 200 seconds of the ULS case using the seeds in Seed pair nr 1 in Table 6.1 was used. Forces, motions and the wave were given as input to the Wasim analysis.

First, the mesh was refined in "Area 1". Four mesh refinemenets were done. Table 6.3 shows the mesh properties that was used.

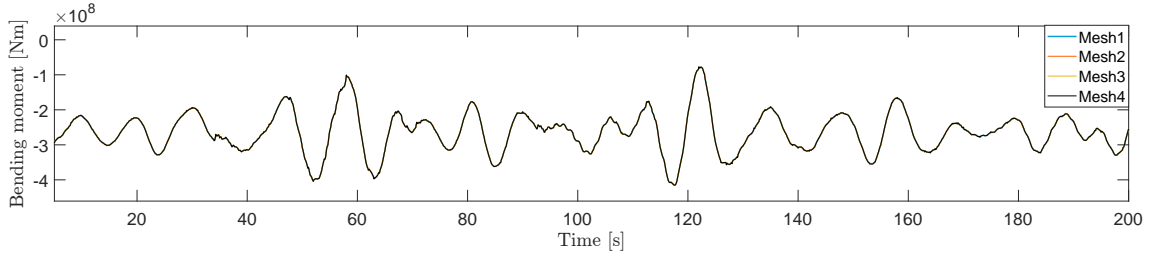
TABLE 6.3: Mesh properties for mesh refinement of "Area 1"

Mesh nr. [-]	1	2	3	4
Nr. elements, Area 1	3464	5040	6920	9104
Nr. elements, Area 2	2700	2700	2700	2700

Table 6.4 below shows the absolute value of the maximum cross sectional bending moment M_y from the 200 seconds of analysis for each refinement together with the relative error. Figure 6.3 shows the 200 second time series of the bending moment.

TABLE 6.4: Bending moments M_y when refining mesh "Area 1"

Mesh nr. [-]	1	2	3	4
Max M_y [Nm]	415516736	415435360	415381568	415340896
Relative error [%]	N/A	0.02	0.01	0.01


 FIGURE 6.3: Local bending moment M_y for different surface mesh densities for "Area 1"

As is seen from Table 6.4, the relative error between each mesh refinement is very small and convergence of results are expected to have occurred. This is also clearly seen from Figure 6.3 where the solutions are impossible to distinguish from each other without zooming very close to the curve.

After refining "Area 1" it was decided to try to refine "Area 2". Table 6.5 shows the number of elements used inside each mesh area. As seen from Table 6.5, the number of elements inside "Area 1" is equal to the coarsest mesh used for "Area 1" from the previous investigation.

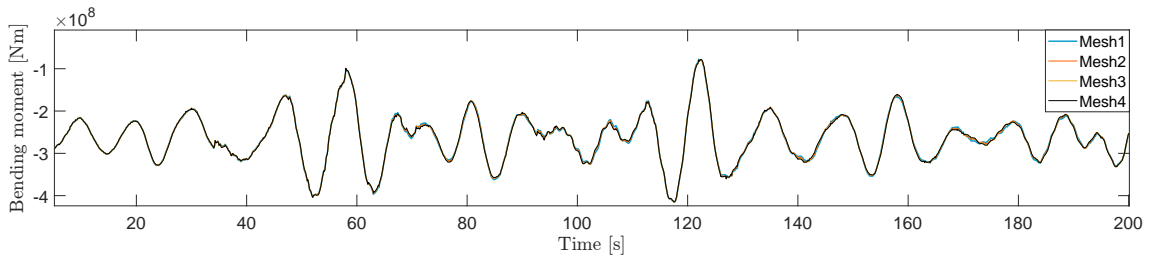
TABLE 6.5: Mesh properties for mesh refinement of "Area 2"

Mesh nr. [-]	1	2	3	4
Nr. elements, Area 1	3464	3464	3464	3464
Nr. elements, Area 2	2700	3600	4500	5400

Table 6.6 shows absolute value of the maximum cross sectional bending moment M_y from the 200 seconds of analysis for each refinement together with the relative error. Figure 6.4 shows the full time series.

 TABLE 6.6: Bending moments M_y when refining mesh "Area 2"

Mesh nr. [-]	1	2	3	4
Max M_y [Nm]	415516736	415279968	414837280	414418496
Relative error [%]	N/A	0.06	0.11	0.10


 FIGURE 6.4: Local bending moment M_y for different surface mesh densities for "Area 2"

As is seen from Table 6.6, the maximum bending moment is not changed significantly when changing the number of elements in "Area 2". The same conclusion can therefore be drawn here as for the previous investigation when changing the mesh size in "Area 1". Some local differences between the solutions can be spotted in Figure 6.4, but these are not considered to be of any significance.

The solutions presented when refining the surface mesh shows that solutions were not significantly affected by refining the mesh. The initial surface mesh that was made before doing this sensitivity

was the coarsest mesh in Table 6.4 and Table 6.5. This mesh was made by intuitively trying to make a sufficiently fine mesh for the analysis. The results shows that this was probably achieved and the coarsest mesh was used for further analysis. This mesh can be seen in Figure 6.5.

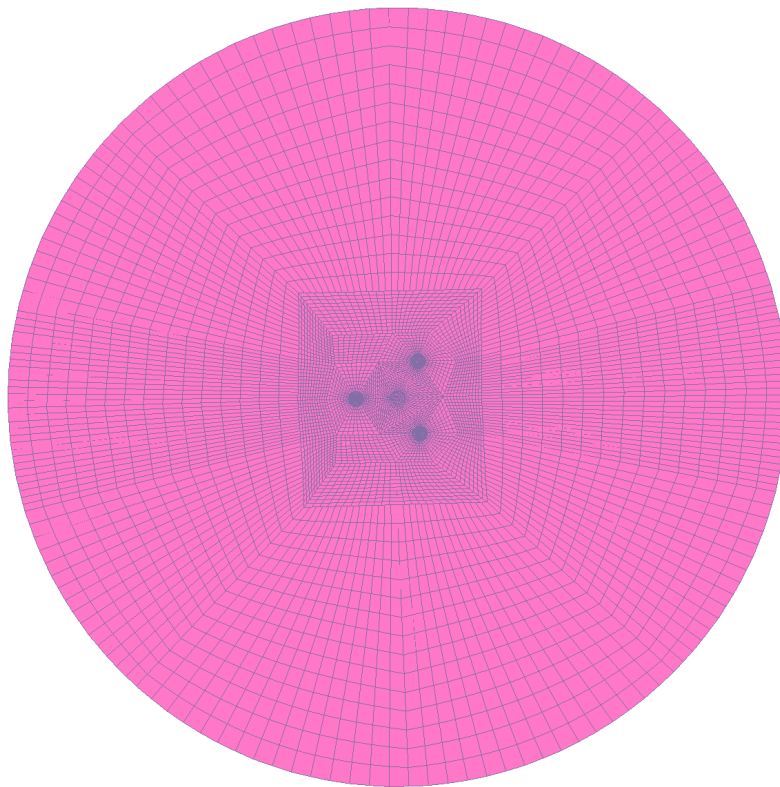


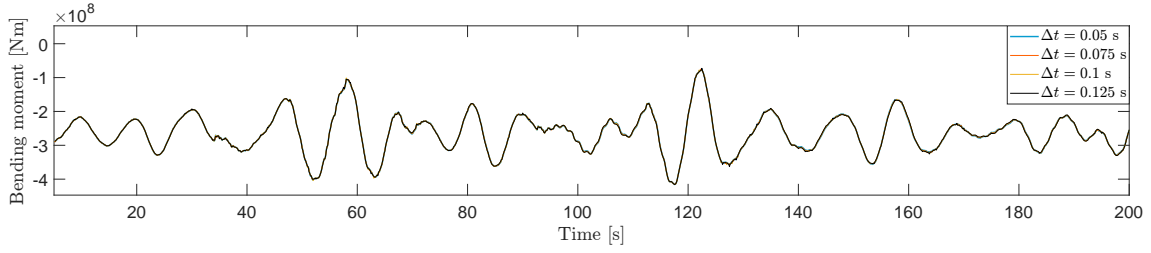
FIGURE 6.5: Surface mesh used for ULS analysis

6.1.2 Time step sensitivity analysis

A time step sensitivity analysis was also done. Table 6.7 shows the time steps that were used for this analysis and the relative difference between the same bending moment that was used for the surface mesh sensitivity. As is seen from Table 6.7, there is very little difference in the maximum bending moment when changing the time step. Figure 6.6 shows time histories for the different time steps and the differences between the solutions seems negligible. A time step of 0.1 s was used for further analysis.

TABLE 6.7: Time step sensitivity analysis

Time step Δt	0.05	0.075	0.1	0.125
Max My [Nm]	415650784	415524800	415516736	415758208
Relative error [%]	N/A	0.0303	0.0019	-0.0581


 FIGURE 6.6: Local bending moment M_y for different time steps

6.2 Sectional bending moments from time domain analysis

Table 6.8 shows the maximum bending moments M_y from all ten realisations in the cross sections defined in Table 6.2. M_y is given in the body frame coordinate system where origo for the different sections are defined in Table 6.2. The bending moments are given as absolute values.

 TABLE 6.8: Maximum bending moments M_y for 10 ULS realisations

Time realisation [-]	1	2	3	4	5	6	7	8	9	10
$M_{y,\max}$, Load cross section 1 [MNm]	584.9	513.0	529.0	523.1	513.1	527.9	524.4	546.4	522.6	513.1
$M_{y,\max}$, Load cross section 2 [MNm]	570.8	493.4	516.1	516.0	500.6	504.0	499.4	526.8	519.5	500.6
$M_{y,\max}$, Load cross section 3 [MNm]	565.2	497.0	525.0	511.3	505.9	519.1	503.6	515.8	522.7	505.9
$M_{y,\max}$, Load cross section 4 [MNm]	211.9	193.3	190.7	195.4	202.7	211.7	209.2	197.9	197.4	190.3

As seen from Table 6.8, the maximum bending moments are occurring for the first time realisation. The pontoon bending moment is seen to be largest at the cross section closest to the central column for all the cases.

The pontoon mean bending moments from all time realisations is seen in Table 6.9 below. The largest mean bending moment is occurring at the cross section closest to the outer column, while the lowest is occurring for the cross section closest to the central column. This is because the pontoon contributes to additional buoyancy which reduces the cross sectional bending moment closer to the central column. A still water analysis in HydroD was also run without any prescribed forces, wave elevation or motion and the same trend was seen here. The differences between the mean bending moments was even larger in this case and this is because of the additional fairlead mooring line force contribution. This bending moment contribution from the fairlead force increases towards the central column and therefore reduces these differences between the stillwater bending moments somewhat.

TABLE 6.9: Static bending moments in pontoons from still water analysis

Load cross section	1	2	3
$M_{y,\text{static}}$ [MNm]	-250.7	-260.0	-293.9

Even though the mean bending moments are larger towards the outer column, the maximum total bending moment is for all the realisations largest in cross section 1. This is because the dynamic bending moment contribution in this cross section is larger. If cross section 2 or cross section 3 have the largest bending moment seems to be more arbitrary.

The bending moments are relatively low at the central column. This is expected as the response is mainly wave driven in idling condition. Blades are pitched in order to minimize the aerodynamic loads and the influence of wind is therefore relatively low. In a case of power producing wind

turbine, the bending moment in the tower would be expected to be much larger.

6.3 Frequency domain comparison

Frequency analysis was done in Wadam with the same ULS sea state, defined in Table 5.1. Since no prescribed tower base forces is applied in Wadam, models of the floater with tower and top mass representation were used. Postresp was used to compute short term statistics for the analysis. Figure 6.7 shows the M_y bending moment spectra for load cross section 1, 2, 3 and 4 in Table 6.2.

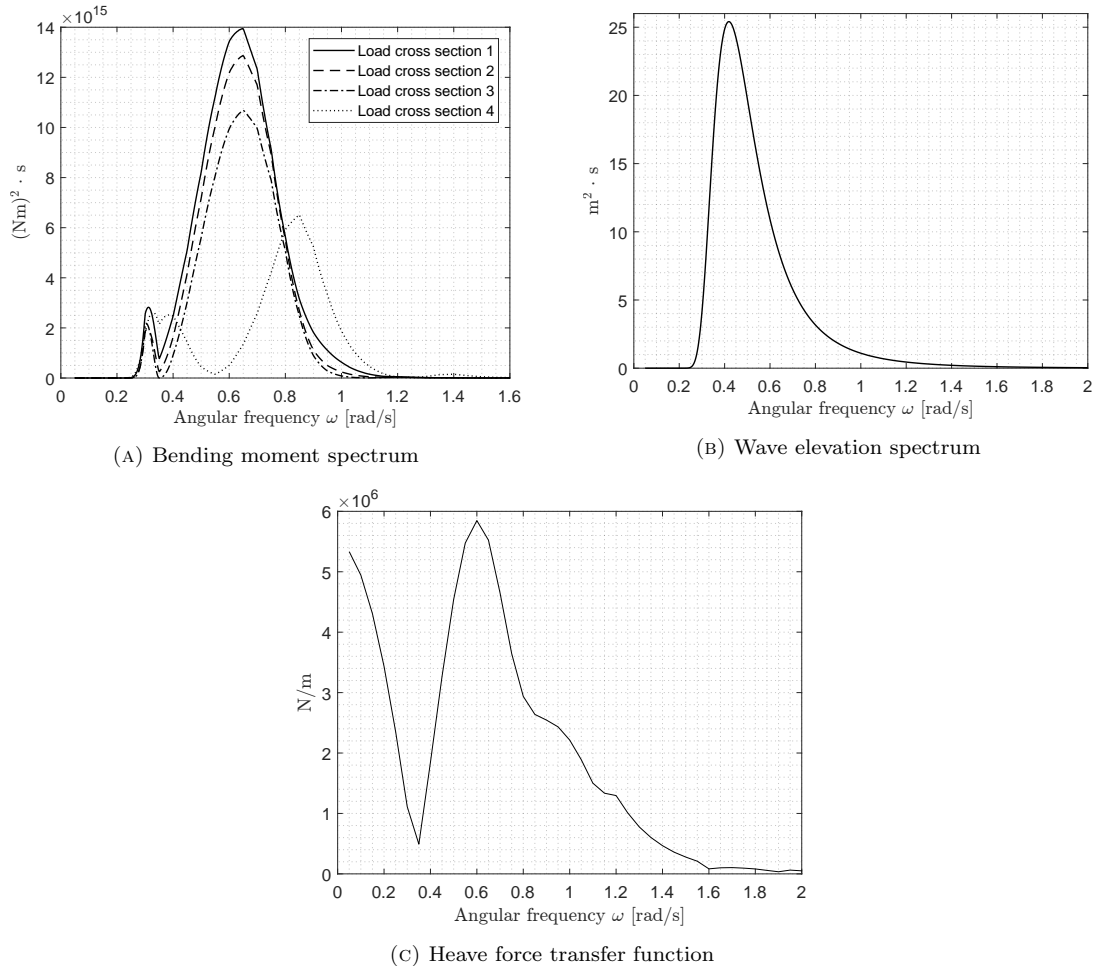


FIGURE 6.7: Data plots from Wadam frequency domain analysis

Most of the energy in the spectra for the three bending moments in the pontoons are located in a frequency range of approximately 0.5 rad/s - 0.9 rad/s. This is in the same region as the wave spectrum has most of its energy located.

A distinct peak can be found for the bending moment spectras at a frequency of 0.3 rad/s. This is the natural frequency in heave. The energy at this frequency is still relatively low since most of the energy in the wave spectrum is located outside this frequency.

The natural frequency in pitch is 0.2 rad/s. This natural frequency can however not be seen in the spectra. The reason for this is that there is no energy in the wave spectrum at this frequency. This is clearly seen in Figure 6.7b, where the spectrum is zero for 0.2 rad/s.

The spectra for the pontoon bending moments are seen to go towards 0 at approximately 0.35 rad/s. This cancellation is also seen in the RAO plots for heave and pitch in Figure 5.7 and is due

to cancellation of the heave force on the structure. This is clearly seen in the heave force transfer function in Figure 6.7c.

The spectrum for load cross section 4 is seen to go towards zero for a angular frequency of approximately 0.55 rad/s. This was somewhat unexpected since there is a lot of wave energy for this frequency. There is also no cancellation in the pitch RAO. The explanation is believed to be due to cancellation effects between the rotational inertia load and the gravity contribution from the mass of the tower and RNA when the structure pitches.

Short term statistical properties from Postresp does not take the static part of the solution into account, while the bending moments in Table 6.8 are for the dynamic and static parts of the solution added together. This means that the static bending moment have to be added to the statistics from Postresp. The static bending moment from a still water analysis in Wasim was therefore added to the results from Postresp.

Table 6.10 shows the mean maximum bending moments from the 10 ULS realisations in Table 6.8 at all four cross sections, together with the expected value of the largest maximum for the same cross sections from frequency domain analysis in Wadam. The expected value of largest maximum was computed using Equation 2.34 The mean-zero-upcrossing period T_x was given directly in Postresp and was used to compute the estimated number of bending moment maximas according to Equation 2.33. The bending moment variances were estimated using the 0th spectral moments which were also given from Postresp.

TABLE 6.10: Bending moments, time domain vs frequency domain

Load cross section	Pontoon			Tower base
	1	2	3	4
$\overline{M}_{y,\max}$, SIMA-WASIM	529.7	514.7	517.1	200.0
$E[M_{y,\max}]$, WADAM	453.5	464.1	493.2	187.9
Ratio [-]	1.17	1.11	1.05	1.06

Solutions for the expected largest bending moment estimates from time domain analyses and frequency domain analysis are seen to be relatively close. The results are for turbine in idling condition. In idling condition, the blades are twisted in an effort to minimize the aerodynamic loads on the turbine blades. The cross sectional floater responses are therefore mostly wave driven.

The bending moments from frequency domain analysis are seen to be non conservative. The time domain analysis has additional contributions from fairlead mooring line loads that has to be corrected for in a frequency domain analysis. The mooring line forces and aerodynamic forces along the tower and on the RNA also have an effect on the global motions of the floater, which in turn will have an effect on the hydrodynamic pressure distribution on the floater. This effect is however believed to be small, especially in the case of idling turbine.

The ratios between solutions from frequency domain analysis and from fully coupled Sima-Wasim analysis are seen to be slightly different for the three load cross sections. The difference is seen to be largest in the cross section closest to the central column and lowest for the cross section closest to the outer column.

The occurrence of slack in the mooring line going parallel to the x-axis was discussed in Section 5.1.2. The mooring line with slack is the mooring line with lowest load level of the three mooring lines since the structure is subjected to strong head wind and sea. The contributions from the two other mooring lines are therefore believed to be more important. Obtained results also seems reasonable and this problem is therefore not expected to have a major influence on the results.

For analyses with power producing wind turbine, the differences are believed to be much larger. Aerodynamic forces on the blades and tower as well as generator torque are then much larger. These effects are not taken into account in a frequency domain analysis and when these effects

become more and more important, the differences will also be larger.

It is important to stress that a frequency domain analysis is not, in any form, equivalent with a fully coupled analysis. A fully coupled analysis takes the simultaneous effect of wind, waves, current and mooring into account. This is a highly nonlinear analysis as opposed to a linear frequency domain analysis. The possibility of using frequency domain analysis could however be considered, especially for idling condition where the response is mainly wave driven. Cross sectional loads should then be multiplied with safety factors larger than those in Table 6.10 in order to obtain conservative values for e.g. bending moments.

7

CONCLUSION

This thesis has investigated a method of combining fully coupled Sima analysis and linear potential theory time domain analysis in Wasim for load transfer of FOWT substructures. Hydrodynamic coefficients from a frequency domain Wadam analysis of the floater are first sent to the floater representation in Sima. Coupled analysis is then carried out and wave elevation, floater motions and forces at the fairleads and tower base are transferred to a floater representation in Wasim for time domain potential flow analysis. This analysis gives the distributed hydro pressure on the floater which together with the prescribed data from Sima can be used to obtain cross sectional loads on the floater or for FEA.

Compatibility of the Sima model and the floater representation in Wasim was ensured by comparing RAOs. RAOs for surge, heave and pitch were compared and were more or less identical except some minor differences at the resonance peaks, which is expected.

The method of transferring data between coupled- and potential flow analysis was done in several steps. First, the input wave elevation from Sima was compared with the reproduced wave elevation in Wasim. Wasim is able reproduce the wave elevation, but how good is highly dependent on the number of wave components that is used to reproduce the wave. This can be specified in the wave elevation input files. More wave components can potentially increase computational time significantly and a sensitivity analysis could be highly beneficial in order to figure out if any wave components could be removed without losing too much information about the wave.

The force resultant in heave from Wasim when using the method of investigation was examined in order to verify correct static balance of forces in the model. This force resultant takes both static and dynamic force contributions into account which means that it should fluctuate with zero mean. This was seen to be the case which means that the buoyancy, weight and the static part of the prescribed forces are in balance.

The prescribed motion in Wasim was verified indirectly by comparing bending moments in a Sima model with simplified top mass representation, with an equivalent model in HydroD. No wind were used in the analysis. Wasim integrates loads from $+\infty$ along the z -axis which means that the tower base loads is calculated from the floater motion if no excitation loads are present above the tower base. The resulting bending moments from Sima and Wasim were almost exactly the same which indicates that motions have been transferred correctly.

Pressure mapping from the Wasim panel model to the structural model from time domain potential flow analysis was checked visually using Xtract. A challenge with this pressure mapping was the

bottom- and top slab modelling in the structural model. These were modelled with the "pizza box" approach, meaning that they are modelled using two separate plates for the top and bottom parts of the slabs, connected with side walls on the "thickness side". This gave good pressure mapping from the panel model, but is not realistic for structural finite element analysis since the top and bottom plating have independent degrees of freedom.

Correctly applied prescribed forces from Sima in the Wasim analysis was checked by collecting cross sectional loads in the vicinity of the applied loads. Comparison between the applied forces and the cross sectional loads strongly indicates that forces have been applied correctly.

The method of investigation was used for obtaining cross sectional M_y bending moments along the pontoon being parallel with the x-axis and in the central shaft for a ULS condition with idling turbine. 10 time realisations were done and the maximum pontoon bending moment occurred at the cross section closest to the central shaft in all cases. The bending moment in the tower base were much lower than in the pontoon which is expected in idling condition.

The mean maximum bending moments from all the time realisations were also compared to the expected largest bending moments from a frequency domain analysis in Wadam. The resulting bending moments were similar in magnitude. The largest ratio between the bending moments from Wadam and the time realisations were found in the cross section closest to the central column with a value of 1.17.

The overall conclusion from investigating the proposed method is that the method works as intended and that it is straightforward to implement.

8

FURTHER WORK

This thesis has presented the work done in running analysis with a combination of fully coupled analysis in Sima and time domain potential flow analysis in Wasim. Time integration is highly time consuming and many more investigations could be done if having more time in hand.

Investigation of hull flexibility The method investigated in this thesis uses the rigid body approximation for the floater. Future work should include comparing results obtained from the rigid body approximation with methods which takes hull flexibility into account. One possible method is to make an equivalent beam model in Sima, where radiation and diffraction pressures are assigned to each individual beam element from a Wamit analysis.

Nonlinear wave elevation Wasim analysis can also be run with nonlinear wave elevation, which could give valuable insight into the effect of higher order waves. It is also expected that the surface mesh density has a larger effect on results obtained from second order wave elevation. The same goes for the mesh density needed on the panel model around the water plane area in order to capture the second order wave elevation. Sensitivity analyses should therefore be run for these mesh properties before evaluating results.

Stress analysis The ULS results presented in chapter 6 does not by any means represent a complete ULS assessment. A stress analysis should be carried out in order to investigate the structural integrity of the structure. "Load transfer" must then be used in Wasim, which means that panel pressures on the structure are stored for FEA after the time domain analysis has been executed.

Using load transfer for the whole time duration of the analysis is not feasible due to the vast amount of data that needs to be stored. Time intervals of interest where structural analysis is done therefore have to be decided in advance before running the analysis. A way to do this is to first run analysis without load transfer and find where cross sectional loads are critical. New time domain analyses with load transfer should then be run for these time intervals before structural analysis is done in Sestra.

Cross sectional loads using load cross sections of finite extent A limitation of using "Load cross sections" in Wasim is that the load cross sections are of infinite extent. This means that e.g. a load cross section in the xy-plane for one of the outer columns would also include the forces in the other four remaining columns. The DNV software Cutres can be used to make load cross sections of finite extent. This should be explored further if investigating cross sectional loads in the outer columns or in the central column where a infinite plane intersects the outer columns.

Floater slab/heaveplate modelling Problems with modelling the top- and bottom slabs for the OO-Star in a realistic manner for structural FEA was discussed in Section 5.2.4.

A possible solution could be to introduce master-slave relationships between DOFs in the upper and lower plates for the slabs. The upper and lower parts would then move together, which would be more realistic than having independent DOFs.

DNV also made it clear in personal communication that the newest version of Wadam has a new element type called "dipole elements". According to DNV, "dipole elements" are suitable for these types of problems. Dipole elements is not yet incorporated in Wasim, but is believed to be implemented in future versions. This could be worth looking further into in future similar investigations.

BIBLIOGRAPHY

- ALEXANDRE, A. et al. (2018). ‘Methodology for calculating floating offshore wind foundation internal loads using bladed and a finite element analysis software’. In: *International Conference on Offshore Mechanics and Arctic Engineering*. Vol. 51319. American Society of Mechanical Engineers, V010T09A084.
- ARAPOGIANNI, ATHANASIA ET. AL. (2013). *Deep water - the next step for offshore wind energy*. Tech. rep. Rue d’Arlon 80. URL: https://windeurope.org/wp-content/uploads/files/about-wind/reports/Deep_Water.pdf.
- BACHYNSKI-POLIĆ, E. E. (2021a). LECTURE NOTES: *Basic aerodynamics for wind turbines*. Can be obtained by request to erin.bachynski@ntnu.no.
- BACHYNSKI-POLIĆ, E. E. (2021b). LECTURE NOTES: *Coupled analysis (1)*. Can be obtained by request to erin.bachynski@ntnu.no.
- BACHYNSKI-POLIĆ, E. E. (2021c). LECTURE NOTES: *Lecture 3 - aerodynamics and turbine controller*. Can be obtained by request to erin.bachynski@ntnu.no.
- BACHYNSKI-POLIĆ, E. E. and GAO, Z. (2021). LECTURE NOTES: *Introduction to offshore wind power and technology*. Can be obtained by request to erin.bachynski@ntnu.no.
- BJERKSETER, C. and ÅGOTNES, A. (2013). ‘Levelised costs of energy for offshore floating wind turbine concepts’. MA thesis. Norwegian University of Life Sciences, Ås.
- BORG, M., BREDMOSE, H. and HANSEN, A. M. (2017). ‘Elastic deformations of floaters for offshore wind turbines: dynamic modelling and sectional load calculations’. In: *International Conference on Offshore Mechanics and Arctic Engineering*. Vol. 57786. American Society of Mechanical Engineers, V010T09A044.
- BORG, M., HANSEN, A. M. and BREDMOSE, H. (2016). ‘Floating substructure flexibility of large-volume 10MW offshore wind turbine platforms in dynamic calculations’. In: *Journal of physics: Conference series*. Vol. 753. 8. IOP Publishing, p. 082024.
- BRETON, S.-P. and MOE, G. (2009). ‘Status, plans and technologies for offshore wind turbines in Europe and North America’. In: *Renewable Energy* 34.3, pp. 646–654. DOI: <https://doi.org/10.1016/j.renene.2008.05.040>. URL: <https://www.sciencedirect.com/science/article/pii/S0960148108002243>.
- BRITISH STANDARD et al. (2002). ‘Eurocode—Basis of structural design’. In: *Eurocode 0*.
- BURTON, T. et al. (2011). *Wind energy handbook*. John Wiley & Sons.
- CARTWRIGHT, D. E. and LONGUET-HIGGINS, M. S. (1956). ‘The statistical distribution of the maxima of a random function’. In: *Proceedings of the royal society of london. series a. mathematical and physical sciences* 237.1209, pp. 212–232.
- CASTRO-SANTOS, L. and DIAZ-CASAS, V. (2016). *Floating offshore wind farms*. Springer.
- CHAKRABARTI, S. K. (1987). *Hydrodynamics of offshore structures*. WIT press.
- CHAKRABARTI, S. K. (2005). *Handbook of Offshore Engineering (2-volume set)*. Elsevier.

- COCHRAN, W. T. et al. (1967). ‘What is the fast Fourier transform?’ In: *Proceedings of the IEEE* 55.10, pp. 1664–1674.
- COOLEY, J. W. and TUKEY, J. W. (1965). ‘An algorithm for the machine calculation of complex Fourier series’. In: *Mathematics of computation* 19.90, pp. 297–301.
- CUMMINS, W., IJHHL, W. and UINM, A. (1962). ‘The impulse response function and ship motions’. In.
- DEWAR, M. J. S. and LONGUET-HIGGINS, H. C. (1952). ‘The correspondence between the resonance and molecular orbital theories’. In: *Proceedings of the Royal Society of London. Series A. Mathematical and Physical Sciences* 214.1119, pp. 482–493.
- DNV (2020). *Floating wind: the power to commercialize*. Tech. rep. Veritasveien 1. URL: <https://www.dnv.com/focus-areas/floating-offshore-wind/commercialize-floating-wind-report.html>.
- DNV (2021). USER MANUAL: *Xtract - Postprocessor for Presentation, Animation and Reporting of Results*. (Visited on 6th June 2022).
- DNV (2022a). USER MANUAL: *HydroD - Wave load & stability analysis of fixed and floating structures*. (Visited on 4th Mar. 2022).
- DNV (2022b). USER MANUAL: *Postresp - Postprocessor for Statistical Response Calculations*. (Visited on 23rd May 2022).
- DNV (2022c). USER MANUAL: *Sesam - Software suite for hydrodynamic and structural analysis of renewable, offshore and maritime structures*. URL: https://www.dnv.com/Images/Sesam-Feature-Description_tcm8-58834.pdf (visited on 8th Dec. 2021).
- DNV (2022d). USER MANUAL: *Sestra - Finite element analysis solver*. (Visited on 6th June 2022).
- DNV (2022e). USER MANUAL: *Wasim - Wave Loads on Vessels with Forward Speed (Valid from V6.3)*. (Visited on 21st Feb. 2022).
- DURAKOVIC, A. (2021a). *10+ MW Floating Wind Turbine Project Kicks Off*. URL: <https://www.offshorewind.biz/2020/09/30/10-mw-floating-wind-turbine-project-kicks-off/> (visited on 7th Dec. 2021).
- DURAKOVIC, A. (2021b). *World’s Largest Floating Offshore Wind Farm Fully Operational*. URL: <https://www.offshorewind.biz/2021/10/19/worlds-largest-floating-offshore-wind-farm-fully-operational/> (visited on 7th Dec. 2021).
- ENERGIAS DE PORTUGAL (2018). *WindFloat Atlantic*. URL: <https://www.edp.com/en/innovation/windfloat>.
- EOLINK (2021). *First prototype*. URL: <http://eolink.fr/en/article-fp-en> (visited on 7th Dec. 2021).
- EQUINOR (2017). *Skapte historie sammen, Ti år siden fusjonen - hva har skjedd?* URL: <https://www.equinor.com/no/about-us/ten-year-merger.html>.
- EQUINOR (2021). *Hywind Tampen: verdens første fornybare kraftkilde for olje- og gassvikrsomhet til havs*. URL: <https://www.equinor.com/no/what-we-do/hywind-tampen.html> (visited on 7th Dec. 2021).
- EUROPEAN COMISSION (2021). *Renewable energy directive*. URL: https://ec.europa.eu/energy/topics/renewable-energy/directive-targets-and-rules/renewable-energy-directive_en (visited on 7th Nov. 2021).
- FALTINSEN, O. M. (1993). *Sea loads on ships and offshore structures*. Vol. 1. Cambridge university press.
- FALTINSEN, O. M. (2005). *Hydrodynamics of high-speed marine vehicles*. Cambridge university press.
- GLOBAL WIND ENERGY COUNCIL (2021a). *Global Offshore Wind Report 2021*. Tech. rep. Rue de Commerce 31 - 1000 Brussels. URL: <https://gwec.net/global-offshore-wind-report-2021/>.

- GLOBAL WIND ENERGY COUNCIL (2021b). *Global Wind Report 2021*. Tech. rep. Rue de Commerce 31 - 1000 Brussels. URL: <https://gwec.net/global-wind-report-2021/>.
- GUIGNIER, L. et al. (2016). ‘Multibody modelling of floating offshore wind turbine foundation for global loads analysis’. In: *The 26th International Ocean and Polar Engineering Conference*. OnePetro.
- HAN, K., VADA, T. and WANG, Q. (2018). ‘Time Domain Coupled Analysis and Load Transfer for Floating Wind Turbine Structures’. In: *International Conference on Offshore Mechanics and Arctic Engineering*. Vol. 51203. American Society of Mechanical Engineers, V001T01A027.
- HANSEN, M. (2015). *Aerodynamics of wind turbines*. Routledge.
- HANSEN, M. O. (2015). *Aerodynamics of wind turbines*. eng. London.
- HASSELMANN, K. et al. (1973). ‘Measurements of wind-wave growth and swell decay during the Joint North Sea Wave Project (JONSWAP)’. In: *Ergaenzungsheft zur Deutschen Hydrographischen Zeitschrift, Reihe A*.
- HESS, J. L. and SMITH, A. (1962). ‘Calculation of non-lifting potential flow about arbitrary three-dimensional bodies’. In: *Journal of Ship Research* 8, pp. 22–44.
- HOFFMAN, D. and KARST, O. J. (Sept. 1975). ‘The Theory of the Rayleigh Distribution and Some of Its Applications’. In: *Journal of Ship Research* 19.03, pp. 172–191. DOI: 10.5957/jsr.1975.19.3.172. eprint: <https://onepetro.org/JSR/article-pdf/19/03/172/2234496/sname-jsr-1975-19-3-172.pdf>. URL: <https://doi.org/10.5957/jsr.1975.19.3.172>.
- HOLTHUIJSEN, L. H. (2007). *Waves in Oceanic and Coastal Waters*. eng. Vol. 9780521860284. Cambridge: Cambridge University Press.
- IDEOL, B. (2021). *A floating foundation that pushes the boundaries of offshore wind*. URL: <https://www.bw-ideol.com/en> (visited on 7th Dec. 2021).
- IEA (2019). *Offshore Wind Outlook 2019*. Tech. rep. 9 rue de la Fédération. URL: https://iea.blob.core.windows.net/assets/495ab264-4ddf-4b68-b9c0-514295ff40a7/Offshore_Wind_Outlook_2019.pdf.
- IRENA (2016). *Floating foundations: A game changer for offshore wind power*.
- JONKMAN, B. J. and KILCHER, L. (2022). USER MANUAL: *TurbSim User’s GUIDE: Version 1.06.00*. (Visited on 10th Apr. 2022).
- JOURNEE, J. and MASSIE, W. (2000). *Offshore hydromechanics*. Undefined/Unknown. Vol. first edition. CITG Section Hydraulic Engineering (j2005).
- KREYSZIG, E. (2006). *Advanced engineering mathematics, 9th edition*. John Wiley & Sons.
- KVITTEM, M. I. (Nov. 2014). ‘Modelling and response analysis for fatigue design of a semi-submersible wind turbine’. PhD thesis.
- LARSEN, C. M. et al. (2019). *Marine Dynamics compendium, TMR4182 Marine dynamics*. Department of Marine Technology, NTNU.
- LIFES50+ (2021). *Lifes50+ - Innovative floating offshore wind energy*. URL: <https://lifes50plus.eu/> (visited on 7th Nov. 2021).
- MANWELL, J. F., MCGOWAN, J. G. and ROGERS, A. L. (2010). *Wind energy explained: theory, design and application*. John Wiley & Sons.
- MANWELL, J. F., MCGOWAN, J. G. and ROGERS, A. L. (2009). *Wind energy explained*. John Wiley & Sons.
- MORISON, J., JOHNSON, J. and SCHAAF, S. (1950). ‘The force exerted by surface waves on piles’. In: *Journal of Petroleum Technology* 2.05, pp. 149–154.
- NEWLAND, D. E. (2012). *An introduction to random vibrations, spectral & wavelet analysis*. Courier Corporation.
- NEWMAN, J. N. (2018). *Marine hydrodynamics*. The MIT press.

- PAIK, J. K. and THAYAMBALLI, A. K. (2003). *Ultimate limit state design of steel-plated structures*. John Wiley & Sons.
- RICE, S. O. (1944). ‘Mathematical analysis of random noise’. In: *The Bell System Technical Journal* 23.3, pp. 282–332.
- RICE, S. O. (1945). ‘Mathematical analysis of random noise’. In: *The Bell System Technical Journal* 24.1, pp. 46–156.
- SEATWIRL (2021). *SeaTwirl S2 1 MW floating offshore wind demonstrator*. URL: <https://webgate.ec.europa.eu/maritimeforum/en/node/5468> (visited on 7th Dec. 2021).
- SILVA DE SOUZA, C. E. and BACHYNSKI, E. E. (2020). ‘Effects of hull flexibility on the structural dynamics of a tension leg platform floating wind turbine’. In: *Journal of Offshore Mechanics and Arctic Engineering* 142.1, p. 011903.
- SINTEF OCEAN (2022a). USER MANUAL: *RIFLEX 4.20.2 Theory Manual*. (Visited on 24th Feb. 2022).
- SINTEF OCEAN (2022b). USER MANUAL: *SIMO 4.20.2 Theory Manual*. (Visited on 23rd May 2022).
- SKAARE, B. et al. (2015). ‘Analysis of measurements and simulations from the Hywind Demo floating wind turbine’. In: *Wind Energy* 18.6, pp. 1105–1122.
- STIESDAL (2021). *The TetraSpar full-scale demonstration project*. URL: <https://www.stiesdal.com/offshore-technologies/the-tetraspar-full-scale-demonstration-project/> (visited on 7th Dec. 2021).
- SVENDSEN, K. F. (2016). ‘Structural design and dynamic analysis of a tension leg platform wind turbine, considering elasticity in the hull’. MA thesis. NTNU.
- UZUNOGLU, E., KARMAKAR, D. and GUEDES SOARES, C. (2016). ‘Floating Offshore Wind Platforms’. In: *Floating Offshore Wind Farms*. Ed. by L. CASTRO-SANTOS and V. DIAZ-CASAS. Cham: Springer International Publishing, pp. 53–76. DOI: 10.1007/978-3-319-27972-5_4. URL: https://doi.org/10.1007/978-3-319-27972-5_4.
- WAFO GROUP (2022). USER MANUAL: *WAFO - a Matlab Toolbox for Analysis of Random Waves and Loads*. (Visited on 23rd May 2022).
- WHITFIELD, S. (Jan. 2020). ‘Offshore Wind: The New Frontier in Powering Platforms?’ In: *Journal of Petroleum Technology* 72.01, pp. 38–40. DOI: 10.2118/0120-0038-JPT. eprint: <https://onepetro.org/JPT/article-pdf/72/01/38/2215990/spe-0120-0038-jpt.pdf>. URL: <https://doi.org/10.2118/0120-0038-JPT>.
- YU, W., MÜLLER, K. and LEMMER, F. (2018). *Qualification of innovative floating substructures for 10MW wind turbines and water depths greater than 50m*. Tech. rep. URL: https://lifes50plus.eu/wp-content/uploads/2018/04/GA.640741.LIFES50_D4.2.pdf.

APPENDIX

A *SIMA_timeseries.m* by Erin Bachynski Polić

```
1 % Makes wave elevation time series for SIMA.
2
3 close all
4 clear all
5 clc
6
7 % Angular frequencies to use
8 omegas = 0.2:0.05:3.0;
9
10 % Matrix with pairs of wave heights H and wave periods T
11 % H_T = zeros(2, length([0.05:0.05:3.00]));
12 H_T = zeros(2, length(omegas));
13
14 % Wave periods
15 % H_T(1, :) = 2*pi./[0.05:0.05:3.00];
16 H_T(1, :) = 2*pi./omegas;
17
18 % Wave heights
19 H_T(2, :) = 2;
20
21 % reg wave H=7.1m, T=12.1s
22 % reg wave H=4m, T=9s
23 dt = 0.1;
24 tic
25
26 test = zeros(length(H_T));
27
28 for iwave = 1:length(H_T)
29
30     % Wave amplitude and angular frequency
31     amp = H_T(2, iwave)/2;
32     w = omegas(iwave);
33     % w = 2*pi/H_T(1, iwave);
34
35     tlength = 1000; % applied time series length SIMA
36
37     % Time series from SIMA
38     t = linspace(0, 1638.4, 16384 + 1);
39     eta = amp*cos(w*t);
40
41     % add a ramp
42     Twave = H_T(1, iwave);
43     % Twave = 2*pi/w;
44     tramp = min(10*Twave,200);
45     iendramp = sum(t<tramp);
46     rampfac = t(1:iendramp)/t(iendramp);
47     eta(1:iendramp)=eta(1:iendramp).*rampfac;
48
49 % figure
50 % plot(t,eta)
51 fid = fopen(sprintf('%s%.1f%s%i%s', 'wave', iwave, 'H', amp*2, '.asc'), 'w');
52 fprintf(fid, '%d\n', length(eta));
```

```
53     fprintf(fid, '%f\n', dt);
54     fprintf(fid, '%s\n', date);
55     fprintf(fid, '%s\n', 'regular waves');
56     for ii = 1:length(eta)
57         fprintf(fid, '%f\n', eta(ii));
58     end
59     fclose(fid);
60
61     test(iwave) = w;
62
63 end
64 toc
```

B *bpass.m* by Halvor Lie

```
1 function xbp = bpass(x, dt, flow, fhigh)
2 %-----
3 % BPASS - Matlab function that will band-pass filter time series stored as
4 %     columns in a matrix.
5 %
6 %     bp = bpass(x, dt, flow, fhigh)
7 %
8 %     x(1:nsamples, 1:ntimeseries) = timeseries matrix
9 %     dt = time step (s)
10 %     flow and fhigh = lower and upper cut-off frequencies, respectively (Hz)
11 %     xbp = band-pass filtered time series
12 % H. Lie, Marintek, 09.04.2002
13 % KEK, 2006-01-13: Minor changes
14 %-----
15 nsamples = length(x(:, 1));
16 domega = 2*pi/(dt*nsamples);           % Frequency interval (rad/s)
17 %
18 % Make frequency array:
19 %
20 Omega = zeros(nsamples, 1);
21 %
22 if ~rem(nsamples, 2),                 % Even number of samples
23     nh = nsamples/2;
24     Omega(1:nh+1) = domega*(0:nh);
25     Omega(nh+2:nsamples) = domega*(-nh+1:-1);
26 else
27     nh = (nsamples-1)/2;
28     Omega(1:nh+1) = domega*(0:nh);
29     Omega(nh+2:nsamples) = domega*(-nh:-1);
30 end
31 %
32 Fx = fft(x);                          % Discrete frequency transform
33 %
34 %---- Band-pass filter signals ----
35 %
36 % Indices corresponding to frequencies to be filtered off:
37 %
38 Ioff = find(abs(Omega) < flow*2*pi | abs(Omega) > fhigh*2*pi);
39
40 Z = zeros(size(Ioff, 1), size(x, 2));  % Block of zeros to be inserted
41 Fx(Ioff, :) = Z;                       % Zero out unwanted components
42 %
43 xbp = real(ifft(Fx));                  % Transform back to time domain.
44
```

C Correct gravity and buoyancy implementation in Sima

The expression for the hydrostatic restoring coefficient C_{55} for a floating structure is given in Equation 1 below. As is seen from the expression, the restoring force has contributions from the

weight of the structure, the buoyancy of the structure and one waterplane stiffness contribution.

$$C_{55} = C_{44} = \rho g I_{wp} + \rho g \Delta z_B - mg z_G \quad (1)$$

The tower, RNA and mooring lines are typically modelled separately from the substructure in Sima using a combination of finite elements for the tower, blades and mooring lines and rigid body representation for the hub, nacelle and substructure.

The tower, RNA and mooring lines have their own mass properties such as total mass, COG, rotational inertias etc. The substructure in Sima therefore has to be assigned the mass properties of the floater alone and not including the other parts of the structure. The same also goes for the hydrostatic stiffness matrix. Equation 1 has to be found using z_G and z_B for the floater alone if the Sima input for the substructure is to be correct. This is important to correct for if a hydrostatic analysis has been carried out for the substructure including the tower and RNA. The output mass values from this analysis will then be wrong since they are not for the floater alone.

Furthermore, there exist some different methods for implementing buoyancy correctly in Sima. This may also make it necessary to modify the hydrostatic stiffness matrix from an initial hydrostatic analysis. This is explained in the following.

When modelling the rigid substructure, it must be decided whether the option "Gravity Included" is to be used or not. If "Gravity Included" is used, Sima will make no assumptions regarding the buoyancy of the substructure. In order to get the correct buoyancy in the model, the total buoyancy force must then be added as a specified force in COB in Sima. The stiffness contribution from buoyancy in Equation 1 is then taken into account directly by this specified force and must be removed from the stiffness in order to not count this effect twice.

If "Gravity Included" is not used, Sima will assume that the buoyancy force on the floater is equal to the gravity force on the floater. This will result in a buoyancy force that is too small since this buoyancy will only balance out the gravity force from the floater. In reality it must carry the weight of the floater, the tower, the RNA and the vertical mooring pre-tension at fairlead. An additional buoyancy force equal to the total weight of the tower, the RNA and the vertical mooring pre-tension at fairlead must then be specified as a point force in Sima. This additional buoyancy force will ensure static equilibrium of the structure. C_{55} and C_{44} does not need to be modified if this force is put in the flotation point of the structure since this will give no restoring moment if the floater rotates. If it is specified somewhere else, C_{44} and C_{55} will have to be modified.

D .wnd input file for TurbSim turbulent wind generation

```

1 TurbSim Input File. Valid for TurbSim v1.50, 25-Sep-2009; Input File for Certification Test #3
  ↳ (Kaimal Spectrum, formatted FF files).
2
3 -----Runtime Options-----
4 501485150          RandSeed1          - First random seed (-2147483648 to 2147483647)
5 1456975012        RandSeed2          - Second random seed (-2147483648 to 2147483647) for intrinsic
  ↳ pRNG, or an alternative pRNG: "RanLux" or "RNSNLW"
6 False            WrBHHTP            - Output hub-height turbulence parameters in GenPro-binary form?
  ↳ (Generates RootName.bin)
7 False            WrFHHTP            - Output hub-height turbulence parameters in formatted form?
  ↳ (Generates RootName.dat)
8 False            WrADHH             - Output hub-height time-series data in AeroDyn form? (Generates
  ↳ RootName.hh)
9 False            WrADFF             - Output full-field time-series data in TurbSim/AeroDyn form?
  ↳ (Generates RootName.bts)
10 True            WrBLFF             - Output full-field time-series data in BLADED/AeroDyn form?
  ↳ (Generates RootName.wnd)
11 False           WrADTWR            - Output tower time-series data? (Generates RootName.twr)
12 False           WrFMTHFF           - Output full-field time-series data in formatted (readable) form?
  ↳ (Generates RootName.u, RootName.v, RootName.w)
13 False           WrACT              - Output coherent turbulence time steps in AeroDyn form? (Generates
  ↳ RootName.cts)

```

```

14 True           Clockwise      - Clockwise rotation looking downwind? (used only for full-field
↳ binary files - not necessary for AeroDyn)
15 0             ScaleIEC        - Scale IEC turbulence models to exact target standard deviation?
↳ [0=no additional scaling; 1=use hub scale uniformly; 2=use individual scales]
16
17 -----Turbine/Model Specifications-----
18 32            NumGrid_Z       - Vertical grid-point matrix dimension
19 32            NumGrid_Y       - Horizontal grid-point matrix dimension
20 0.05          TimeStep        - Time step [seconds]
21 12000.0       AnalysisTime    - Length of analysis time series [seconds] (program will add
↳ time if necessary: AnalysisTime = MAX(AnalysisTime, UsableTime+GridWidth/MeanHHWS) )
22 12000.0       UsableTime      - Usable length of output time series [seconds] (program will
↳ add GridWidth/MeanHHWS seconds)
23 119.00        HubHt           - Hub height [m] (should be > 0.5*GridHeight)
24 200.00        GridHeight      - Grid height [m]
25 200.00        GridWidth       - Grid width [m] (should be >= 2*(RotorRadius+ShaftLength))
26 0             VFlowAng        - Vertical mean flow (uptilt) angle [degrees]
27 0             HFlowAng        - Horizontal mean flow (skew) angle [degrees]
28
29 -----Meteorological Boundary Conditions-----
30 "IECKAI"      TurbModel        - Turbulence model ("IECKAI"=Kaimal, "IECVKM"=von Karman, "GP_LLJ",
↳ "NWTCCUP", "SMOOTH", "WF_UPW", "WF_07D", "WF_14D", or "NONE")
31 "3"          IECstandard     - Number of IEC 61400-x standard (x=1,2, or 3 with optional 61400-1
↳ edition number (i.e. "1-Ed2") )
32 8.9           IECturbc        - IEC turbulence characteristic ("A", "B", "C" or the turbulence
↳ intensity in percent) ("KHTEST" option with NWTCCUP, not used for other models)
33 "NTM"        IEC_WindType     - IEC turbulence type ("NTM"=normal, "xETM"=extreme turbulence,
↳ "xEWM1"=extreme 1-year wind, "xEWM50"=extreme 50-year wind, where x=wind turbine class 1, 2, or
↳ 3)
34 default      ETMc            - IEC ETM "c" parameter [m/s] (or "default")
35 "PL"         WindProfileType - Wind profile type ("JET"=Low-level
↳ jet, "LOG"=Logarithmic, "PL"=Power law, or "default")
36 119.00        RefHt            - Height of the reference wind speed [m]
37 39.6          URef            - Mean (total) wind speed at the reference height [m/s]
38 350           ZJetMax         - Jet height [m] (used only for JET wind profile, valid 70-490 m)
39 0.11          PLExp           - Power law exponent (or "default")
40 0.0003        Z0             - Surface roughness length [m] (or "default")
41
42 -----Non-IEC Meteorological Boundary Conditions-----
43 default      Latitude        - Site latitude [degrees] (or "default")
44 0.05          RICH_NO         - Gradient Richardson number
45 default      UStar           - Friction or shear velocity [m/s] (or "default")
46 default      ZI             - Mixing layer depth [m] (or "default")
47 default      PC_UW           - Mean hub u'w' Reynolds stress (or "default" or "none")
48 default      PC_UV           - Mean hub u'v' Reynolds stress (or "default" or "none")
49 default      PC_VW           - Mean hub v'w' Reynolds stress (or "default" or "none")
50 default      IncDec1         - u-component coherence parameters (e.g. "10.0 0.3e-3" in quotes)
↳ (or "default")
51 default      IncDec2         - v-component coherence parameters (e.g. "10.0 0.3e-3" in quotes)
↳ (or "default")
52 default      IncDec3         - w-component coherence parameters (e.g. "10.0 0.3e-3" in quotes)
↳ (or "default")
53 default      CohExp          - Coherence exponent (or "default")
54
55 -----Coherent Turbulence Scaling Parameters-----
56 ".\EventData" CTEventPath    - Name of the path where event data files are located
57 random       CTEventFile    - Type of event files ("random", "les" or "dns")
58 true         Randomize       - Randomize disturbance scale and location? (true/false)
59 1.0          DistScI         - Disturbance scale (ratio of dataset height to rotor disk).
60 0.5          CTly            - Fractional location of tower centerline from right (looking
↳ downwind) to left side of the dataset.
61 0.5          CTLz            - Fractional location of hub height from the bottom of the dataset.
62 30.0         CTStartTime     - Minimum start time for coherent structures in RootName.cts
↳ [seconds]
63
64 =====
65 NOTE: Do not add or remove any lines in this file!
66 =====

```

E Buoyancy correction force in Sima

E.1 Estimation of vertical pretension at fairlead

The vertical pretension at fairlead is equal to the mass in water of the mooring line part that is not resting on the ground. The list below summarizes the procedure on how this vertical pretension was estimated.

1. The node "dummy1" serves as the floater connection and floater origo. Fix this node to its initial position (0 m, 0 m, 0 m).
2. Run static calculation in Sima with "dummy1" fixed. After completion of the static analysis, the mooring lines should have the correct equilibrium configuration at the design draft of 22 m.
3. Find the mooring line length of the part that is not resting on the ground by taking the whole line length and subtracting the part that is resting on the ground. The length of the line that is resting on the ground was found by plotting the static line configuration of one of the mooring lines.
4. Multiply the mooring line length of the part not resting on the ground with the mass coefficient for the mooring lines that is specified in Sima and add the clump weight. These masses should be mass in water in order to account for buoyancy.

Figure A1 shows the resulting static configuration of one of the mooring lines after fixing the node "dummy1" to (0 m, 0 m, 0 m). This is the mooring line that is laying in the xz-plane in its initial position and the line length resting on the ground can therefore easily be found by reading of the touch down point in the plot.

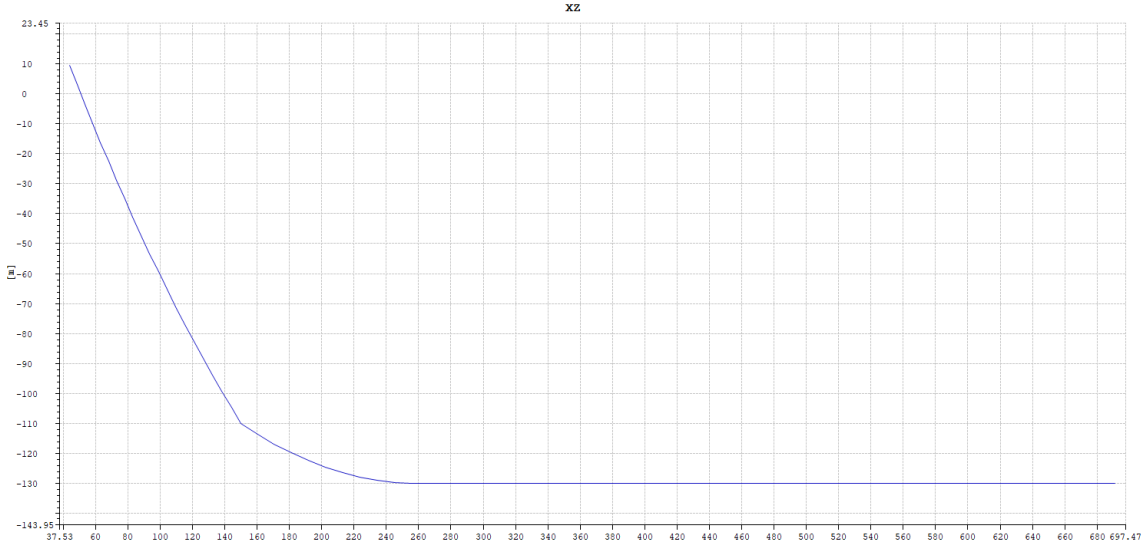


FIGURE A1: Static mooring line configuration of the mooring line in the xz-plane

The anchor point radius is seen in Section 3.4, Table 3.4 to be 691 m and the radius of the touch down point is seen to be at approximately 250 m when reading of the plot. The mooring line length resting on the ground is therefore 691 m - 250 m = 441 m. The total mooring line length is seen in Table 3.4 to be 703 m. This means that the line length not resting on the ground is 703 m - 441 m = 262 m. The mass of the mooring lines not resting on the ground is now easily found by multiplying this line length with the mass coefficient of the mooring line chain cross section and adding the clump weight which is located at 118 meters down on the mooring line. The mass

coefficient of the mooring line cross section and the clump weight in Sima were given as mass in water and buoyancy will therefore also be taken into account in a proper way. The mass coefficient of the mooring line chain cross section and the clump weight in water are seen in the MatLab code *buoyancy_correction.m* below to be 375.38 kg/m and 51025 kg respectively. The calculation of the vertical pretension can also be found in the script *buoyancy_correction.m* below. The vertical pretension of one line was found to be $1.4654 \cdot 10^6$ N and hence the total buoyancy correction force was calculated to be $3 \cdot 1.4654 \cdot 10^6 = 4.3961 \cdot 10^6$ N.

E.2 *buoyancy_correction.m*

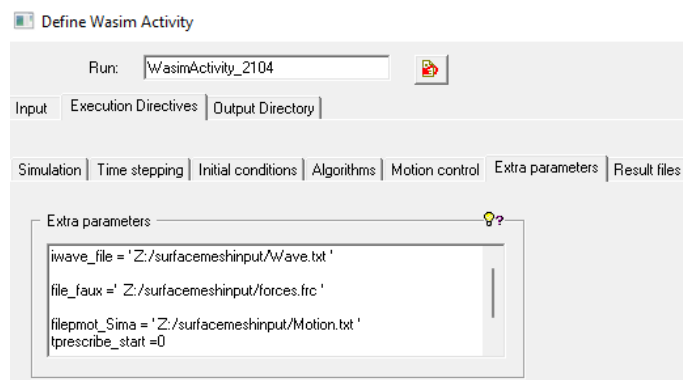
```

1  %% Mass directly from Sima
2
3  m_SIMA_tower = 1.2561*10^6; % Mass of the tower line in Sima
4  m_SIMA_blades = 3*41721; % Mass of the 3 blade lines in Sima
5  m_SIMA_eccentricities = 3*2.8; % Mass of the 3 eccentricity lines in Sima
6  m_SIMA_nacelle = 4.4454*10^5; % Mass of the nacelle line in Sima
7  m_SIMA_shaft = 500.5; % Mass of the shaft line in Sima
8  m_SIMA_nacellebody = 1.0; % Mass of the nacelle "dummy Simo body" in Sima
9  m_SIMA_hub = 1.0502*10^5; % Mass of the hub Simo body in Sima
10
11 % Total mass of the tower line and the rotor nacelle assembly (RNA)
12 m_SIMA_tower_and_RNA = m_SIMA_tower + m_SIMA_blades + m_SIMA_eccentricities + m_SIMA_nacelle +
   ↵ m_SIMA_shaft + m_SIMA_nacellebody + m_SIMA_hub;
13
14 g = 9.81; % Acceleration of gravity [m/s2]
15
16 m_c = 51025; % Equivalent clump mass in water on mooring lines [kg];
17 l = 703; % Mooring line length [m]
18 l_sf = 691 - 250; % Mooring line segment length resting on the ground [m]
19 Cm = 375.38; % Mass coefficient of mooring lines
20           % (mass per unit length in water) [-]
21 m_tot = l*Cm; % Total mass in water of one mooring line excluding clump
22 m_eff = m_tot - Cm*l_sf; % Mass in water of mooring line part not resting on ground, one line [kg]
23 pret = m_eff*g + m_c*g; % Vertical pretension at fairlead of one line [N]
24 pret_3 = 3*pret; % Total vertical pretension of all mooring lines together [N]
25
26 % Resulting Sima buoyancy correction force
27 SIMA_buoyancy_correction_force = m_SIMA_tower_and_RNA*9.81 + pret_3;

```

F Applying prescribed data from Sima in Wasim analysis

Prescribed data is specified under the tabs "Execution Directives" and "Extra parameters" in the Wasim activity in HydroD. This can be seen in Figure A2a. Figure A2b shows all the text inside the "Extra parameters" text field.



(A)

```

iwave_file = ' Z:/surfacemeshinput/Wave.txt '
file_faux = ' Z:/surfacemeshinput/forces.frc '
filepmot_Sima = ' Z:/surfacemeshinput/Motion.txt '
tprescribe_start = 0
tprescribe = 200
IMSTEP = 0

```

(B)

FIGURE A2: Prescribed motion, point forces and wave elevation specification in HydroD for Wasim analysis

`tprescribe_start = 0` and `tprescribe = 20` means that the prescribed data should start at 0 s and end at 20 s, while `IMSTEP = 0` is a command that tells Wasim to use motions from the `motion.txt` file instead of solving the motion in the analysis.

The file `Force.frc` contains all information about the prescribed forces in the Wasim analysis. This includes the position of the forces and the time history. Two seconds of such a `Force.txt` file can be seen in at the end of this section. The `Force.frc` file also contains some additional parameters in the first few lines. Interested readers are advised to look up these parameters and what they mean in Wasim user manuals (DNV 2022e).

The file `Motion.txt` is a file containing the applied motion of the analysis. The file contains 19 columns where column 1 is the time steps, 2-7 is the motion, 8-13 is velocity and 14-19 is the acceleration. The motion, velocity and acceleration have one column per rigid body mode. Two seconds of such a `Motion.txt` file can be found at the end of this section.

The wave elevation can be given either directly as a time series. Alternatively, the wave elevation can be given as a list of regular waves. The `Wave.txt` file at the end of this section shows an example of the latter method using 3496 waves. Note that there are only 11 wave components in the text file presented due to the large size of the full file. As for the `forces.frc` file, interested readers are recommended to read the Wasim user manuals for a detailed description of the first few lines of the `Wave.txt` file. The Wasim user manual also describes in detail how the other method of inputting the wave elevation time series directly works (DNV 2022e).

DNV have made it easy to output floater motion, forces and wave elevation from Sima analyses for use in Wasim by using the "Export results to WASIM" option under "Dynamic Calculation" in the Calculations Parameters folder in Sima. This option in Sima can be seen in Figure A3 below.

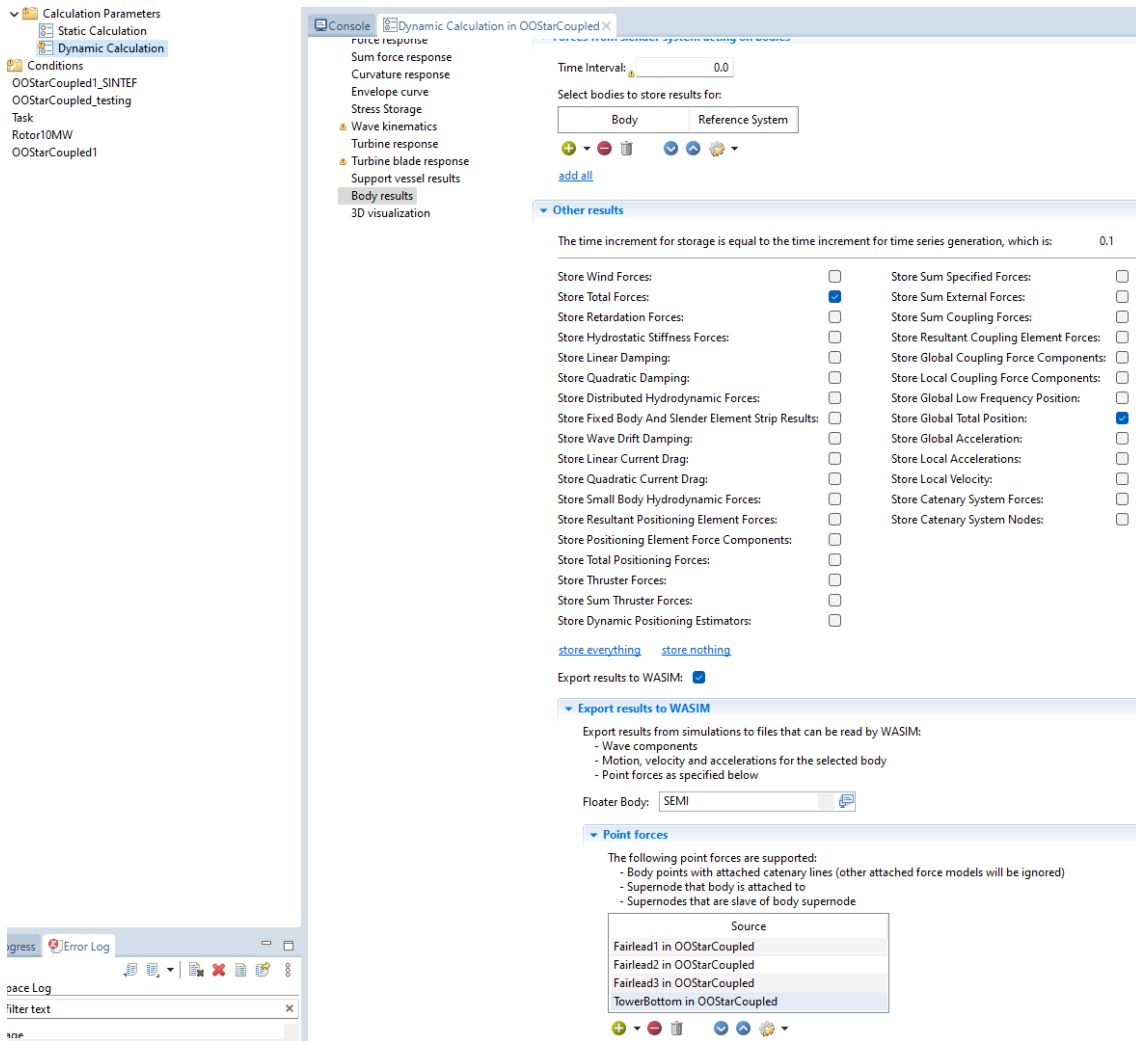


FIGURE A3: "Export results to Wasim" option in Sima

The "Export results to Wasim" option seen in Figure A3 outputs the files "Motion.txt", "Force.txt" and "Wave.txt" in the Sima working directory. Motion.txt and Wave.txt can be used directly as seen in Figure A2. The Force.txt file needs a slight modification of the first few lines in order to be consistent with the correct format as described in the Wasim user manual. The file extension also has to be changed to .frc.

F.1 Wave.txt

1	V2				
2	-1.0	0.0	1.0	0.0	
3		3496			
4	0.300623837E+02	0.652564268E-04	0.000000000E+00	0.321501846E+02	
5	0.299935913E+02	0.711348257E-04	0.000000000E+00	0.564382439E+02	
6	0.299251118E+02	0.774628425E-04	0.000000000E+00	0.258156071E+02	
7	0.298569450E+02	0.842677327E-04	0.000000000E+00	-0.870495148E+02	
8	0.297890911E+02	0.915782875E-04	0.000000000E+00	0.110550812E+03	
9	0.297215424E+02	0.994246293E-04	0.000000000E+00	0.364841461E+02	
10	0.296542988E+02	0.107837630E-03	0.000000000E+00	-0.330705681E+02	
11	0.295873585E+02	0.116849493E-03	0.000000000E+00	0.679648972E+02	
12	0.295207195E+02	0.126494313E-03	0.000000000E+00	-0.137366171E+02	
13	0.294543800E+02	0.136806804E-03	0.000000000E+00	-0.725663300E+02	
14	0.293883400E+02	0.147823128E-03	0.000000000E+00	-0.162282982E+02	

F.2 forces.frc

```
1 4 1
2 44.0 0.0 9.5 -21.999999999999999 38.105117766515306 9.5 -22.000000000000002 -38.10511776651529 9.5 0.0
  ↪ 0.0 11.0
3 0 0 1
4 0.10000000149011612 966195.9838867188 0.32097750226967037 -1347663.2080078125 0.0 0.0 0.0
  ↪ -486575.4089355469 842006.7138671875 -1354250.48828125 0.0 0.0 0.0 -486452.2705078125
  ↪ -841793.0297851562 -1353906.6162109375 0.0 0.0 0.0 -7963.873863220215 -60260.80322265625
  ↪ -1.79897890625E7 1501508.4228515625 -878682.9833984375 -50073.03237915039
5 0.20000000298023224 963082.8247070312 2.736708614975214 -1343154.541015625 0.0 0.0 0.0
  ↪ -487798.0041503906 844378.90625 -1358057.2509765625 0.0 0.0 0.0 -487864.44091796875
  ↪ -844490.4174804688 -1358239.990234375 0.0 0.0 0.0 -89527.16064453125 68095.77941894531
  ↪ -1.8427609375E7 -3810238.28125 -3690836.181640625 -211317.19970703125
6 0.30000000447034836 962405.8227539062 -8.320106193423271 -1341663.818359375 0.0 0.0 0.0
  ↪ -488192.8405761719 845932.6782226562 -1360491.2109375 0.0 0.0 0.0 -488741.27197265625
  ↪ -846907.2265625 -1362057.2509765625 0.0 0.0 0.0 -168879.53186035156 31495.325088500977
  ↪ -1.811050390625E7 -3375052.734375 -8852357.421875 -269699.70703125
7 0.4000000059604645 960748.291015625 -17.128819599747658 -1338731.0791015625 0.0 0.0 0.0
  ↪ -487910.4309082031 846460.205078125 -1361234.130859375 0.0 0.0 0.0 -489066.40625
  ↪ -848514.9536132812 -1364522.705078125 0.0 0.0 0.0 -206739.0594482422 -4818.4099197387695
  ↪ -1.82340546875E7 -1512525.5126953125 -1.34248359375E7 -151291.24450683594
8 0.5000000074505806 954092.28515625 -12.726154178380966 -1328890.380859375 0.0 0.0 0.0
  ↪ -488182.9528808594 847981.2622070312 -1363540.8935546875 0.0 0.0 0.0 -489075.2258300781
  ↪ -849575.9887695312 -1366071.2890625 0.0 0.0 0.0 -238021.728515625 -54939.334869384766
  ↪ -1.833669921875E7 -202009.38415527344 -1.6625060546875E7 207271.8505859375
9 0.6000000089406967 946524.2919921875 -3.529045032337308 -1317955.078125 0.0 0.0 0.0
  ↪ -488618.1335449219 849758.6059570312 -1366217.6513671875 0.0 0.0 0.0 -488948.0285644531
  ↪ -850354.9194335938 -1367142.4560546875 0.0 0.0 0.0 -196993.14880371094 -28388.7939453125
  ↪ -1.8250376953125E7 -3448455.322265625 -1.6846943359375E7 495194.4580078125
10 0.7000000104308128 943524.169921875 -7.354155648499727 -1313553.7109375 0.0 0.0 0.0
  ↪ -488318.3288574219 850198.73046875 -1366709.8388671875 0.0 0.0 0.0 -488913.9099121094
  ↪ -851257.1411132812 -1368402.4658203125 0.0 0.0 0.0 -236487.85400390625 75414.2837524414
  ↪ -1.833863671875E7 -8941333.0078125 -2.002244921875E7 413142.7307128906
11 0.800000011920929 943384.8876953125 -22.70342968404293 -1313203.857421875 0.0 0.0 0.0
  ↪ -487942.4133300781 850472.2900390625 -1366911.4990234375 0.0 0.0 0.0 -489336.1511230469
  ↪ -852947.0825195312 -1370908.3251953125 0.0 0.0 0.0 -283831.48193359375 -38127.39944458008
  ↪ -1.8277447265625E7 -5339292.48046875 -2.29363984375E7 142551.89514160156
12 0.9000000134110451 942689.2700195312 -21.208997815847397 -1312089.84375 0.0 0.0 0.0
  ↪ -488077.2399902344 851635.009765625 -1368515.380859375 0.0 0.0 0.0 -490082.45849609375
  ↪ -855173.0346679688 -1374243.1640625 0.0 0.0 0.0 -253461.45629882812 -33007.40432739258
  ↪ -1.831899609375E7 -5331803.7109375 -2.0961453125E7 85382.26318359375
13 1.0000000149011612 941755.9814453125 -9.468847885727882 -1310651.85546875 0.0 0.0 0.0
  ↪ -488465.27099609375 853216.6748046875 -1370764.0380859375 0.0 0.0 0.0 -490425.5065917969
  ↪ -856652.5268554688 -1376345.21484375 0.0 0.0 0.0 -197469.74182128906 -111451.18713378906
  ↪ -1.8338583984375E7 -3430135.25390625 -1.6698427734375E7 397686.70654296875
14 1.1000000163912773 943011.5356445312 9.761459194123745 -1312252.3193359375 0.0 0.0 0.0
  ↪ -488035.4309082031 853341.7358398438 -1370650.390625 0.0 0.0 0.0 -489790.52734375
  ↪ -856372.1313476562 -1375614.74609375 0.0 0.0 0.0 -168866.3330078125 -66057.47985839844
  ↪ -1.825663671875E7 -6941715.33203125 -1.3446033203125E7 876746.1547851562
15 1.2000000178813934 945322.2045898438 20.981423556804657 -1315258.544921875 0.0 0.0 0.0
  ↪ -486822.265625 852075.68359375 -1368313.8427734375 0.0 0.0 0.0 -488325.62255859375
  ↪ -854625.0610351562 -1372564.0869140625 0.0 0.0 0.0 -176095.93200683594 -53954.60510253906
  ↪ -1.8345396484375E7 -1.05524951171875E7 -1.129708984375E7 1018028.2592773438
16 1.3000000193715096 946467.8955078125 21.088847890496254 -1316554.0771484375 0.0 0.0 0.0
  ↪ -485233.70361328125 850137.8784179688 -1364935.05859375 0.0 0.0 0.0 -487154.6630859375
  ↪ -853396.9116210938 -1370412.7197265625 0.0 0.0 0.0 -103194.4580078125 22530.576705932617
  ↪ -1.8336134765625E7 -1.63605546875E7 -5509154.78515625 678517.9443359375
17 1.4000000208616257 947486.0229492188 10.248900391161442 -1317590.576171875 0.0 0.0 0.0
  ↪ -483377.5634765625 847704.58984375 -1360817.9931640625 0.0 0.0 0.0 -486913.4521484375
  ↪ -853802.5512695312 -1370952.392578125 0.0 0.0 0.0 -15652.990341186523 23308.7100982666
  ↪ -1.83595E7 -1.8120076171875E7 551765.625 280779.3273925781
18 1.5000000223517418 950997.9248046875 4.662723280489445 -1321999.267578125 0.0 0.0 0.0
  ↪ -481421.0205078125 845087.890625 -1356469.970703125 0.0 0.0 0.0 -487149.10888671875
  ↪ -855039.794921875 -1372867.1875 0.0 0.0 0.0 -5840.962886810303 -32118.911743164062
  ↪ -1.832101171875E7 -1.51983203125E7 1596488.6474609375 190710.1593017578
19 1.600000023841858 956660.4614257812 27.061987668275833 -1329248.53515625 0.0 0.0 0.0
  ↪ -480314.02587890625 844022.3388671875 -1354653.4423828125 0.0 0.0 0.0 -486386.9323730469
  ↪ -854533.9965820312 -1371998.1689453125 0.0 0.0 0.0 -53096.38595581055 -127708.04595947266
  ↪ -1.838102734375E7 -1.20896572265625E7 -535518.5546875 561111.7553710938
```

20 1.700000025331974 961045.8984375 65.50265103578568 -1334532.8369140625 0.0 0.0 0.0 -480024.169921875
↪ 844492.919921875 -1355302.1240234375 0.0 0.0 0.0 -484997.6806640625 -852986.1450195312
↪ -1369486.9384765625 0.0 0.0 0.0 13785.748481750488 -7190.803527832031 -1.8367525390625E7
↪ -1.82960546875E7 1616349.609375 1121941.162109375

21 1.8000000268220901 962895.0805664062 88.71445059776306 -1336138.916015625 0.0 0.0 0.0
↪ -479674.5910644531 844902.34375 -1355829.9560546875 0.0 0.0 0.0 -483755.0048828125
↪ -851754.150390625 -1367544.7998046875 0.0 0.0 0.0 42176.92947387695 39589.87045288086
↪ -1.8425390625E7 -2.1351623046875E7 2113126.220703125 1364401.0009765625

22 1.9000000283122063 963779.2358398438 107.58595913648605 -1336332.3974609375 0.0 0.0 0.0
↪ -478400.6042480469 843669.6166992188 -1353703.0029296875 0.0 0.0 0.0 -483086.4562988281
↪ -851519.1040039062 -1367267.2119140625 0.0 0.0 0.0 61393.42498779297 -4239.546775817871
↪ -1.8393205078125E7 -1.785187109375E7 923595.5810546875 1206322.8759765625

23 2.0000000298023224 964929.3212890625 153.9715826511383 -1336849.853515625 0.0 0.0 0.0
↪ -476923.88916015625 842131.0424804688 -1351092.8955078125 0.0 0.0 0.0 -482252.38037109375
↪ -850997.3754882812 -1366571.1669921875 0.0 0.0 0.0 -8739.243507385254 -153128.81469726562
↪ -1.84218046875E7 -9587075.1953125 -3910407.958984375 953834.47265625

F.3 Motion.txt

1 0.0 0.02857310138642788 -5.841060897182615E-7 0.004526882898062468 -2.803354561820015E-7
↪ -0.013642745092511177 1.6052763385232538E-6 0.0 0.0 0.0 0.0 0.0 0.0 0.0 0.0 0.0 0.0 0.0 0.0 0.0 0.0

2 0.10000000149011612 0.02904040925204754 -1.2908852795590064E-6 0.004486742429435253
↪ 2.2991598598309793E-6 -0.013412972912192345 1.4771746918995632E-6 0.009601340629160404
↪ -1.6415317077189684E-4 -5.329496925696731E-4 3.734862257260829E-4 0.004764520097523928
↪ -5.432059424492763E-6 0.10212509334087372 -0.002162978518754244 -0.0022049900144338608
↪ 0.00486280120435818 0.056241898719787395 -8.947767587518527E-5

3 0.20000000298023224 0.030515659600496292 -1.2988794878765475E-5 0.004400279838591814
↪ 2.5559204004821368E-5 -0.012672464363276958 -4.351411746483791E-7 0.019946279004216194
↪ 6.478086288552731E-5 -0.0013364609330892563 -2.5512094725854695E-4 0.010102762840688229
↪ -3.6928875488229096E-5 0.1022268682718277 0.006647508591413498 -0.009651140309870243
↪ -0.017082071327997148 0.04990158218963133 -4.519225471893848E-4

4 0.30000000447034836 0.0330394022166729 2.2704041839460842E-5 0.004236686509102583
↪ -7.851251575630158E-5 -0.011405552737414837 -6.532718089147238E-6 0.030426155775785446
↪ 6.011110381223261E-4 -0.0018402866553515196 -0.0017279558815062046 0.014946763403713703
↪ -8.639221778139472E-5 0.100550077855587 0.00393701670691371 -0.004906039219349623
↪ -0.011654859876163876 0.037560657659034775 -5.522982718526383E-4

5 0.4000000059604645 0.03660481795668602 1.0030651901615784E-4 0.004014825448393822
↪ -3.0328260618261993E-4 -0.00970761850476265 -1.766648711054586E-5 0.040794193744659424
↪ 8.988859481178224E-4 -0.002627018140628934 -0.002631520386785269 0.018758857622742653
↪ -1.3236267841421068E-4 0.09975960105657578 7.425396324833855E-5 -0.006266809534281492
↪ -0.0019724632914633064 0.027967130031329574 -2.891231446629753E-4

6 0.5000000074505806 0.04119117185473442 1.781746104825288E-4 0.003724084235727787
↪ -5.481123807840049E-4 -0.007693284656852484 -3.12165284412913E-5 0.050849009305238724
↪ 6.161888595670462E-4 -0.0032564240973442793 -0.0021748985163867474 0.02132008597254753
↪ -1.263964077224955E-4 0.09916949272155762 -0.002617496997117996 -0.00862942636013031
↪ 0.0037232555948586263 0.022296058648022365 4.388949431039023E-4

7 0.6000000089406967 0.04679159075021744 2.3437928757630289E-4 0.0033573838882148266
↪ -7.681086426600814E-4 -0.0054122069850564 -4.06137369282078E-5 0.061154238879680634
↪ 5.669493111781776E-4 -0.004043332301080227 -0.002408567350357771 0.024300402030348778
↪ -5.2058549044886604E-5 0.10164309293031693 0.0014133390504866838 -0.006618037354201078
↪ -0.0083875998665646 0.026987809970912675 9.670157981272917E-4

8 0.7000000104308128 0.05341076850891113 3.1663692789152265E-4 0.0029183533042669296
↪ -0.00109816191252321 -0.0028526694513857365 -4.11490436817985E-5 0.07112425565719604
↪ 0.0012484301114454865 -0.0047789402306079865 -0.004618789069354534 0.026673462241888046
↪ 3.787636524066329E-5 0.0968489721417427 0.010458498261868954 -0.00820055790245533
↪ -0.03128672536492808 0.017899027653280792 7.191785550353024E-4

9 0.800000011920929 0.06099658086895943 4.7969823936000466E-4 0.0024025640450417995
↪ -0.0016849355306476355 -1.0253767686663195E-4 -3.479341103229672E-5 0.080473393201828
↪ 0.0018454407108947635 -0.005514062941074371 -0.006731202360242605 0.028113223612308502
↪ 8.189716027118266E-5 0.08980366587638855 0.001371258869767189 -0.007070811465382576
↪ -0.01046904081892981 0.00775447084526173 1.828615199070849E-4

10 0.9000000134110451 0.06947863847017288 6.697932258248329E-4 0.0018122614128515124
↪ -0.0024069673381745815 0.002750586485490203 -2.6169798729824834E-5 0.08918481320142746
↪ 0.0019780374132096767 -0.006299810018390417 -0.007752363104373217 0.029111068695783615
↪ 9.114761633099988E-5 0.08897417038679123 0.0016904011135920882 -0.007477795705199242
↪ -0.010908093916514693 0.01794771442896362 1.0261650919943263E-4

11 1.0000000149011612 0.07883193343877792 8.654825505800545E-4 0.0011472466867417097
↪ -0.0032132817432284355 0.005780728068202734 -1.5892186638666317E-5 0.09791503846645355
↪ 0.0018282652599737048 -0.006997711956501007 -0.00814061239361763 0.031740546226501465
↪ 1.287257473450154E-4 0.08783763647079468 -0.0035920029040426016 -0.007940048351883888
↪ 3.8745969267064306E-4 0.032516999848963404 7.657856644310053E-4

12 1.1000000163912773 0.08903811872005463 0.0010380300227552652 4.082804371137172E-4
↪ -0.004046284593641758 0.009126372635364532 2.1974719857098535E-6 0.10621701925992966
↪ 0.0017113068606704473 -0.007707825396209955 -0.008761672303080559 0.03538232669234276
↪ 2.534446248319E-4 0.08315028250217438 0.0015756076900288463 -0.005890471860766411
↪ -0.013821271316650953 0.04224321924254131 0.0016901525924445538

13 1.2000000178813934 0.10004019737243652 0.001221124897710979 -3.95843613659963E-4
↪ -0.00500689959153533 0.012870791368186474 3.647819539764896E-5 0.11376771330833435
↪ 0.0020000599324703217 -0.008353417739272118 -0.01062367856502533 0.03959392383694649
↪ 4.417473392095417E-4 0.07408804446458817 0.005075466353446245 -0.006967822089791298
↪ -0.02552377493057631 0.04532684954960373 0.0019011037812043743

14 1.3000000193715096 0.11175453662872314 0.001460137078538537 -0.001266595791094005
↪ -0.006234744098037481 0.017068885266780853 8.881333633325994E-5 0.12057781964540482
↪ 0.0029185819439589977 -0.008978222496807575 -0.014308852143585682 0.04476245492696762
↪ 6.004481110721827E-4 0.0704149529337883 0.013182726688683033 -0.006043518427759409
↪ -0.04769326997317514 0.06469267700241128 0.0011523037516999793

15 1.4000000208616257 0.12413210421800613 0.0018211555434390903 -0.0021998046431690454
↪ -0.007915559224784374 0.02189021185040474 1.5258674102369696E-4 0.12702111899852753
↪ 0.005525386426597834 -0.009586518630385399 -0.01933666318655014 0.052047356963157654
↪ 6.737110088579357E-4 0.0654749795794487 0.013763480819761753 -0.0052522276528179646
↪ -0.05063680136097296 0.08321069388427779 3.563055527667635E-4

16 1.5000000223517418 0.1371157169342041 0.0023172032088041306 -0.003185402601957321
↪ -0.010093670338392258 0.027502749115228653 2.203474286943674E-4 0.13255438208580017
↪ 0.005525386426597834 -0.0099806422367692 -0.02397930808365345 0.06022683158516884
↪ 6.965430802665651E-4 0.0514945387840271 0.007136164698749781 -0.003538423217833042
↪ -0.033816326611692635 0.08018547370081089 2.207142967611308E-4

17 1.600000023841858 0.15056699514389038 0.0028809159994125366 -0.004209481179714203
↪ -0.012603582814335823 0.03388189151883125 2.9094243654981256E-4 0.13627924025058746
↪ 0.005647368263453245 -0.01035162340849638 -0.0259796641767025 0.06715875118970871
↪ 7.540041697211564E-4 0.03242139518260956 0.001138303428888321 -0.0029365583322942257
↪ -0.020107658367327676 0.06576809162125112 0.0010214122892898427

18 1.700000025331974 0.1643112301826477 0.003474254859611392 -0.0052613322623074055
↪ -0.015358475968241692 0.04092090576887131 3.716222709044814E-4 0.13856451213359833
↪ 0.006409625988453627 -0.010478362441062927 -0.02958928979933262 0.07379518449306488
↪ 9.120241738855839E-4 0.021635912358760834 0.01167414989322424 -0.001182568958029151
↪ -0.04677049407402923 0.07195811063913385 0.0020911624243104077

19 1.8000000268220901 0.17822732031345367 0.004179369192570448 -0.00632456736639142
↪ -0.01856861263513565 0.048647552728652954 4.721084551420063E-4 0.1396358460187912
↪ 0.007777057122439146 -0.010542414151132107 -0.03482292965054512 0.08072668313980103
↪ 0.0011502749985083938 0.00668039545416832 0.01646246202290058 4.060915671288967E-5
↪ -0.05914549617930312 0.06861493314361095 0.002504131861550811

20 1.9000000283122063 0.19217541813850403 0.005040381569415331 -0.007386977318674326
↪ -0.022346194833517075 0.05704523250460625 5.963409203104675E-4 0.13917985558509827
↪ 0.009340076707303524 -0.0103855449706316 -0.040434159338474274 0.08713879436254501
↪ 0.001388503354974091 -0.010099048726260662 0.009808184579014778 0.0033064938616007566
↪ -0.04107304575412747 0.05958090739867821 0.002178964998011284

21 2.0000000298023224 0.205983504652977 0.005994681268930435 -0.008419978432357311
↪ -0.026522086933255196 0.06600921601057053 7.41503550671041E-4 0.13669390976428986
↪ 0.009517033584415913 -0.009936216287314892 -0.04248052090406418 0.09172277897596359
↪ 0.0015838365070521832 -0.03368181735277176 -0.0036658651661127806 0.005803230218589306
↪ -0.006113112271772307 0.03408946080732042 0.0017449041625637429

